

https://dspace.org/

Analysis of peptidoglycan degrading amidases in Mycobacterium smegmatis

Senzani, Sibusiso

2014-02-18
http://hdl.handle.net10539/13852

Downloaded from a DSpace repository. https://dspace.org/

Analysis of peptidoglycan degrading amidases in *Mycobacterium smegmatis*

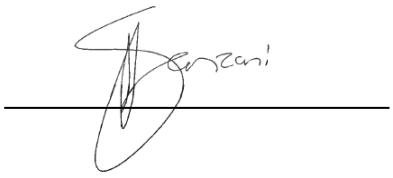
Sibusiso Senzani (0603371N)

Dissertation submitted to the Faculty of Health Science, University of the Witwatersrand, Johannesburg, in fulfilment of the requirements for the degree of Master of Science in Medicine.

May 2013

Declaration

I, Sibusiso Senzani declare that this Dissertation is my own work. It is being submitted for the Degree of Master in Medicine in the University of the Witwatersrand, Johannesburg. It has not been submitted before for any degree or examination at this or any other University.



Sibusiso Senzani

29th Day of May 2013

Dedication

I dedicate this work to my parents Mr Alpheus Tholisizwe Senzani and Mrs Hellen Senzani for their complete support of everything I do, and for teaching me to do what makes me happy and not just what makes me money and I thank them for that.

Presentations from this dissertation

Conference	: SASBMB/FASBMB conference
Presentation	: Poster
Year	: 2012

Conference	: Wits Research Day and Postgraduate Expo
Presentation	: Poster
Year	: 2012

Conference	: MRC Early Career Scientists Conference
Presentation	: Oral
Year	: 2012
Achievement	: **Second prize in the MRC Early Career Scientists Conference oral category**

Abstract

Tuberculosis (TB) is a worldwide pandemic, which claims approximately 2 million lives annually. Though treatable through chemotherapy, TB still causes 8-10 million new infections annually. The problem is further complicated by the emergence of multi-drug resistant strains of *Mycobacterium tuberculosis* (Mtb) the causative agent of TB. The unabated spread of this disease and associated high levels of mortality has prompted the search for new drugs with novel modes of action. The peptidoglycan (PG) component of the cell wall of Mtb is an incredibly complex structure and has been the focus of antimicrobial development in other organisms. In this study, we characterize PG remodelling *N*-acetylmuramyl-L-alanine amidases (cell wall amidases) in *Mycobacterium smegmatis* (Msm), a model organism for TB research by gene knockout/knockdown. Cell wall amidases cleave the bond between the stem peptide and the glycan backbone in PG and have been shown to play an essential role in cell growth, cell signalling and antibiotic resistance in other organisms. Our bioinformatics analysis revealed that *M. smegmatis* encodes three possible amidase homologues designated *ami1, ami2* and *ami3.* Deletion mutagenesis in Msm resulted in successful deletion of *ami1* whilst repeated attempts to delete *ami2* did not yield a knockout mutant, suggesting that *ami2* is essential for growth. Deletion of *ami1* results in the formation of long filaments consisting of 3 to 8 cells attached to each other due to incomplete resolution of the septum. In these filaments, lateral growth at both the internal septation sites and extreme poles resulted in irregular cell width, strongly implicating Ami1 in bacterial cell division, the maintenance of bacterial cell shape and possibly balancing the growth at the cell pole. Since deletion of *ami2* was not possible, a knockdown strain allowing for anhydrotetracycline (ATC)-regulated conditional gene expression of *ami2* was generated. In this system, withdrawal of ATC results in repression of expression. Expression analysis of *ami2* in this strain revealed that

whilst significant gene knockdown was achieved, *ami2* expression was not completely abolished in the absence of the inducer ATC, suggesting the presence of basal level *ami2* expression. The repression of *ami2* expression results in retarded growth, diminished motility, unusual colony morphology consisting of miniature colonies lacking any form of serpentine cording and the formation of miniature cells consisting of globular bulges. These data implicate Ami2 in bacterial growth and maintenance of bacterial cell shape. Collectively, our data comprise the first demonstration of an important role for peptidoglycan degrading amidases in mycobacterial growth and cell division. Furthermore, the phenotypic defects in colony formation due to deletion or depletion of amidases suggest that these enzymes play an important role in cell-cell communication during colony formation. These data validate this class of enzymes as an untapped, legitimate source of novel targets for anti-tubercular drug discovery.

Acknowledgements

I would like to thank my family for the support structure and encouragement throughout the past two years.

The **NRF** (National Research Foundation) and the University of the Witwatersrand for the financial support they offered me allowing me the opportunity to do my MSc.

Thank you to the **MMU** (Microscopy and Microanalysis Unit) at the University of the Witwatersrand for affording me the opportunity to work with their Confocal microscope and the **Microscopy unit** at the University of Cape Town for giving me the opportunity to work on their Scanning and Transmission electron microscope at odd hours in the night

I would also like to thank my supervisor **Dr Bavesh Kana** not only for the guidance and supervision but also for giving me the freedom to try different unorthodox experiments throughout the project allowing me to learn how to think 'out of the box'.

I would like also thank my colleagues and senior staff, at the CBTBR, for assistance, support and the occasional laugh to lighten the spirit when nothing was working; this allowed me to surpass many challenges faced throughout my studies.

Table of Contents

Declaration i
Dedication ii
Presentations from this dissertation iii
Abstract iv
Acknowledgements vi
List of Figures x
List of Tables xi
Nomenclature xii
1. Introduction 1
1.1 Background 1
1.2 Latent TB Infection 5
1.3 The Mycobacterial Envelope 8
1.4 PG 11
1.4.1 Antibiotics that target PG synthesis 13
1.4.1.1 β-lactam antibiotics 13
1.4.1.2 Cycloserine 14
1.4.1.3 Ramoplanin 15
1.4.1.4 Vancomycin 15
1.5 PG hydrolases 16
1.5.1 Carboxypeptidases (CPases) 16
1.5.2 Endopeptidases (EPases) 17
1.5.3 Lysozymes 17
1.5.4 Lytic transglycosylases 18
1.5.4.1 Resuscitation promoting factors (Rpfs) 18
1.5.5 *N*–Acetyl-β-D-glucosaminidases 19
1.6 *N*-acetylmuramyl-L-alanine amidases 20
1.6.1 Viral and eukaryotic amidases 20
1.6.2 Bacterial amidases 21
1.7 Aims and objectives 26
2. Materials and Methods 27
2.1 Bacterial strains, plasmids and growth conditions 27
2.1.1 Growth of *E. coli* DH5α and derivative strains 28
2.1.2 Growth of Msm strains 29
2.2 DNA manipulation 29
2.2.1 Mycobacterial chromosomal DNA extraction 29
2.2.1.1 Cetyltrymethylammonium bromide (CTAB) DNA extraction 29
2.2.1.2 Small scale DNA extraction for PCR 30
2.2.2 *E. coli* plasmid extraction 30
2.2.2.1 Bulk plasmid preparation using Nucleobond plasmid purification kit 30
2.2.2.2 Plasmid miniprep using alkaline lysis method 31
2.2.3 Sodium acetate DNA precipitation 32
2.2.4 DNA restriction enzyme digestion 32
2.2.5 Phosphorylation of DNA 32
2.2.6 Dephosphorylation of 5'ends of plasmid DNA 33
2.2.7 DNA ligation 33
2.2.8 Agarose gel electrophoresis 33

2.2.9 Purification of DNA fragments 34
2.2.10 Nucleic acid quantification 34
2.2.11 DNA Sequencing 35
2.3 Standard Polymerase chain Reaction (PCR) 35
2.3.1 Roche Fast-Start Taq PCR 35
2.3.2 Phusion High-Fidelity DNA polymerase 36
2.4 Transformation of bacterial cells 36
2.4.1 Transformation of chemically competent DH5α 36
2.4.2 Electroporation into Msm 37
2.5 Southern Blotting 38
2.5.1 Labelling of Probe DNA 38
2.5.2 Blotting 38
2.6 Assessment of gene expression 40
2.6.1 RNA extraction from mycobacterial cells 40
2.6.2 Reverse Transcriptase PCR (RT-PCR) 41
2.6.3 Quantitative real-time PCR (qPCR) amplification 42
2.7 Analysis of bacteria growth 42
2.7.1 Growth rate analysis 42
2.7.2 Analysis of mycobacterial biofilm formation 43
2.7.3 Analysis of mycobacterial sliding motility 43
2.7.4 Bacterial spotting assay 44
2.8 Microscopic analysis 44
2.8.1 Confocal microscopy 44
2.8.2 Scanning electron microscopy (SEM) 45
2.8.3 Transmission electron microscopy (TEM) 45
2.8.4 Atomic force microscopy (AFM) 46
2.9 Bio-informatic analysis 46
2.10 Construction of knock out strains 47
2.10.1 Construction of *ami1* and *ami2* knockout vectors 48
2.10.1.1 PCR reactions 48
2.10.1.2 Cloning 50
2.10.1.2.1 pGEM cloning 50
2.10.1.2.2 Three Way cloning 51
2.10.1.2.3 Pac cassette cloning 52
2.10.1.3 Testing for acquired sucrose sensitivity 53
2.10.1.4 Two-step homologues recombination 53
2.10.1.5 PCR Screening 54
2.11 Complementation of Msm Δ*ami1* strain 54
2.11.1 Construction of the complementation vector 56
2.11.2 pMVAmi1 integration into Δ*ami1* strain genomic DNA 57
2.12 Construction of *ami2* knockdown strain 58
2.12.1 Construction of *ami2* knockdown vector 60
2.13 Msm *ami2*KDP associated Phenotyping 60
2.13.1 Msm *ami2*KDP preculture preparation 60
2.13.2 Analysis of regulated gene expression 61
2.13.3 Msm *ami2*KDP growth kinetics 62
3. Results 63
3.1 Bioinformatics analyses and identification of putative amidase-encoding genes in mycobacteria 63
3.1.1 Conservation of catalytic residues within the Amidase 3 domain 66

3.1.2 Conservation of catalytic residues within the Amidase 2 domain 68
3.2 Construction of deletion mutants defective in the *ami1* and *ami2* genes. 69
3.2.1 Construction of vectors for deletion of *ami1* and *ami2*. 70
3.2.2 Two-step homologues recombination and gene knockout..... 75
3.3 Complementation of the Msm Δ*ami1* strain 77
3.3.1 Construction of the *ami1* complementation vector..... 79
3.3.2 pMVAmi1 integration into Δ*ami1* strain genomic DNA..... 80
3.4 Construction of an *ami2* knockdown strain 81
3.4.1 Construction of *ami2* knockdown vector..... 82
3.4.2 Incorporation of pSEAmi2P into Msm to create a gene knockdown strain..... 83
3.5 The Role of Ami1 in cell division and structural maintenance..... 83
3.5.1 Ami1 does not play a significant role in determining growth rate 85
3.5.2 Ami1 does not play a significant role in biofilm formation..... 86
3.5.3 Ami1 does not play a significant role in sliding motility..... 87
3.5.4 Ami1 plays an important role in cell division, cell growth and cell shape maintenance..... 88
3.6 The Role of Ami2 in cell growth..... 100
3.6.1 Confirmation of regulated gene expression in the *ami2* knockdown strain.... 100
3.6.2 Ami2 plays a role in determining growth rate..... 102
3.6.3 Ami2 plays role in sliding motility..... 103
3.6.4 Ami2 plays role in determining colony morphology..... 105
3.6.5 A role for Ami2 in determining cell morphology 105
4. Discussion 110
5. Appendices..... 120
6. Bibliography..... 126

List of Figures

Figure 1.1: Diagrammatic representation of the estimated 2011 global TB incidents rate…….. 2
Figure 1.2: Diagrammatic representation of the structure of mycobacterial cell envelope…….. 8
Figure 1.3: Representation of the structure of PG and cleavage sites for various PG associated hydrolases…….....12
Figure 1.4: Diagrammatic representation of the PG biosynthetic pathway……... 13
Figure 1.5: Diagrammatic representation of the proposed mechanism for EnvC and NlpD mediated amidase activation……. 23
Figure 2.1: Diagrammatic representation of the allelic exchange process……... 48
Figure 2.2: Diagrammatic representation of the construction of knockout vectors..51
Figure 2.3: Schematic representation of the PCR screen for deletion mutants…....55
Figure 2.4: Schematic representation of the tetracycline operator knockdown system……..... 59
Figure 2.5: Schematic representation of the ATC-regulated knockdown strain…...59
Figure 3.1: Schematic representing the mycobacterial amidases and their *E. coli* homologues……..…… 64
Figure 3.2: Diagrammatic representation of the Msm cell wall amidases and their respective protein domains…….……... 64
Figure 3.3: ClustalW analysis of amidase_3 domain containing amidases……..67
Figure 3.4: ClustalW analysis of amidase_2 domain containing amidases…….....69
Figure 3.5: Restriction profile of p2NILAmi1……...……...71
Figure 3.6: Restriction profile of p2NILAmi2……...……...72
Figure 3.7: Restriction profile of p2ΔAmi1G19……...…… 73
Figure 3.8: Restriction profile of p2ΔAmi2G19……...…… 74
Figure 3.9: Confirmation of sucrose sensitivity in strains carrying knockout constructs…… 75
Figure 3.10: PCR screen for deletion mutants of *ami1* and *ami2*…….…… 76
Figure 3.11: Southern Blot analysis of the Msm Δ*ami1* strain……...…….. 78
Figure 3.12: Restriction profile of pMVami1……...…… 79
Figure 3.13: PCR Screen for integration of pMVami1…...……..81
Figure 3.14: Restriction profile of pSEAmi2P……..82
Figure 3.15: Southern Blot analysis of the Msm *ami2*KDP knockdown strain…… 84
Figure 3.16: Growth kinetics of the Δ*ami1* strain……85
Figure 3.17: Biofilm formation with Δ*ami1 s*train……...…… 86
Figure 3.18: Sliding motility of the mc^2155 and Δ*ami1 s*trains on 7H9 and M63 agar..…… 88
Figure 3.19: Confocal microscopy comparing mc^2155, Δ*ami1* and Δ*ami1::*pMVami1..…….. 90
Figure 3.20: SEM images of mc^2155, Δ*ami1* and Δ*ami1::*pMVami1 strains..……. 93
Figure 3.21: TEM images of the mc^2155, Δ*ami1* and Δ*ami1::*pMVami1 strains… 97
Figure 3.22: AFM images of the mc^2155, Δ*ami1* and Δ*ami1::*pMVami1 strains… 99
Figure 3.23: Expression analysis of ATC regulated gene expression..……... 101
Figure 3.24: Depletion of *ami2* results in reduced growth of Msm……..... 102
Figure 3.25: Sliding motility assays with the *ami2* depletion strains……104
Figure 3.26: The impact of *ami2* depletion on colony morphology……. 105
Figure 3.27: SEM images of the mc^2155 and *ami2*KDP strains…….. 107
Figure 3.28: Confocal microscopy of the mc^2155 and *ami2*KDP strains……. 108

List of Tables

Table 2.1: Bacterial strains created and/or used in this study…….. 27
Table 2.2: Plasmids created and/or used in this study…….. 27
Table 2.3: Primer3 parameters used when designing primers using the Primer3 tool…….. 35
Table 2.4: Primers used for amplification of upstream and downstream regions of the *ami1* and *ami2* genes…… 49
Table 2.5: Double cross over screening primers……... 56
Table 2.6: Primer used for expression analysis ……61

Nomenclature

$(NH_4)_2SO_4$	: Ammonium sulphate
µ	: Micro
AAP	: Antarctic Alkaline Phosphatase
AFM	: Atomic force microscopy
AIDS	: Acquired Immunodeficiency Syndrome
Ami	: Amidase
Amp	: Ampicillin
ATC	: Anhydrotetracycline
bp	: Base pairs
cDNA	: Complementary Deoxyribonucleic acid
	Cetyltrymethylammonium bromide
CFU	: Colony forming unit
CSPD	: Chloro-5-substituted adamantyl-1, 2-dioxetane phosphateCTAB
DAP	: Diaminopimelic acid
DCO	: Double cross over
DDSA	: Dodecenyl Succinic Anhydride
DIG	: Digoxigenin
DMP	: Tris-2,3,6-(dimethylaminomethyl)phenol
DNA	: Deoxyribonucleic acid
dNTP	: Deoxynucleotide triphosphate
DST	: Drug susceptibility testing
EDTA	: Ethylenediaminetetraacetic acid
$FeSO_4.7H_2O$	: Iron sulphate
g	: gram
HCl	: Hydrochloric acid
HIV	: Human I immunodeficiency Virus
Hyg	: Hygromycin
hyg	: Gene encoding hygromycin B resistance
Hyg^R	: Hygromycin Resistance
Kan	: Kanamycin
Kan^R	: Kanamycin Resistance
kb	: Kilo base pair
KH_2PO_4	: Potassium dihydrogen phosphate
KOH	: Potassium hydroxide
LA	: Luria-Bertani agar
lacZ	: Gene encoding galactosidase
LB	: Luria-Bertani broth
LGFP	: Leucine, Glycine, Phenyalanine, Proline repeat Domain
LTBI	: Latent tuberculosis infection
MDR	: Multi-Drug resistant
MDR-TB	: Multidrug-Resistant Tuberculosis
min	: minutes
ml	: Millilitre
mRNA	: messenger Ribonucleic acids
Msm	: *Mycobacterium smegmatis*
Mtb	: *Mycobacterium tuberculosis*
NaCl	: Sodium chloride
NAG	: *N*-acetylglucosamine mine

NAM : *N*-acetylmuramic acid
NaOH : Sodium hydroxide
OD_{600} : Optical density at 600 nanometre wavelength
PBP : Penicillin Binding Proteins
PCR : Polymerase Chain Reaction
PG : Peptidoglycan
PGRS : Peptidoglycan recognition proteins
PNK : Polynucleotide Kinase
R : Resistant
RBS : Ribosomal Binding Site
RNA : Ribonucleic acids
Rpf : Resuscitation promoting factor
rpm : Revolutions per minute
RT : Reverse Transcriptase
sacB : Gene encoding levansucrase
SCO : Single cross over
sdH2O : Sterile distilled water
SDS : Sodium dodecylsulphate
SEM : Scanning electron microscopy
TB : Tuberculosis
TBE : Tris-Borate-EDTA
TDR : Total-Drug resistant
TE : Tris-EDTA
TEM : Transmission electron microscopy
Tris : Tris (hydroxymethyl) aminomethane
Tween : Polyoxyethylene sorbitan monooleate
TY : Tryptone, Yeast Extract
U : Enzyme Unit
UDP : Uridine diphospate
v/v : Volume per volume
VBNC : Viable but non culturable
w/v : Weight per volume
WHO : World Health Organisation
XDR : Extensively-Drug resistant
XDR-TB : Extensively Drug Resistant Tuberculosis
X-gal : 5-bromo-4-chloro-3-indolyl-D-thiogalactopyranoside
Δ : Delta
η : Nano

1. Introduction

1.1 Background

Over the past century, Tuberculosis (TB) has been a significant source of human suffering and has historically been attributed as responsible for the largest number of deaths due to a single bacterial infectious disease agent (Zhang, 2005). Currently, TB is responsible for approximately 1.5 - 2 million deaths annually, with 30 % of these being HIV/AIDS related incidents (World Health Organization statistics, 430 000 HIV-TB cases of 1.4 million total cases in 2011); a further 8 to 10 million new TB cases are reported annually (WHO, 2011). The recent WHO report indicates that vaccination and effective chemotherapeutic interventions for TB have resulted in the global decline of TB incidence but frustratingly, these effects have not been felt in the developing world. This is mainly due to the disproportionately high burden of disease in these countries, particularly Southern Africa, where high population density, increased urbanisation, high HIV incidents and poor socio-economic conditions, have fuelled the TB pandemic (WHO, 2011, Tripathi *et al*., 2005). This has led to the current situation where the developing world accounts for 82 % of all non HIV related TB deaths, Figure 1.1 (Tripathi *et al*., 2005, WHO, 2011).

TB is caused by infection with *Mycobacterium tuberculosis* (Mtb), an extremely well adapted human pathogen, that causes a multitude of disease outcomes upon infection ranging from subclinical latent infection, to chronic active granulomatous disease (Chao and Rubin, 2010). TB is treatable through a combinatorial treatment regimen that involes two phases: an intial two month treatment phase with four first line drugs, isoniazid, rifampicin, ethambutol and pyrazinamide followed by a continuation 4 month treatment phase with rifampicin and isoniazid (WHO, 2009, WHO, 2011, Zhang, 2005). Despite the presence of this robust treatment program, TB still remains a global health concern due to

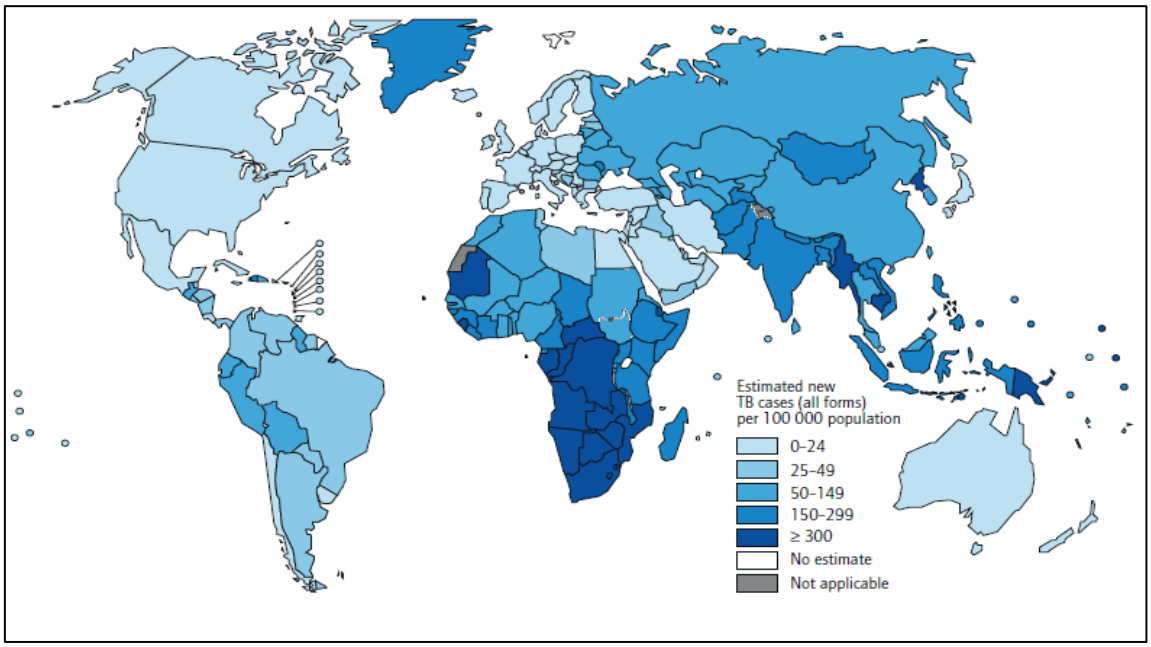


Figure 1.1: Diagrammatic representation of the estimated 2011 global TB incidents rates. The southern and central African regions are representative of the highest global burden with an estimated greater than 300 new incidents per 100 000 population in 2011. Other high burden regions include the Far East and South East Asia. Lower burden areas include more developed regions such as North America, Europe and Australia, averaging 0-24 new TB incidents per 100 000 population in 2011(WHO, 2011).

multiple factors. These include inherent cellular mechanisms in the tubercle bacillus for resisting host innate and adaptive immunity, the ability to establish latent infection and the multiple mechanisms of inherent or acquired drug resistance/tolerance (Zhang, 2005, Hett and Rubin, 2008). Furthermore, the highly impermeable cell envelope, the presence of numerous multi-drug efflux pumps, the expression of antibiotic degrading ezymes and most principally, the chromosomal mutation of drug targets resulting in the emergence of multi-drug (MDR), extensively-drug (XDR), and totally-drug (TDR) resistant strains have all been contributing factors to the success of TB (Zhang 2005; Hett and Rubin 2008; Velayati *et al*., 2009). MDR strains are those disease causing strains that are resistant to rifampicin and isoniazid, XDR strains represent a further step in the evolution of drug resistance since in addition to being MDR, they are resistant to aminoglycosides and flouroquinolones (WHO, 2009). The combination of the above-mentioned facets of Mtb

biology makes it quiet resilient to TB treatment protocols and necessitates the protracted treatment period that is currently used.

The rapid emergence of drug resistant strains is a major cause for concern and further undermines the national TB treatment programs of many high-burden countries, like India and South Africa (WHO, 2011, Okeke *et al*., 2005). The increased prevalence of these strains has been, in part, attributed to the current treatment protocols and patient non-compliance (Mitchison, 1998, Yagui *et al*., 2006), the latter relates to the fact that TB chemotherapy is a lengthy, intense process, which is toxic to the host. This results in a reduction in the bio-availability of antibiotic in patients, leading to the evolution of drug resistance (Zhang, 2005, Velayati *et al*., 2009, Tripathi *et al*., 2005, Mitchison, 1998). Out of the estimated 1.4 million new TB incidents in 2011, an estimated 310 000 of these were MDR-TB strains of, which approximately 60 % were in India, China and The Russian Federation (WHO, 2011).

Diagnosis of MDR and XDR TB is a lengthy and costly process involving drug susceptibility testing (DST), which does not form part of the initial diagnosis protocol due to the cost and extended time associated with these methods (Yagui *et al*., 2006). This has now changed with the advent of nucleic acid-based diagnostic platforms that allow for the identification of drug resistance alleles rapidly (Van Rie *et al*., 2010). Previously, DST was only done when a patient was failing standard therapy due to the lengthy time period required to collect more sputum material, followed by culturing of Mtb, which takes weeks. This allows ample time for further propagation of these drug resistant strains in patients, leading to subsequent spread in the community (WHO, 2009, Kimerling *et al*., 1999, Yagui *et al*., 2006, Storla *et al*., 2008). Infection with MDR strains is usually treated

with the use of less efficient, more toxic, second line drugs such as cycloserine, ethionamide, pyrazinamide, injectable aminoglycosides (amikacin, cepreomycin or kanamycin) or fluoroquinolones (ciprofloxin or ofloxicin) (WHO, 2009). The cost and length (up to two years) of the therapy renders this form of TB control highly impractical and economically challenging at best.

The chromosomal mutation of drug targets or enzymes required for drug activation is the most common mechanism of drug resistance in Mtb. A number of drug targets have been identified wherein chromosomal mutations lead to phenotypic resistance to specific antibiotics. These include: isoniazid resistance resulting from mutations in either *katG, inhA, aphC, nhd* and *kasA* genes, rifampicin resistance resulting from mutations in the *rpoB* gene, ethambutol resistance resulting from mutations in the *emb* gene, pyrazinamide resistance resulting from mutations in the *pncA* gene and fluoroquinolone resistance resulting from mutation in the *gyrA* or *gyrB* genes (Heifets and Cangelosi, 1999, Zhang *et al*., 1992, Banerjee *et al*., 1994, Nachega and Chaisson, 2003). There are other, less characterized, mechanisms that contribute to the emergence of drug resistance. These include the presence of cellular processes, which target antibiotics directly such as antibiotic degrading enzymes like β-lactamases, which are induced by the presence of β-lactam antibiotics (penicillins) and efflux pumps, which actively remove toxic elements out of the cytoplasm, including antibiotics (Chambers *et al*., 1995, McKeegan *et al*., 2004). Mtb has an additional, mimetic mechanism for evading antibiotic activity by producing compounds, which structurally resemble antibiotic targets, thus reducing the efficiency of antibiotics, which then bind the 'mimetic' compound leading to reduced overall drug potency (Nguyen and Thompson, 2006).

1.2 Latent TB Infection

The most significant barrier to the complete eradication of TB from human society is the large reservoir of individuals that harbour latent TB infection (LTBI). This is defined as a clinical state where an individual is infected with Mtb but does not present with any clinical symptoms of disease (Chao and Rubin, 2010, Barry *et al*., 2009). It is estimated that one third of the world's population carries LTBI - all of whom carry a defined lifetime risk (10 % per averaged lifetime) of progressing to active TB disease (Chao and Rubin, 2010, Barry *et al*., 2009). Despite significant research effort, very little is known about the bacterial and host innate factors that allow for the establishment and subsequent control of LTBI. There are currently two principal hypotheses with regards to LTBI, the first posits that latency is a result of a distinct transition from active growth to dormancy in the infecting bacteria and the second is based on the idea that LTBI is the result of a dynamic bacterial population (of growing and dying organisms) that is kept in control by a robust immune response. In both cases it has been hypothesized that some of the infecting organisms enter a metabolically quiescent or dormant-like state.

Dormancy is a complex microbiological phenomenon that is usually attributed to bacteria, grown in the laboratory, and is defined as a reversible state of low metabolic activity, which the bacterium enters under conditions of stress such as antimicrobial assault or nutrient starvation (Driks, 2009, Chao and Rubin, 2010). Current antimicrobial protocols involve the use of antibiotics, which target cellular processes that are essential for bacterial growth and survival (Zhang, 2005, Tripathi *et al*., 2005). The most significant problem with this approach is that these antibiotics will inherently target actively growing organisms only, which results in phenotypic drug tolerance with non-replicating dormant organisms thus allowing these bacteria to resist treatment and the host immune response

(Chao and Rubin, 2010, Barry *et al*., 2009). This ability to enter into a dormant state allows Mtb to survive in the host for years in the face of robust immunity until conditions become favourable for growth (host becomes immune-compromised), which results in exit from this state of metabolic quiescence and the resumption of active growth (Scanga *et al*., 1999). The dormant phenomenon, and mechanisms associated with entry and exit from this phase, have been extensively described in *Bacillus* species with respect to spore formation [reviewed in (Higgins and Dworkin, 2011)]. Numerous studies have demonstrated that several species of pathogenic and non-pathogenic mycobacteria have the ability to enter into a viable but non culturable (VBNC) state, where the organisms are unable to grow on solid media but remain viable as demonstrated by the use of live/dead staining systems and moreover by the fact that they can resume growth when cultured in specialized, conditioned media (Biketov *et al*., 2000, Shleeva *et al*., 2002, Wayne, 1994, Oliver, 2010, Wayne, 1960, Shleeva *et al*., 2004). An important point to note here is that mycobacteria do not possess the canonical genes, required for entry into spore-like dormancy, which are normally found in *Bacillus* and other spore forming organisms (Feucht *et al*., 2003). The mechanisms, which ultimately result the mycobacterial dormant form, if indeed this form exists during TB infection, are currently unknown and the search to uncover this, is the underlying hypothesis of this MSc project.

The hypothesis that LTBI is characterized by a dynamic bacterial population is rapidly gaining traction in the field since recent data on the immunology associated with LTBI supports this idea (Barry *et al*., 2009, Berry *et al*., 2010). From a microbiological perspective, it has been shown that in axenic bacterial cultures, there is a subset of organisms, which are phenotypically tolerant to antibiotic attack, these have been termed persisters (Bigger, 1944, Gefen and Balaban, 2009). The exact metabolic nature of these

cells is currently unknown however; there are a number of theories, which attempt to explain their presence in culture. The first theory, which was introduced by the researcher who originally observed these organisms, states that persisters comprise a subpopulation of dormant cells within an actively growing population (Bigger, 1944), since then a few more theories have been proposed suggesting these could either be, cells, which are defective in programmed cell death modules initiated by antibiotic treatment (Sat *et al*., 2001, Wang and Wood, 2011), cells in some protective stage in the cell cycle (Miller *et al*., 2004) or cells that have adapted rapidly to antibiotic stress (Gefen and Balaban, 2009, Bigger, 1944, Miller *et al*., 2004). Regardless of the underlying mechanism of the phenomenon, persistence provides these cells with a phenotypic advantage against antibiotics, which is not genetically transmitted. This has been confirmed by the demonstration that cultures grown from persister cells are still susceptible to attack by the same antibiotic that induced/unmasked the persister population (Bigger, 1944, Gefen and Balaban, 2009). Consequently, reactivation from LTBI may simply be a result of the immune system's inability to deal with the next wave of actively growing organisms, which spawn from the persister population.

Both these theories premise a level of communication between bacterial cells and between bacterial cells and their environment in order to inform them of possible danger, presumably allowing them to enter a state of dormancy for the ultimate survival of the population. One structure, which has been shown to possess the capacity to induce signalling pathways is the bacterial cell wall (Shah *et al*., 2008, Lee *et al*., 2012). This is evidenced by the ability of cell wall breakdown products to act as ligands for the induction of complex signalling pathways involved in the immune response and reactivation of dormant bacterial cells (Shah *et al*., 2008, Lee *et al*., 2012).

1.3 The Mycobacterial Envelope

Mtb is a gram variable organism, which shares some similarity to both gram positive and gram negative bacteria (Hett and Rubin, 2008). Genomic analysis of various sequenced mycobacterial genomes has revealed some correlation between mycobacteria and gram positive organisms. Structurally mycobacteria are more similar to gram negative organisms, mainly with respect to their cell envelope (Fu and Fu-Liu, 2002). The mycobacterial cell envelope consists of multiple, complex layers, which include a capsule like layer, a mycolic acid-arabinogalactan-peptidoglycan (PG) layer (cell wall layer) and the cell membrane, Figure 1.2, unlike the conventional two-layer gram positive cell envelope (Hett and Rubin, 2008, Vollmer *et al*., 2008).

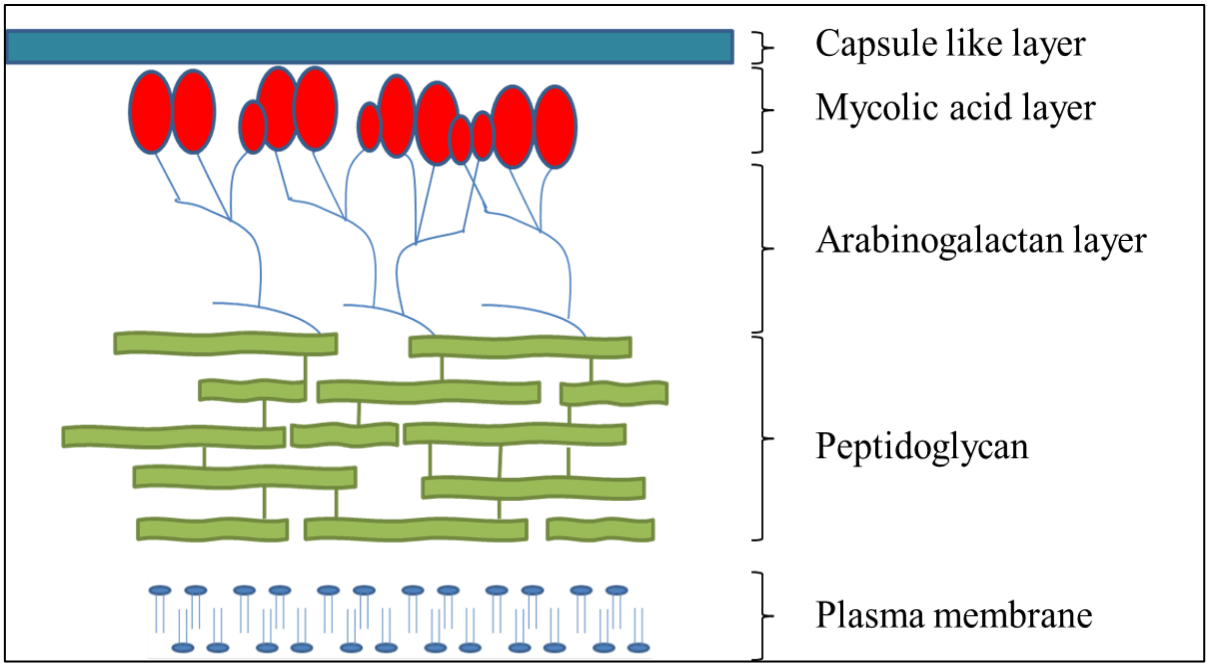


Figure 1.2: Diagrammatic representation of the structure of mycobacterial cell envelope. Blue circles represent cell membrane phospholipid bilayer, green rectangles represent PG, green lines are the cross-links between PG, blue lines are arabinogalactan, red circles represent mycolic acids. (Adapted from Hett and Rubin, 2008)

The outer most layer of the mycobacterial cell envelope, the capsule, is a non-covalently attached layer consisting of a conglomerate of lipids, polysaccharides and proteins (Daffe and Etienne, 1999, Alderwick *et al*., 2007, Mishra *et al*., 2011, Lee *et al*., 2012, Niederweis

et al., 2010). The polysaccharide constituent consists mainly of 3 major saccharides, which are glucan, mannan and arabinomannan saccharides, there is also a range of various sugars, which have not been characterized as yet (Daffe and Etienne, 1999). The glucan saccharides are structurally similar to glycogen however, they are 1000-fold smaller. The mannan constituents are made up of small branched mannose chains and the arabinomannan is a hetero-polysaccharide, which consists of a mannan component identical to the capsule mannan and an arabinan component consisting of arabinose and galactan (Daffe and Etienne, 1999, Mishra *et al*., 2011, Geurtsen *et al*., 2009).

The lipid component of the cell envelope is made up of a range of lipids including lipopolysaccharides (which are a group of highly bioactive lipids thought to be involved in modulating the host immune responses), phospholipids, lipooligosaccharides, trehalose dimycolates (which have been associated to the cording phenotype of mycobacterial colonies) and several other lipids (Daffe and Etienne, 1999, Lee *et al*., 2012, Neyrolles and Guilhot, 2011). The protein component consists of a wide range of exported enzymes involved in the catalysis of diverse substrates. This includes a variety of proteins ranging from the β-lactamase, involved in β-lactam antibiotic degradation, to superoxide dismutase, involved in the detoxification of reactive oxygen intermediates (Daffe and Etienne, 1999, Niederweis *et al*., 2010).

The second layer of the cell wall is made up 3 distinct components, which are covalently linked; these are mycolic acids, arabinogalactan and the PG components. The mycolic acid layer comprises a variety of short α-alkyl and long β-hydroxyl fatty acid chains consisting of 60 to 90 carbons per chains (Besra and Brennan, 1997). These chains form tetramycolyl-penta-arabinofuranosyl clusters, which are covalently attached to the arabinogalactan layer

by way of an ester bond and have been shown to also associate with capsule lipids and protein components of the cell wall (Besra and Brennan, 1997, Hett and Rubin, 2008). Due to their hydrophobic nature, the mycolic acids are postulated to play a central role in the inherent reduced permeability to small molecules, which is characteristic of mycobacteria (Besra and Brennan, 1997, Hett and Rubin, 2008). Furthermore, mycolic acids have also been linked to the reduction of host inflammatory responses induced by Mtb infection (Rao *et al*., 2005, Hett and Rubin, 2008). The next component is the arabinogalactan layer, which is covalently attached to both the mycolic acid and PG layers. The arabinogalactan consists of branched polysaccharide chains consisting of arabinan and galactan polymers (Daffe *et al*., 1990). The galactan polymers consists of approximately 30 galactose residues, which are linked in an alternate 1-5, 1-6 conformation. The arabinan polymers are linked at the 5^{th} position to form branches (Daffe *et al*., 1990, McNeil *et al*., 1990). The arabinogalactan layer contributes to the maintenance of cell envelope integrity and also plays an important role in modulating cell permeability by serving as an anchor for the impermeable mycolic acid layer (Hett and Rubin, 2008). The third component of the cell wall layer is the PG layer. PG is a protective structure, which consists of long glycan chains linked via peptide stems. The PG layer will be discussed in further detail later.

The complexity of the cell envelope makes Mtb naturally resistant to many antibiotics (Rastogi *et al*., 1981, Hett and Rubin, 2008). The cell envelope also plays a role in the establishment of Mtb infection in the host by providing inherent protection from harmful host derived elements such as enzymes and bacteriocidal peptides (Daffe and Etienne, 1999). The cell wall has further been implicated in the development of lung granolomas, which play a vital role in Mtb infection. This is evidenced by the demonstration that trehalose 6,6'- dimycolates, which are found on the inner coat of the capsule like layer, are

released during initial degradation of Mtb during early stages of infection and have been linked to granuloma induction (Daffe and Etienne, 1999, Rastogi and David, 1988, Lee *et al*., 2012).

The critical role that the cell wall plays in Mtb infection underscores the need to develop new drugs that target cell wall biogenesis and/or remodelling (Boshoff and Barry, 2006). In this regard, the mycobacterial PG represents a rich area for drug discovery

1.4 PG

PG or murein is a rigid structure surrounding the cell, which is involved in a number of cellular processes, most importantly, maintenance of cell shape and size (Hett and Rubin, 2008). PG plays a role in a number of other cellular functions including, cell growth, division, cell to cell signalling, resistance to environmental pressures and maintenance of osmotic pressure (Hett and Rubin, 2008). It consists of glycan strands composed of alternating *N*-acetylglucosamine (NAG) and *N*-acetylmuramic acid (NAM) carbohydrate residues (Hett and Rubin, 2008, Vollmer *et al*., 2008). These glycan strands are cross linked by stem peptides, which are attached to the NAM residues, Figure 1.3, (Vollmer *et al*., 2008, Hett and Rubin, 2008).

PG biosynthesis is a multistep process, which involves a range of enzymes located either in the cytoplasmic or periplasmic compartments of the cell. PG precursors are produced in the cytoplasm and transported to the periplasm for incorporation into the growing PG layer (Hett and Rubin, 2008). Synthesis, shown in Figure 1.4, begins with a NAG residue, which is first linked to a uridine diphospate (UDP) to form UDP-NAG (Bouhss *et al*., 2008). The NAG residue is then converted to NAM by linking enoyl pyruvate at the NAG C_5 position

(Bouhss *et al*., 2008). The stem peptide is then attached to the NAM residue sequentially, beginning with the L-alanine then D-glutamine, diaminopimelic acid (DAP) and finally the two terminal D-alanine residues are attached simultaneously (Bouhss *et al*., 2008). The UDP is removed (to form Lipid I) and UDP-NAG is then linked to the NAM residue and this compound, referred to as Lipid II, is transported to the plasma membrane where it is translocated to the periplasm with the possible aid of a flippase (Mahapatra *et al*., 2005, Bouhss *et al*., 2008, Ehlert and Holtje, 1996). The lipid II compound is then incorporated into the PG where stem peptide crosslinking occurs (Vollmer *et al*., 2008), Figure 1.4.

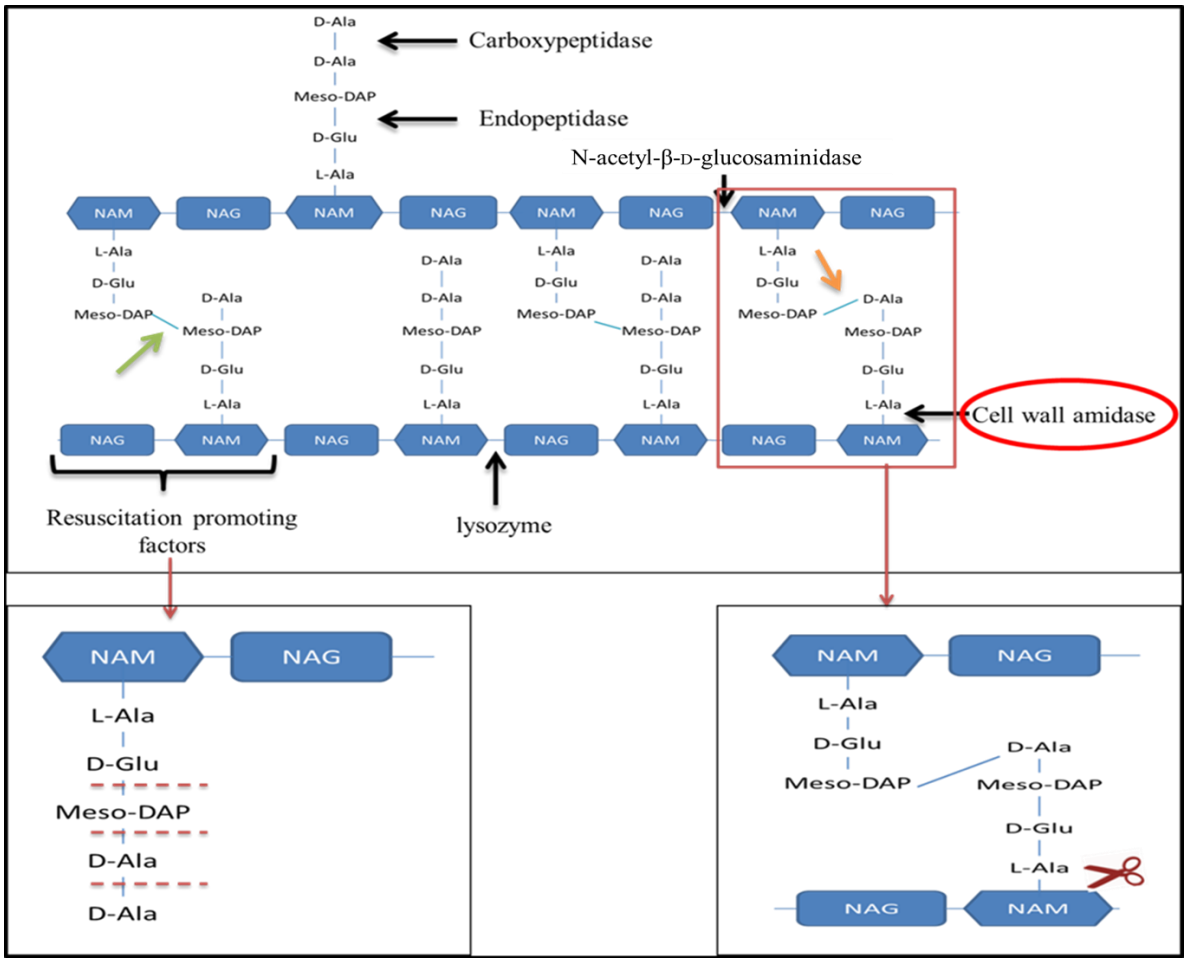


Figure 1.3: Representation of the structure of PG and cleavage sites for various PG associated hydrolases. The diagram also shows the predicted cleavage points of the resuscitation promoting factors and lysozyme. Red scissors indicate *N*-acetylmuramyl-L-alanine amidases (cell wall amidases) hydrolysis site, red dotted line indicates various stem peptide lengths found on muropeptides. Green arrow indicates 3' - 3' crosslink and the orange arrow indicates 3' – 4' crosslink (adapted from Vollmer *et al*., 2008 and Kana *et al*., 2009).

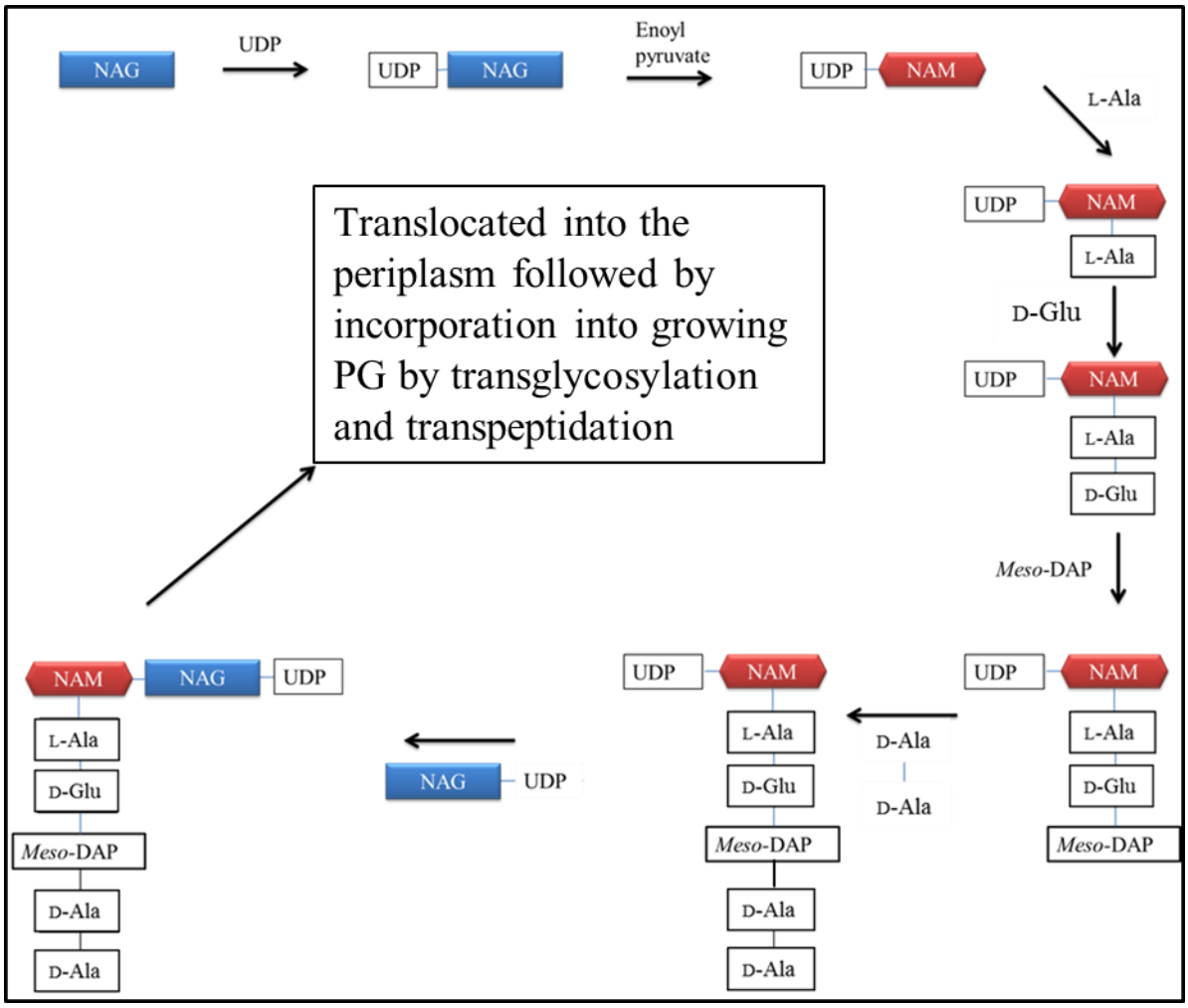


Figure 1.4: Diagrammatic representation of the PG biosynthetic pathway. The pathway begins with initiation of PG synthesis by association of UDP with NAG and ends with the incorporation of the PG precursor into pre-existing bacterial PG.

1.4.1 Antibiotics that target PG synthesis

1.4.1.1 *β-lactam antibiotics*

β-lactams are a class of antibiotics, which inhibit PG synthesis by preventing stem peptide crosslinking (Waxman and Strominger, 1983). These drugs contain a β-lactam ring, which is structurally similar to the terminal D-alanine dimer in the pentapeptide of newly synthesized PG (Waxman and Strominger, 1983). Consequently, molecules belonging to this class of antibiotics bind the D, D-transpeptidases (Penicillin Binding Proteins – PBPs), which are responsible for stem peptide crosslinking, this ultimately inhibits the subsequent formation of crosslinks between the 4th D-alanine residue and adjacent *meso*-DAP residue,

Figure 1.4, (Waxman and Strominger, 1983, Hett and Rubin, 2008). These antibiotics are not efficient in killing mycobacterial strains mainly due expression of a highly active mycobacterial β-lactamase, which immediately inactivates the antibiotic through cleavage of the β-lactam ring structure (Flores *et al*., 2005). One exception is a class of antibiotics called carbapenems. These are β-lactam antibiotics, which display high tolerance to β-lactamase induced degradation (Livermore and Woodford, 2000). Recently, it has been shown that a combination of meropenem (a carbapenem) and clavulanate (β-lactamase inhibitor) provides potent antitubercular activity against drug susceptible and XDR-TB (Hugonnet *et al*., 2009, Hugonnet and Blanchard, 2007).

1.4.1.2 *Cycloserine*

Cycloserine targets PG synthesis by inhibiting the activity of D-alanine racemase (Alr), which is responsible for the conversion of L-alanine to D-alanine, required for the two terminal alanine residues found on the stem peptide (Zhang, 2005). Though naturally occurring, cycloserine resistant Mtb strains are yet to be reported extensively in the clinical setting. Research into the mechanisms governing cycloserine resistance has shown that in *Mycobacterium smegmatis* (Msm), overexpression of the alanine racemase-encoding gene, *alr*, results in acquired antimicrobial resistance to cycloserine (Feng and Barletta, 2003, Caceres *et al*., 1997). In this specific case, mutation of the *alr* promoter region was predicted to be responsible for overexpression of the target gene, which led to resistance (Johnson *et al*., 2003).

1.4.1.3 *Ramoplanin*

Ramoplanin is a lipoglycopeptide antibiotic, which inhibits PG synthesis at two distinct levels. The first is inhibition of the *H*-acetylglucosaminyltransferase reaction (carried out by MurG), responsible for linking the NAG residue to the NAM–pentapeptide (Somner and Reynolds, 1990). The inhibitory effect is achieved by ramoplanin binding to Lipid I thus preventing MurG association resulting in a halt in the PG biosynthetic pathway (Somner and Reynolds, 1990). The second level is by association with lipid II, leading to inhibition of the transglycosylation reaction responsible for the integration of new PG units into the cell wall (Lo *et al*., 2000). This antibiotic possesses clinical significance mainly due to its activity against infectious gram positive bacteria, including methicillin-resistant *Staphylococcus aureus*, which cause an estimated 18000 fatalities in the United States of America annually (Schmidt *et al*., 2010). Though no naturally occurring resistant strains have been isolated, a ramoplanin resistant *S. aureus* strain has been generated *in vitro* however the genetic basis of resistance remains unknown (Schmidt *et al*., 2010).

1.4.1.4 *Vancomycin*

Vancomycin is a glycopeptide, which inhibits PG synthesis by binding to the two terminal D-alanine residues thus inhibiting crosslinking between the 4th D-alanine residue and adjacent *meso*-DAP residue (Barna and Williams, 1984). Vancomycin is generally used for the treatment of gram positive bacterial infections including methicillin-resistant *S. aureus* (Weigel *et al*., 2003). Vancomycin resistant strains have been isolated in *S. aureus* and *Enterococcus faecium*, in both cases resistance is the result of the *vanG* gene located on a multi-resistance conjugative plasmid (Weigel *et al*., 2003). VanG produces a D-alanine, D-lactate dimer, which is incorporated into the NAM-tripeptide (instead of a D-alanine, D-alanine dimer) during PG synthesis (Bugg *et al*., 1991). Incorporation of this dimer has

been shown to result in 1000-fold reduction in the binding affinity of vancomycin thus resulting in diminished potency and subsequent resistance (Weigel *et al*., 2003, Bugg *et al*., 1991).

1.5 PG hydrolases

Though rigid, the PG layer is also a highly dynamic structure, which continuously undergoes remodelling, required for cell expansion, cell signalling, insertion of new PG units, insertion of structural features such as flagella and other PG associated processes (Vollmer *et al*., 2008). Before any form of remodelling occurs, existing PG needs to be degraded to create space for the insertion of new PG units. This function is carried out by a group of enzymes called PG hydrolases. PG hydrolases are a class of enzymes, also referred to as autolysins, ubiquitously found in bacteria and have the capacity to degrade bacterial PG at various sites, Figure 1.3 (Vollmer *et al*., 2008, Hett and Rubin, 2008). PG hydrolases can be classified into six major groups namely D, D – and L, D - carboxypeptidases, endopeptidases, lysozymes, lytic transglycosylases, *N*–Acetyl-β-D-glucosaminidases and the *N*-acetylmuramyl-L-alanine amidases (Vollmer *et al*., 2008). These are discussed further below.

1.5.1 Carboxypeptidases (CPases)

CPases are a class of PG hydrolases, which are responsible for cleaving the C-terminal amino acid/s of the stem peptide, Figure 1.3. These enzymes play role in PG synthesis by removing the terminal D-alanine of the pentapeptide stem peptide thus allowing transpeptidation between the D-alanine in the 4th position and the *meso*-DAP residue of an adjacent stem peptide (Vollmer *et al*., 2008, Vollmer, 2012). These enzymes can be categorised into two main classes, which are the L, D- and D, D- CPases. D, D-CPases

hydrolyse the bond between two terminal amino acids, which are both arranged in the D steric conformation, while L, D-CPases hydrolyse the stem peptide link between the 4th D-alanine and the *meso*-DAP residue, the latter being in the L steric confirmation, Figure 1.3, (Vollmer *et al*., 2008, Vollmer, 2012).

1.5.2 Endopeptidases (EPases)

EPases play a similar role to CPases; however this class of enzymes cleaves non-terminal peptide bonds within the stem peptide, Figure 1.3. There are 2 main types of EPases, which are the PBP-4 and PBP-7 classes of EPases. The PBP-4 class consists of enzymes that function in multi-protein complexes consisting of several EPases (Vollmer *et al*., 2008). Extensive research done on this class of enzymes has suggested that they possess the capacity to interact with teichoic acids in addition to PG (Sauvage *et al*., 2008). Though the exact role of these enzymes is still unknown they have been indirectly linked to daughter cell separation and maintenance of cell morphology (Meberg *et al*., 2004, Sauvage *et al*., 2008, Vollmer, 2012). The PBP-7 class consists of membrane associated, β-lactam-sensitive EPases, which play a role in PG remodelling by cleaving the 4-3 stem peptide crosslink allowing for insertion new PG and the formation of a *meso*-DAP to *meso*-DAP crosslink, see Figure 1.3 (Vollmer *et al*., 2008, Vollmer, 2012).

1.5.3 Lysozymes

Lysozymes are a group PG hydrolysing enzymes, which cleave the 1-4 glycosidic bond between the NAM and NAG residue, Figure 1.3 (Vollmer *et al*., 2008). Lysozymes are a class of enzymes whose specific role in bacterial growth is yet to be elucidated mainly due to the redundancy of glycan degrading enzymes (Vollmer *et al*., 2008). They are, however,

predicted to play some role in septation by hydrolysing septal PG and cell expansion, by hydrolysing the glycan bond allowing for insertion of new PG (Holtje, 1996).

1.5.4 Lytic transglycosylases

Lytic transglycosylases are similar to lysozymes as they also hydrolyse the β 1-4 glycosidic bond between the NAM and NAG residues, Figure 1.3 (Vollmer *et al*., 2008). The difference between these two classes is that lytic transglycosylases further modify the NAM residue during catalysis resulting in the formation of a 1-6 anhydromuramyl ring on the NAM residue (Vollmer *et al*., 2008). The second difference is that while lysozymes are endo-lytic hydrolases cleaving within the glycan strand, lytic transglycosylases exhibit exo-lytic activity cleaving the terminal NAM residue, resulting in the production of a 1,6 anhydromuropeptide, which consists of NAG residue attached to the 1,6 anhydro NAM residue and the stem peptide (Vollmer *et al*., 2008). Another class of cell wall hydrolases, which are structurally and functionally similar to the lytic transglycosylases are resuscitation promoting factors (Keep *et al*., 2006, Vollmer *et al*., 2008, Mukamolova *et al*., 2006), which are discussed further below.

1.5.4.1 *Resuscitation promoting factors (Rpfs)*

Rpf is an enzyme, which was discovered in *Micrococcus luteus* and found to play an important role in the reactivation of dormant bacteria (Mukamolova *et al*., 1998). Mtb has five Rpf homologues (designated RpfA-E), which were shown to be dispensable for growth in vitro, but are essential for resuscitation from a dormant state in vitro and important for virulence in mice (Kana *et al*., 2008). The mechanism of Rpf-mediated growth stimulation is not fully understood but it has been proposed that Rpfs act as lytic transglycosylases and cleave the glycan component of the PG backbone (Kana and

Mizrahi, 2009, Vollmer *et al*., 2008, Keep *et al*., 2006, Mukamolova *et al*., 2006). How this catalytic activity relates to resuscitation remains a mystery. The structural differences between PG found from actively growing bacteria and stationary phase organisms (with regard to increased level of *meso*-DAP to *meso*-DAP crosslinks in stationary phase organisms, Figure 1.3) have led to the suggestion that the PG structure of dormant bacteria may be different from that of actively growing bacteria in terms of glycan subunit composition and/or peptide crosslinks (Lavollay *et al*., 2008). It has been hypothesized that Rpfs may be responsible for cleavage of these specialist bonds in PG, which prevail during dormancy resulting in the release of muropeptides as shown in Figure 1.3 (Keep *et al*., 2006). These muropeptides have been linked to the induction of signalling pathways by association with, and subsequent activation of, a eukaryotic like membrane associated Ser/Thr kinase (PknB) resulting in signalling cascade, which leads to bacterial reactivation from dormancy (Kana and Mizrahi, 2010, Vollmer *et al*., 2008, Kana and Mizrahi, 2009, Shah *et al*., 2008). Furthermore, Rpf-mediated hydrolysis of PG could result in the formation of insertion points for new PG and perhaps activate other essential signalling pathways involved in growth (Kana and Mizrahi, 2010, Kana and Mizrahi, 2009, Hett and Rubin, 2008).

1.5.5 *N*–Acetyl-β-D-glucosaminidases

N–Acetyl-β-D-glucosaminidases are a class of enzymes, which hydrolyse the glycosidic bond between the NAG and NAM residue, Figure 1.3. This class of enzymes plays a role in cell wall turnover as it releases components, which can be used for the production of new PG (Vollmer *et al*., 2008). Not much research has been done on these enzymes.

1.6 *N*-acetylmuramyl-L-alanine amidases

N-acetylmuramyl-L-alanine amidases or cell wall amidases are a group zinc metalloenzymes responsible for hydrolysing the bond between the glycan strand and stem peptide resulting in release of the stem peptide, Figure 1.3 (Heidrich *et al*., 2001, Uehara and Park, 2007, McCall *et al*., 2000). Cell wall amidases can be organized into 2 main classes determined by the type of amidase domain present in the protein, which can be either an amidase_2 or amidase_3 - type domain (Vollmer *et al*., 2008). These enzymes are found in a wide range of organism including bacteria, viruses and eukaryotic organisms.

1.6.1 Viral and eukaryotic amidases

Cell wall amidases from different organisms catalyse the same reaction but their fundamental role in various organisms differs, in some cases individual organisms encode a multiplicity of amidases, each with a discrete function. This adaptability has led to the amidase being one of the most ubiquitously distributed cell wall hydrolase in existence. The most extensively researched viral cell wall amidase is the T7 lysozyme. T7 lysozyme is an amidase_3 domain-containing viral cell wall amidase, which was found to play an essential role in T7 viral infection (Silberstein and Inouye, 1975, Cheng *et al*., 1994). The T7 lysozyme plays two distinct roles during phage infection, however none involve PG hydrolysis. The first function involves the release of bacterial host DNA from the associated membrane capsule, possibly mediated by the T7 lysozyme hydrolysis of the membrane, resulting in subsequent degradation of DNA by alternate enzymes and utilization of digested DNA in viral DNA replication (Silberstein and Inouye, 1975). Loss of the T7 lysozyme results in a reduction in viral replication and elevated bacterial survival, most likely due to reduced availability of bacterial DNA for viral replication (Silberstein and Inouye, 1975). The second function involves inhibition of T7 gene

expression during late infection (Cheng *et al*., 1994). T7 lysozyme has the ability to interact with T7 RNA polymerase (Moffatt and Studier, 1987). This interaction results in inhibition of RNA polymerase activity leading to a halt in gene transcription, this halt in transcription initiates viral DNA replication resulting in subsequent viral replication (Cheng *et al*., 1994, Moffatt and Studier, 1987).

PG recognition proteins (PGRPs) are a group of eukaryotic proteins, which form part of the innate immune response (Steiner, 2004). They regulate induction of the bacterial mediated Toll-I immune response. This regulation of immune responses is achieved by activation of the Toll-I ligand, in response to binding of PGRPs to muropeptides, resulting in the induction of the Toll-I response (Steiner, 2004). However, PGRPs can also reduce the levels of Toll-I induction by cleaving the stem peptide thus inactivating the muropeptide (Steiner, 2004, Mellroth and Steiner, 2006). This function is carried out by a cell wall amidase-like PGRP found in a variety of organisms including *Drosophila* and humans (Steiner, 2004).

1.6.2 Bacterial amidases

In bacteria, investigation of the role of these enzymes in cell growth has been extensively conducted in *E. coli*. Thus far, five PG associated amidases have been identified in *E. coli*; AmiA, AmiB, AmiC, AmiD (periplasmic) and AmpD (cytoplasmic) (Heidrich *et al*., 2001, Korsak *et al*., 2005). All five amidases hydrolyse the same substrate but their ability to hydrolyse the substrate is dependent on the conformation of PG. AmiA, AmiB, and AmiC can only hydrolyse PG in the conformation that is found in the cell wall, consisting of alternating NAG and NAM subunits bound to the stem peptide. AmpD can only hydrolyse PG in the form of anhydromuropeptides consisting of an anhydrous NAM subunit bound to

the stem peptide (Heidrich *et al*., 2001). AmiD is able hydrolyse PG regardless of substrate conformation (Korsak *et al*., 2005, Heidrich *et al*., 2001, Uehara and Park, 2007).

Research conducted by Heidrich *et al.* (2001) has significantly enhanced our understanding of the role of three periplasmic amidases, AmiA, AmiB and AmiC in *E. coli* and possibly other organisms. Their work was predominantly based on the characterisation of amidase knock-out mutants and demonstrated that a significant percentage of cells in liquid culture have a tendency of growing in chains when *amiA* or *amiC* was deleted individually. This phenotype was more pronounced in the *amiC* deletion mutant (Heidrich *et al*., 2001). The *amiB* deletion mutant did not display a similar phenotype. When double and triple mutants, defective in different combinations of the *amiA*, *amiB* and *amiC* genes were constructed, the chaining phenotype was more prominent with a greater proportion of cells growing in this chain conformation and an increase in average chain size (Heidrich *et al*., 2001). The presence of miniature cells (which form part of the chains) in amidase triple mutants was also observed, which led to the hypothesis that these amidase genes are involved in cell growth and division (Heidrich *et al*., 2001).

It has also been demonstrated that triple amidase knockouts have increased susceptibility to certain antibiotics suggesting that these enzymes may play an important role in modulating the inherent resistance to antibiotics in bacteria (Korsak *et al*., 2005). These observations led to the hypothesis that the *amiA*, *amiB* and *amiC* amidase gene products could play a role in antibiotic resistance through structural maintenance of the cell envelope by hydrolysis, which could lead to envelope remodelling (Korsak *et al*., 2005).

Further studies have led to the discovery of two proteins responsible for activating the amidase_3 domain-containing family of amidases, these are EnvC and NlpD. These are LytM containing PG degrading enzymes, which possess the ability to activate specific

amidases; EnvC activates AmiA and AmiB while NlpD activates AmiC (Uehara *et al*., 2009, Uehara *et al*., 2010). The proposed mode of activation suggests that the native conformation of the three amidases consists of a closed active site preventing PG attachment (Yang *et al*., 2012). Binding of the EnvC and NlpD accessory factors induces a conformational change, possibly through direct association with the amidases, resulting in an open active site conformation, which is then capable of binding and hydrolysing PG, Figure 1.5 (Yang *et al*., 2012).

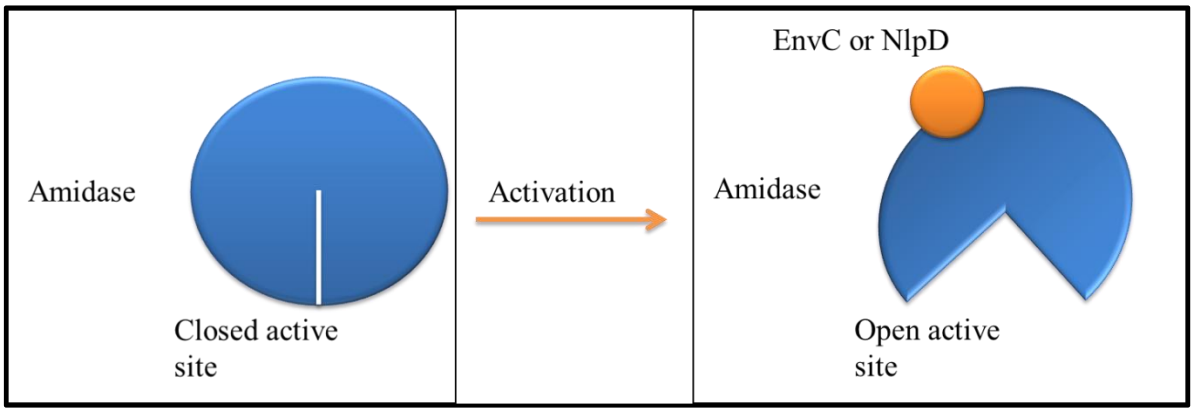


Figure 1.5: Diagrammatic representation of the proposed mechanism for EnvC and NlpD mediated amidase activation. Left shows the native form (inactive) of the cell wall amidase, which consists of a closed active site, inhibiting substrate binding. Binding of the activator results in a conformational change leading to an open active site thus allowing substrate binding and catalytic activity (Adapted from Yang *et al*., 2012)

Not much is known about the cellular role of AmiD but its catalytic activity has been researched extensively. AmiD is a periplasmic lipoprotein bound to the plasma membrane (Uehara and Park, 2007). As stated before, AmiD has the ability to hydrolyse PG and release of the stem peptide regardless of PG conformation (Uehara and Park, 2007). This flexibility in function has led to speculation that AmiD could be involved in immune evasion (Uehara and Park, 2007).

Work conducted on the innate immune response and bacterial reactivation, including germination of spores, has revealed the importance of muropeptides in the activation of these processes (Lim *et al*., 2006, Werner *et al*., 2000, Shah *et al*., 2008). Muropeptides form part of the products released from PG catalysis by the different enzymes shown in Figure 1.3. These can be in the form of muramyl dipeptides or muramyl tripeptides consisting of a NAG-NAM disaccharide linked to stem peptides of varying length, or as anhydromuropeptides, which contain a NAM residue with a 1, 6 anhydromuramoyl ring (Lim *et al*., 2006, Werner *et al*., 2000, Jacobs *et al*., 1994). Research conducted in *Drosophila melanogaster* has revealed that the minimal structural requirement for induction of PG associated innate immune response is a disaccharide muropeptide consisting of a stem peptide, which contains a minimal of 3 peptides, the third peptide being a *meso*-DAP (Werner *et al*., 2000). The same result was also observed when investigating the importance of muropeptides in germination of *B. subtilis* spores (Lim *et al*., 2006, Shah *et al*., 2008). Due to the importance of the overall structure it is speculated that AmiD may remove the stem peptide resulting in the release of molecules, which cannot be detected by the host immune system (Uehara and Park, 2007). This hydrolysis would also result in the formation of the disaccharide and stem peptide. These cannot independently induce signalling pathways involved in bacterial growth stimulation and dormant spore reactivation, thus keeping the cells in their dormant state, which could aid in the formation and maintenance of the LTBI phenomenon (Shah *et al*., 2008). Collectively, these studies demonstrate that cell wall amidases play an important role in bacterial and host signalling processes that regulate bacterial growth and/or reactivation and activation of innate immune responses respectively. In this context, we hypothesize that amidases play a similar role in Mtb infection, thus may also contribute to the reactivation from dormancy.

AmpD is the first extensively studied PG associated amidase. This is mainly due to its role in the expression of β-lactamase, which degrades β-lactam antibiotics such as penicillin, a widely used antibiotic for the treatment of bacterial infection (Jacobs *et al*., 1994). This is the only cytoplasmic PG-associated amidase identified thus far. This amidase can only hydrolyse substrates in the form of anhydromuropeptides, which have been linked to β-lactamase induction (Heidrich *et al*., 2001). It has been proposed that the hydrolysis of these muropeptides by AmpD has a negative regulatory effect on the expression of β-lactamase, and consequently a negative effect on bacterial resistance to β-lactam antibiotics (Jacobs *et al*., 1994).

Though different bacteria contain varying numbers of cell wall amidases the general role of these enzymes remains the same. Research done in *B. subtilis* also confirmed that cell wall amidases play a role in septation as seen by the formation of abnormally long chains in LytC deficient strains (Blackman *et al*., 1998, Smith *et al*., 2000). Further research in *Bacillus* also revealed additional processes wherein cell wall amidases are utilised including mother cell lysis during spore formation and formation of the δ-lactam structure in the spore cortex, indicating their importance in the formation of dormant spores (Smith *et al*., 2000, Popham *et al*., 1996). Cell wall amidases also play a role in bacteria, which are normally filamentous. In this regard, it has been demonstrated that *Cyanobacterium Anabaena* PCC 7120, a photosynthetic prokaryotic organism, requires a cell wall amidase for cell to cell communication with neighbouring cells and the ultimate formation of heterocysts from vegetative cells (Berendt *et al*., 2012). Heterocysts are nitrogenase containing cells, which are responsible for filamentous nitrogen assimilation (Berendt *et al*., 2012). These cells are morphologically different from vegetative cells to allow for protection of nitrogenases from the O_2 produced by photosynthetic cells (Berendt *et al*., 2012).

The role of amidases in bacterial growth, virulence and resuscitation from dormancy in mycobacteria has not been investigated. The impact of these amidases on mycobacterial antibiotic resistance is also unknown.

1.7 Aims and objectives

Aim

In this research, the function of putative amidase-encoding genes will be investigated in Msm, which serves as a model organism for Mtb research since it is a close relative of Mtb but easier and faster to work with and is also non-pathogenic. We hypothesize that cell wall amidases play important roles mycobacterial growth and cell division, which may be functionally redundant across the class and/or complementary with other cell wall amidases and/or other classes of cell wall hydrolases

Specific objectives

- To identify putative amidase-encoding genes in Msm and Mtb through bioinformatics analysis
- To construct knockout/knockdown mutant strains defective in putative amidase-encoding genes in Msm
- To characterise phenotypic differences between wild type and amidase mutant strains using the following phenotypic assays:
    - Growth kinetics analysis
    - Analysis of biofilm formation
    - Bacterial motility assays
    - Colony morphology analysis
    - Bacterial microscopic analysis

2. Materials and Methods

A brief summary of the project experimental layout is illustrated as a flow chart in the appendix section (Appendix E).

2.1 Bacterial strains, plasmids and growth conditions

All bacterial strains and plasmids created and/or used in this study are listed in Table 2.1 and 2.2 respectively. Glycerol stocks of each strain were prepared in media containing 6.6 % (v/v) glycerol and stored at -80 °C.

Table 2.1: Bacterial strains created and/or used in this study

Strain	**Genotype**	**Reference**
Escherichia coli DH5α	*SupE44 ΔlacU169 hsdR17 recA1 endA1 gyrA96 thi-1 relA1*	Promega, Madison, WI
mc^2155	High frequency transformation mutant of Msm ATCC 607	(Snapper *et al*., 1990)
Δ*ami1*	Derivative of mc^2155 carrying an unmarked, out-of-frame deletion in *ami1*	This study
SRS	Derivative of mc^2155 carrying pMC1s integrated at the *attB* bacterial phage attachment site, Kan^R	C. Ealand (CBTBR)
*ami2*KDP	Derivative of SRS carrying pSEAmi2P integrated in the upstream promoter region of *ami2* to allow for ATC-regulation, Kan^R, Hyg^R	This study
Δ*ami1::*pMVami1	Derivative of Δ*ami1* carrying pMVami1 integrated at the bacterial *attB* phage attachment site, Hyg^R	This study

Kan^R: Kanamycin Resistance, Hyg^R: Hygromycin Resistance

Table 2.2: Plasmids created and/or used in this study

Plasmids	**Genotype**	**Reference**
p2NIL	*E. coli* cloning vector; Kan^R	(Parish and Stoker, 2000)
pSE100	*E. coli*-Mycobacterium shuttle vector carrying P_{myc1}*tetO*; Hyg^R	(Ehrt *et al*., 2005)
pOLYG	*E. coli*-Mycobacterium shuttle vector; Hyg^R	(O'Gaora *et al*., 1997)

pMC1s	Shuttle vector carrying P_{SMYC}–*tetR*, integrates at the *attB* site on the mycobacterial genome; Kan^R	(Ehrt *et al*., 2005)
pGEM3Z(+)f	*E. coli* cloning vector; Amp^R	Promega
pGOAL19	Plasmid carrying *lacZ*, *sacB* and *hyg* genes as a *Pac*I cassette; Amp^R	(Parish and Stoker 2000)
pMV306	Complementation vector, which integrates at the *attB* site on mycobacterial genome; Kan^R	(Stover *et al*., 1991)
pMV306(H)	pMV306 derivative carrying Hyg^R marker	H. Boshoff
pGEMAmi1us	Derivative of pGEM3Z(+)f carrying 1704 bp of the upstream homologous region of *ami1*, containing 1655 bp upstream of *ami1* and 31 bp of the 3' end of *ami1*; Amp^R	This study
pGEMAmi1ds	Derivative of pGEM3Z(+)f carrying 1674 bp of the downstream homologous region of *ami1*, containing1626 bp downstream of *ami1* and 13 bp of the 3' end of *ami1*; Amp^R	This study
pGEMAmi2us	Derivative of pGEM3Z(+)f carrying 1436 bp of the upstream homologous region of *ami2*, containing 1310 bp upstream of *ami2* and 98 bp of the 3' end of *ami2*; Amp^R	This study
pGEMAmi2ds	Derivative of pGEM3Z(+)f carrying the 1316 bp of the downstream homologous region of *ami2*, containing 1216 bp downstream, of *ami2* and 72 bp of the 3' end of *ami2*; Amp^R	This study
p2NILΔAmi1	Derivative of p2NIL carrying the Δ*ami1* deletion allele, with a 751 bp internal deletion; Kan^R	This study
p2NILΔAmi2	Derivative of p2NIL carrying the Δ*ami2* deletion allele, with a 1021 bp internal deletion; Kan^R	This study
p2ΔAmi1G19	Derivative of p2NILΔAmi1 carrying the *lacZ*, *sacB* and *hyg* genes from pGOAL19; Hyg^R, Kan^R	This study
p2ΔAmi2G19	Derivative of p2NILΔAmi2 carrying the *lacZ*, *sacB* and *hyg* genes from pGOAL19; Hyg^R, Kan^R	This study
pMVAmi1	Derivative of pMV306(H) carrying a functional *ami1*gene and the upstream native promoter region; Hyg^R	This study
pSEAmi2P	Derivative of pSE100 carrying the first 350 bp region of the *ami2*gene and the *panC* ribosomal binding site; Hyg^R	This study

Kan^R: Kanamycin Resistance, Hyg^R: Hygromycin Resistance, Amp^R: Ampicillin Resistance

2.1.1 Growth of *E. coli* DH5α and derivative strains

E. coli strains were grown in Luria-Bertani broth (LB) at 37 °C with shaking at 100 rpm and supplementation of media with the appropriate antibiotic. Antibiotic concentrations

were as follows: Kanamycin (Kan) 50 µg/ml, Hygromycin (Hyg) 200 µg/ml and Ampicillin (Amp) 100 µg/ml. The strains were also grown on Luria-Bertani agar (LA) containing the abovementioned concentration of antibiotics, when appropriate, at 37 °C unless stated otherwise. *E. coli* strains containing plasmids for bulk plasmid extraction were grown in LB containing appropriate antibiotic at 37 °C shaking at 250 rpm, unless stated otherwise.

2.1.2 Growth of Msm strains

Msm strains were grown in Middlebrook 7H9 liquid media supplemented with 0.2 % glucose, 0.5 % glycerol, 0.085 % NaCl, 0.05 % Tween 80 and appropriate antibiotic at 37 °C (herein referred to as 7H9 media) with shaking at 100 rpm unless stated otherwise. Antibiotic concentrations used were as follows: Kan 25 µg/ml and Hyg 50 µg/ml. Strains were also grown on Middlebrook 7H10 solid media supplemented with 0.2 % glucose, 0.5 % glycerol, 0.085 % NaCl and appropriate antibiotics at 37 °C unless stated otherwise (herein referred to as 7H10 media).

2.2 DNA manipulation

2.2.1 Mycobacterial chromosomal DNA extraction

2.2.1.1 *Cetyltrimethylammonium bromide (CTAB) DNA extraction*

Bacterial strains were grown on 7H10 agar for 2 days and the resulting cells were harvested by scraping the surface of the agar plate and resuspending the cells in 500 µl TE buffer followed by incubation at 65 °C for 35 min. The cells were incubated at room temperature to cool down. Thereafter, a 50 µl aliquot of lysozyme (10 mg/ml) was added to the sample and incubated at 37 °C for 1 hour, subsequently 70 µl of 10 % SDS and 6 µl of proteinase K (10 mg/ml) was added and the sample was incubated at 65 °C for 2 hours.

Following incubation, 100 µl 5 M NaCl and 80 µl pre-warmed CTAB/NaCl was added, mixed and incubated at 65 °C for 10 min. An equal volume of 24:1/Chloroform:Isoamyl alcohol was added, followed by mixing and centrifugation at maximum speed for 5 min at room temperature. The aqueous layer was subsequently transferred into a clean Eppendorf tube followed by addition of 0.6 volume equivalent isopropanol and centrifugation for 20 min at room temperature. The supernatant was discarded; the pellet was washed in 70 % ethanol and dried using an Eppendorf Concentrator 5301. The DNA pellet was resuspended in 50 µl sterile distilled water (sdH_2O), quantified using NanoDrop and stored at 4 °C.

2.2.1.2 *Small scale DNA extraction for PCR*

A single colony was scraped from an agar plate and resuspend in 30 µl sdH_2O. Thereafter a 10 µl sample was spotted on 7H10 agar for a sample reference and 40 µl of chloroform was added to the remaining solution and incubated at 95 °C for 5 min. The sample was centrifuged at 16 000 × g for 5 min, the resulting aqueous layer was transferred into a fresh Eppendorf tube and 2 µl was used as template for PCR.

2.2.2 *E. coli* plasmid extraction

2.2.2.1 *Bulk plasmid preparation using Nucleobond plasmid purification kit*

Plasmid DNA preparation using the Nucleobond kit was done as per manufacturer's instructions (Macherey Nagel). Briefly, a 50 ml *E. coli* culture was grown in LB containing appropriate antibiotic at 37 °C with shaking at 250 rpm to an OD_{600nm} of 3 to 5. The culture was centrifuged at 3 900 × g for 10 min. The supernatant was discarded and the cells were resuspended in 4 ml of Buffer S1 containing RNAse A. Thereafter 4 ml of the lysis buffer, Buffer S2, was added to the sample and mixed gently by inverting 8 to 10 times followed

by incubation at room temperature for 3 min. Following incubation, 4 ml of Buffer S3 was added to the sample, which was then mixed gently by inverting the tube 10 times. The sample was placed on ice for 5 min and thereafter centrifuged at 3 900 × g for 25 min. During the 25 min centrifugation stage, a new Nucleobond AX100 column was equilibrated by adding 2.5 ml Buffer N2 and allowing the buffer to flow through by gravity. After centrifugation, the supernatant was decanted into the column and allowed to flow through. Thereafter, the column was washed with 10 ml Buffer N3. The DNA was eluted by addition of 5 ml Buffer N5, the flow-through was collected in a sterile tube. The DNA was precipitated by adding 3.5 ml of isopropanol into the tube, followed by centrifugation at 16 000 × g at 4 °C for 30 min. The resulting supernatant was discarded and the pellet was washed with 70 % ethanol. Thereafter the pellet was dried, resuspended in 50 µl sdH_2O and quantified using the NanoDrop.

2.2.2.2 *Plasmid miniprep using alkaline lysis method*

A single colony was grown in 2 ml LB containing appropriate antibiotic at 37 °C. A 10 µl sample was spotted on LA containing appropriate antibiotics for reference. The remaining culture was centrifuged 9 300 × g and resuspended in 100 µl cold solution I. Thereafter 200 µl of room temperature solution II was added to the sample, which was mixed by inverting 10 times and placed on ice for 5 min. Following incubation, 150 µl of cold solution III was added and the sample was placed on ice for a further 10 min. The sample was centrifuged at room temperature for 10 min and the supernatant was transferred to a clean Eppendorf tube. A 300 µl aliquot of isopropanol was added, and the mixture was centrifuged at room temperature for 20 min. The supernatant was discarded; the pellet washed with 70 % ethanol and dried using an Eppendorf Concentrator 5301. The DNA

pellet was then resuspended in 10 µl sdH_2O and used for restriction endonuclease reactions.

2.2.3 Sodium acetate DNA precipitation

A one-tenth volume equivalent of 3 M sodium acetate, pH 5.2, and 2.5 volume equivalent of cold 100 % ethanol was added to the DNA solution. The sample was mixed and incubated at -20 °C for 20 min. Thereafter the sample was centrifuged at room temperature for 20 min, the supernatant was discarded and the pellet washed in 70 % ethanol. The pellet was dried using the Eppendorf Concentrator 5301 and resuspend in 50 µl sdH_2O.

2.2.4 DNA restriction enzyme digestion

Restriction digests were carried out using Roche (Roche Applied Sciences), NEB (New England Biolab) and Fermentas (Fermentas) enzymes and reactions were set up as per manufacturer's instructions. Briefly, 20 µl restriction enzyme reactions containing 1 × appropriate restriction buffer, 1 µg DNA, 1 U restriction enzyme and sdH_2O were set up in an Eppendorf tube and incubated at the appropriate temperature for 1 hour. Bovine serum albumin (BSA) was added to the reaction when necessary to a final concentration of 10 µg/ml. The reaction was heat inactivated at 65 ºC for 10 min unless advised differently by supplier.

2.2.5 Phosphorylation of DNA

Phosphorylation of PCR products was carried out using Polynucleotide kinase (PNK) (Roche Applied Sciences) in 20 µl reactions containing 1 × PNK buffer, 1 µg of PCR product, 1 U of PNK and sdH_2O. This was incubated at 37 ºC for 30 min and then heat inactivated at 65 ºC for 20 min.

2.2.6 Dephosphorylation of 5'ends of plasmid DNA

Dephosphorylation of 5' ends was carried out using Antarctic Alkaline Phosphotase (AAP) (Roche Applied Sciences) in 20 µl reactions containing 1 × AAP buffer, 1 µg of digested DNA, 1 U of AAP and sdH_2O. This reaction was incubated at 37 ºC for 1 hour, then heat inactivated at 65 ºC for 20 min.

2.2.7 DNA ligation

All ligations were carried out using the Fermentas T4 Ligase (Fermentas). For optimal ligation conditions a molar ratio of 1:1 vector: insert was used in all reactions. A constant amount of vector, 50 ηg, was used for all ligation reactions and the insert mass required to make up a molar ratio of 1:1 was calculated using the following equation:

$$\text{Amount of insert } \eta\text{g} = \frac{\text{Amount of vector } \ 50\ \eta\text{g} \ \times \text{Size of insert (bp)}}{\text{Size of vector (bp)}}$$

Ligation reactions were set up in 20 µl volumes containing 1 × ligation buffer, 50 ηg vector DNA, 1 molar equivalent insert DNA, 5 U T4 ligase and sdH_2O, which were incubated at 22 ºC for 10 min. In the case of blunt end ligations the reaction was supplemented with one-tenth volume PEG4000 and incubated at 22 ºC for 1 hour. T4 ligase was then heat inactivated at 75 ºC for 10 min.

2.2.8 Agarose gel electrophoresis

DNA was run on agarose gels containing 0.5 µg/ml ethidium bromide. Separation of high molecular weight DNA was accomplished by using 0.8 – 1 % agarose gels made in 1 × TAE buffer (40 mM Tris-acetate, 1 mM EDTA) and low molecular weight DNA separation was accomplished by using 2 % agarose gels. Electrophoresis was conducted in 1 × TAE buffer at 80 – 100 V in electrophoresis tanks (Bio-Rab laboratories). In all cases,

DNA molecular weight markers for size determination were run on the same gel. Gels were visualized using a G:Box SYNGENE system in conjunction with the GeneSnap image acquisition software (Syngene).

2.2.9 Purification of DNA fragments

Fragment purification was carried out for either PCR products or DNA restriction products for use in subsequent DNA manipulation/cloning steps. In both cases, purification was conducted using the Nucleospin PCR and Gel purification Kit (Macherey-Nagel) as per manufacturer's instructions. In the case of PCR products, a small sample was run on a gel to make sure the desired product was amplified. Thereafter, a 2 volume equivalent of binding Buffer was added to the remaining product, which was loaded on the provided column and spun at 11 000 × g for 30 s. The flow-through was discarded, 700 µl wash buffer was added and spun at 11 000 × g for 2 min. The DNA was eluted by adding 50 µl dH_2O to the column and centrifuging at 11000 × g for 1 min. The DNA was quantified using the NanoDrop. In the case of gel extractions, the desired fragment was excised from the gel and melted in binding buffer at 42 ºC. The product was then loaded on the column provided and purified as per PCR products.

2.2.10 Nucleic acid quantification

All DNA and RNA was quantified using the NanoDrop ND-1000 Spectrophotometer (NanoDrop Technologies) used in conjunction with software provided by the manufacturer (Coleman Technologies).

2.2.11 DNA Sequencing

Sequencing, which was outsourced to the DNA Sequencing Facility of Stellenbosch University, was performed using the Big Dye terminator v3.1 Cycle Sequencing kit and Bioline Half Dye Mix. Finch TV version 1.4 and the Seqman module of the Lasergene suite software were used to analyse the sequencing data.

2.3 Standard Polymerase chain Reaction (PCR)

Screening for clones/knockout mutants and optimization of PCR parameters for all primers was conducted using the Roche Fast-Start kit (Roche Applied Science). Amplification of products for cloning was done using the Phusion High-Fidelity DNA polymerase (Finnzymes), which retains DNA proofreading capacity to ensure that no inadvertent second-site mutations were introduced into the resulting PCR products. Primer design was carried out using the Primer3 online tool (http://frodo.wi.mit.edu/) using the following parameters:

Table 2.3: Primer3 parameters used when designing primers using the Primer3 tool

	Size (bp)	**Tm (**ºC)	**% GC**
Minimum	18	55	55
Maximum	22	65	65
Optimum	20	60	62

2.3.1 Roche Fast-Start Taq PCR

PCR reactions were set up in a 50 µl volume each containing 1 × PCR buffer, 2 mM $MgCl_2$, 0.2 mM dNTP, 0.5 mM forward and reverse primers, 1 × GC rich buffer, 50 ηg

DNA template, 2 U of Taq polymerase and sdH_2O in 200 µl PCR tubes. These reactions were incubated in a thermo cycler using the following parameters: enzyme activation at 95 ºC for 4 min, then 35 cycles of denaturation at 95 ºC for 30 s, annealing temperature, which was dependent on the specific primer set for 30 s and elongation at 72 ºC for a time period dependent on the length of the desired product (Fast start Taq amplifies 1 Kb/min), then final elongation at 72 ºC for 10 min.

2.3.2 Phusion High-Fidelity DNA polymerase

PCR reactions were set up in 20 µl or 50 µl volumes containing 1 × GC buffer, 0.2 mM dNTP, 0.5 mM forward and reverse primers, 3 % DMSO, 50 ηg template, 1 U Phusion polymerase and sdH_2O in 200 µl PCR tubes. The reactions were incubated in a thermo cycler using the following parameters: enzyme activation at 98 ºC for 30 s, then 35 cycles of denaturation at 98 ºC for 10 s, annealing temperature, which was dependent on the specific primer set for 30 s and elongation at 72 ºC for a time period dependent on the length of the desired product (Phusion polymerase amplifies at 1 Kb/30 s), followed by a final elongation stage of 72 ºC for 10 min.

2.4 Transformation of bacterial cells

2.4.1 Transformation of chemically competent DH5α

Chemically competent cells were prepared using rubidium chloride. For this, 1 ml of a stationary phase overnight *E. coli* culture was inoculated in 100 ml LB broth and grown to an optical density $(OD)_{600nm}$ of between 0.48 - 0.55. The cells were placed on ice for 15 min and centrifuged at 3 900 × g for 5 min at 4 °C to harvest cells. The pellet was then resuspended in 20 ml TfbI solution (30 mM potassium acetate, 100 mM rubidium chloride, 10 mM calcium chloride, 50 mM manganese chloride, and 15 % v/v glycerol - pH 5.8),

and placed on ice for 15 min. The cells were then centrifuged at 3 900 × g for 5 min at 4 °C, resuspended in 2 ml TfbII solution (10 mM MOPS, 75 mM calcium chloride, 10 mM rubidium chloride and 15 % v/v glycerol-pH 6.5), 500 µl aliquots were flash-frozen in ethanol and stored at -80 °C until further use.

For transformations, *E. coli* DH5α competent cells were thawed on ice and 100 µl of the cell suspension was used per transformation. Up to 1 µg plasmid DNA was incubated with the cells on ice for 20 min, heat-shocked for 90 s at 42 °C and placed on ice for 2 min. Thereafter, 750 µl of 2 × TY was added to rescue the cells followed by incubation at 37 °C for 1 hour. The cells were plated on LA media containing the appropriate antibiotics, and incubated for 1 - 2 days at 37 °C with the exception of larger plasmids (>8 Kb), which were incubated at 30 ºC for 2 days.

2.4.2 Electroporation into Msm

Msm was grown to an OD_{600nm} of 0.6 - 0.8 in a final volume of 100 ml 7H9 media, using a stationary phase preculture as an inoculum. The cells were harvested at 2 630 × g for 10 min at 4 °C and the pellet washed 4 times by gentle resuspension in successive steps of 45 ml, 20 ml, 10 ml and 5 ml of ice-cold 10 % glycerol followed by centrifugation at 2 630 × g for 10 min at 4 °C. The final cell pellet was resuspended in 2 ml ice-cold 10 % glycerol and these competent cells were used immediately. Up to 5 µg plasmid DNA was added to a 400 µl aliquot of Msm competent cells. This was transferred to a 0.2 cm electroporation cuvette (Bio-Rad laboratories) and pulsed using the following conditions: 2.5 kV, 25 µF and 1000 Ω using the Gene PulserX cell (Bio-Rad Laboratories). The cells were rescued immediately with 800 µl 2 × TY for at least 3 hours at 37 °C and thereafter

plated on Middlebrook 7H10 media containing the appropriate supplements and antibiotics, followed by incubation for 3 - 7 days at 37 °C before scoring CFUs.

2.5 Southern Blotting

2.5.1 Labelling of Probe DNA

Alkali-labile digoxigenin (DIG)-dUTP probes were constructed using a commercially available kit (PCR DIG Probe Synthesis Kit -Roche Applied Sciences) by PCR as per manufacturer's instructions. Briefly two 50 µl reactions (labelled and unlabelled) were set up containing 1 × PCR buffer, 1 mM forward and reverse primer and 0.75 µl enzyme mix. The labelling reaction was supplemented with 5 µl PCR DIG labelling mix while the negative control was supplemented with 5 µl of a dNTP stock solution. The PCR amplification conditions were first optimized using Roche Fast-start Taq to ensure that a single, pure product was produced during the labelling reaction. The DIG-labelled and unlabelled reactions were run on the same agarose gel to confirm labelling since incorporation of the DIG label results in a molecular weight shift on agarose gels.

2.5.2 Blotting

For restriction digests, 2 µg of chromosomal DNA was digested with 5 U of selected enzyme overnight. DNA was then separated on 0.8 % agarose gel with either Lambda pUC mix 4 Marker (Fermentas) or Roche marker IV (Roche) at 80 V for 2 to 3 hours. After photographing of the gel, using the G-Box SYNGENE system, the DNA was depurinated by soaking the gel in 0.2 M HCl for 15 min with gentle shaking. The depurination solution was then removed and the gel was washed with 1 × TBE buffer followed by soaking in a solution of 0.5 M NaOH and 1.5 M NaCl for 30 min to denature the DNA. The gel was then washed in 1 × TBE, overlaid with Hybond™ -N nitrocellulose membrane,

sandwiched between 4 Whitman filter papers and 2 sponges, and pre-soaked in 1 × TBE (89 mM Tris-Borate, 2 mM EDTA, pH 8.3). The sandwich was carefully placed in a gel cassette (Bio-Rad Laboratories) and transferred to an SB10 tank (Bio-Rad Laboratories) containing 1 × TBE. DNA was transferred to the nitrocellulose membrane at 600 mA for 2 hours. The DNA was cross-linked to the nitrocellulose membrane by UV irradiation twice, at 2500 mJ/cm^3 in a UV Stratalinker 1800 (Stratagene). The membrane was incubated in 10 ml of DIG-EASY-HYB solution for 30 min at 42 ºC. The DIG labelled probe was added to the hybridization solution and incubated at 42 ºC overnight. The DIG-EASY-HYB and probe mixture was decanted into a 50 ml Falcon tube and stored at -20 ºC for future use. The membrane was washed with a solution containing 2 × SSC (300 mM NaCl, 30 mM Sodium citrate) and 0.1 % SDS for 5 min at room temperature. This was followed by two washes in a solution containing 0.5 × SSC and 0.1 % SDS for 15 min at 68 ºC. The membrane was rinsed in wash buffer (0.1 M maleic acid buffer and 0.3 % Tween 20) for 5 min at room temperature and incubated in 1 × blocking solution (made by diluting 10 × blocking solution – Roche Applied Sciences - in 0.1 M maleic acid buffer) for 30 min. Thereafter, the membrane was incubated in 20 ml of antibody solution (20 ml 1 × blocking solution and 2 µl Anti-Digoxigenin-AP [Roche Applied Sciences]) for 30 min, followed by rinsing twice for 15 min in wash buffer. The membrane was placed in a hybridization bag (Roche Diagnostics; Mannheim, Germany) DNA side facing up and 1 ml chloro-5-substituted adamantyl-1, 2-dioxetane phosphate (CSPD) substrate was aliquoted on to the DNA side of the membrane and incubated at room temperature for 10 min, the excess CSPD was then removed, the hybridization bag was sealed and incubated at 37 ºC for 5 min. The membrane was exposed to X-ray film (Kodak Biomax Light or CL-Xposure™ Film-Thermo Scientific) for 10 min and the film was developed using an automated Axim developer.

2.6 Assessment of gene expression

PCR Primers for gene expression work are listed in Table 2.6. Expression primer sets for genes of interest were designed to contain a forward and reverse primer pair for amplification and a second reverse primer (RT primer) for cDNA synthesis. Expression analysis was conducted in two steps, the first being cDNA synthesis from purified RNA, using RT primers, followed by real-time amplification of cDNA.

2.6.1 RNA extraction from mycobacterial cells

RNA extraction was carried out using the Nucleospin RNA purification Kit (Macherey-Nagel) as per manufacturer's instructions. Cells were grown in Middlebrook 7H9 media containing the appropriate antibiotics to an OD_{600nm} of 0.3. The cells were harvested at 3 900 × g for 10 min at 4 ºC. Pellets were resuspended in 350 µl lysis buffer and 3.5 µl β-mercaptoethanol was added to the sample. The suspension was transferred to lysis matrix B tubes (IEPSA) and ribolysed 3 times using the FastPrep Savant FP-120 Ribolyser for 45 s (Speed = 6) and placing the tubes on ice for 2 min between each ribolysis. Lysates were transferred to violet ring containing lipid filters, supplied by the manufacturer and centrifuged at 11 000 × g for 30 s. Thereafter, 350 µl of 70 % ethanol was added to the flow-through and the solution was transferred to nucleic acid binding blue ring containing columns, centrifuged at 11 000 × g for 30 s and the flow-through was discarded. A 350 µl aliquot of Membrane desalting buffer (MBD) was added to the column, which was centrifuged at 11 000 × g for 30 s and the flow-though was discarded. A 100 µl aliquot of DNAse reaction mixture containing 10 µl of reconstituted rDNAse (reconstituted as per manufacturer's instruction) to 90 µl of Reaction buffer for rDNAse was added to the column followed by incubation at room temperature for 30 min. Thereafter the column was

washed by aliquoting 200 µl of Buffer RA2 into the membrane and centrifuging for 30 s at 11 000 × g. A second and third wash was conducted using 600 µl Buffer RA3 at 11 000 × g for 30 s, followed by 250 µl Buffer RA3 at 11 000 × g for 2 min. Following the third wash, the column was placed in a fresh Eppendorf tube, 60 µl of RNAse free water was aliquoted onto the membrane, incubated at room temperature for 10 min and RNA eluted by centrifugation at 11 000 × g for 1 min. RNA was then quantified using the NanoDrop.

2.6.2 Reverse Transcriptase PCR (RT-PCR)

RT-PCR was carried out using the Superscript III reverse transcriptase [RT] (Invitrogen). A 25 µl reaction was set up containing 1 µg of DNA free RNA and 0.2 mM reverse primer mix consisting of the s*igA* mRNA conversion primer and the *ami2* mRNA conversion primer. The *sigA* gene is a housekeeping gene, which is expressed at a consistent level throughout different growth phases and is used for normalization to standardize for differential RNA amounts isolated or used in the analysis. Primers were annealed to RNA by incubation at 94 ºC for 90 s, 65 ºC for 3 min and 57 ºC for 3 min followed by incubation on ice. The nucleic acid mix was split into two 12.5 µl aliquots, one for the RT reaction and another to serve as an RT free reaction control to confirm the absence of any contamination/residual DNA in these samples. To the RT conversion sample, the following was added: 5 µl 5 × first strand buffer, 4 µl 25 mM $MgCl_2$, 2 µl 0.1 mM Dithiotreitol, 1 µl 10 mM dNTP and 0.5 µl Superscript III reverse transcriptase (SSIII). The RT free control contained the same components, however the SSIII was substituted by sterile nuclease free water. These reactions were incubated at 50 ºC for 50 min followed by heat inactivation of the enzyme at 85 ºC for 5 min. The cDNA was then used for qPCR.

2.6.3 Quantitative real-time PCR (qPCR) amplification

qPCR amplification was conducted using the Biorad SsoFast Evergreen Supermix (Bio-Rad Laboratories). In this case, 20 µl reactions containing 10 µl supermix, 0.25 mM qPCR forward primer and the qPCR reverse primer, 2 µl template cDNA and sterile distilled nuclease free water were set up and incubated in the CFX96 Real-Time PCR detection system (Bio-Rad Laboratories) using the following parameters: enzyme activation step of 95 ºC for 30 s, followed by a ten cycle touchdown stage consisting of 3 steps; denaturation at 95 ºC for 10 s, annealing beginning at 65 ºC for 10 s and gradually decreasing by 0.5 ºC after each cycle, elongation at 72 ºC for 10 s followed by SYBR Green quantification at the end of each cycle. The touchdown was followed by a 35 cycle stage consisting of a 95 ºC denaturation step for 10 s, a 60 ºC annealing step for 10 s and a 72 ºC elongation step for 10 s followed by SYBR Green quantification at the end of each cycle. Melt curve analysis was conducted beginning at a temperature of 50 ºC then gradually increasing by 0.5 ºC every 0.05 s to 95 °C, SYBR Green quantification was conducted continuously throughout this stage. Raw data was then processed using the Biorad CFX Manager 2.1 software (Bio-Rad Laboratories).

2.7 Analysis of bacteria growth

2.7.1 Growth rate analysis

Growth rates of wild type and mutant strains were determined by conducting growth curve experiments. For this, a pre-culture was set up by inoculating either 1 ml of frozen culture or a single colony into 15 ml 7H9 containing appropriate antibiotics and incubated overnight at 37 ºC shaking at 100 rpm. The preculture was then diluted to a final OD_{600nm}

of 0.05 in 25 ml 7H9 containing appropriate antibiotic, when necessary, and incubated at 37 ºC with shaking at 100 rpm. Growth was determined by recording OD_{600nm} measurements at 3 hour intervals and data was displayed as a scatter plot.

2.7.2 Analysis of mycobacterial biofilm formation

Biofilm analysis was carried out using the protocol described by Ojha *et al*. (2008). Briefly, cells were grown to stationary phase ($OD_{600nm} > 2$). These cells were then washed in Sauton's media twice. The OD_{600nm} was recorded and adjusted to 2, then a ten-fold serial dilution of the adjusted cultures was conducted ranging from 10^0 to 10^5 and 100 µl of each dilution was inoculated into 10 ml Sauton's media. This was done to determine whether variation in the starting inoculum may result in a more dramatic phenotypic difference since the initial bacterial population size would be reduced with each dilution. The plates were incubated at 37 ºC for five days and images were taken; high magnification images were also taken using the Stemi 2000-C stereomicroscope (Zeiss). Biofilm formation in this case was defined as the formation of a pellicle on the surface of the liquid media. The CFUs were calculated by plating the serial dilutions on 7H10 solid media to determine the number of bacteria used in each experiment.

2.7.3 Analysis of mycobacterial sliding motility

Sliding motility assays were carried out using the protocol described by Martinez *et al*. (1999). Briefly, strains were streaked on 7H10 containing appropriate antibiotics and incubated at 37 ºC until single colonies could be observed. A colony was then taken and spotted on 7H9 plates (7H9 media containing 0.3 % agar with 0.5 % glycerol as carbon source) and M63 minimal media (100 mM KH_2PO_4, 15 mM $(NH_4)_2SO_4$, 1.7 µM $FeSO_4.7H_2O$, containing 0.3 % agar with 0.5 % glycerol as a carbon source) pH to 7.0 with

KOH. The plates were sealed with parafilm and incubated at 37 °C for two weeks and images were taken using the G-Box SYNGENE system

2.7.4 Bacterial spotting assay

Spotting assays were conducted to observe the morphologies of bacterial strains when grown on solid media. Cultures were grown in 7H9 containing appropriate antibiotics to an OD_{600nm} of 0.8. A ten-fold serial dilution series from 10^0– 10^6 was made and 10 µl of each dilution was spotted on 7H10 media containing appropriate antibiotic and incubated at 37 ºC.

2.8 Microscopic analysis

2.8.1 Confocal microscopy

Cells were grown in 10 ml 7H9 containing appropriate antibiotics to an OD_{600nm} equal 0.8 followed by harvesting and washing twice in PBS. Cells were then resuspended in 1 ml of 7H9 containing appropriate antibiotics. Thereafter, 0.2 µl of 5 mg/ml vancomycin and 1 µl of 1 mg/ml BODIPY-fluorescent vancomycin (Invitrogen) was added to the culture followed by incubation at 37 ºC for 1.5 hours. Following this, 2 µl of 5 mg/ml 4',6-diamidino-2-phenylindole (DAPI) (Sigma-Aldrich) and 1 µl of 500 ηg/µl Cellmask™ Orange (Invitrogen) was added to the culture and incubated at 37 °C for 20 min. Following incubation, the cells were washed twice in 7H9 and resuspended in 50 µl 7H9. 5 µl was then spread on a coverslip and allowed to dry. A drop of fluoramount (Sigma) was deposited on a slide and the cover slip was placed on the fluoramount and allowed to dry. The slides were then viewed on the Zeiss LSM-780 Confocal microscope and images processed with ZEN black Ver. 7.0 software (Zeiss).

2.8.2 Scanning electron microscopy (SEM)

For cell preparation, 50 ml cultures were grown in 7H9 containing appropriate antibiotic to an OD_{600nm} of 0.8. The cells were harvested by centrifugation, washed twice with PBS and resuspended in 2.5 % gluteraldehyde in PBS overnight at 4 °C. The cells were then washed twice with PBS and resuspended in 100 µl 2 % osmium tetraoxide in PBS and incubated at room temperature for 1 hour. Cells were then washed twice with PBS and dehydrated by submerging in a series of ethanol concentrations for 2 min at each concentration beginning with 30 % then 50 %, 70 % and twice at 100 % ethanol followed by storage in 100 % ethanol. Cells were spotted on a filter, coated twice with carbon and viewed using the FEI Nova NenoSEM 230.

2.8.3 Transmission electron microscopy (TEM)

A 50 ml culture was grown in 7H9 containing appropriate antibiotic to an OD_{600nm} equal 0.8. The cells were harvested by centrifugation and washed twice in 1 ml PBS. Cells were resuspended in fixing solution containing 0.1 mM HEPES, 2 % (v/v) formaldehyde, 2.5 % (v/v) gluteraldehyde and 0.05 % (w/v) ruthenuim red and incubated at room temperature for 1 hour. The cells were then harvested and resuspended in 100 µl of 2 % osmium tetraoxide in PBS and incubated at room temperature for one hour. The samples were then washed twice in PBS and dehydrated by submerging in a series of ethanol concentrations for two min at each concentration beginning with 30 % then 50 %, 70 % and twice at 100 % ethanol. The dehydrated samples were then washed in propylene oxide twice and incubated for one hour in a solution made up of 50 % propylene oxide and 50 % resin mixture, which consists of 5.62 g araldite, 7.75 g epon 812 and 15 g DDSA. The propylene oxide resin mixture was then removed and the cells were resuspended in 100 % resin mixture and incubated at room temperature overnight. Cells were pelleted, the resin

mixture was removed and fresh resin mixture containing DMP 30 at a ratio of 1:40 (g: g) of DMP 30 to resin mixture was added to the cells and these were incubated at 60 °C for 48 hours. The solidified resin was sectioned using a Relchert Ultracut Ultramucrotome (Circa) and viewed using a Tecnai F20 TEM.

2.8.4 Atomic force microscopy (AFM)

AFM was conducted to analyze the surface structure of individual cells. For cell preparation, 50 ml cultures were grown in 7H9 containing appropriate antibiotic to an OD_{600nm} of 0.8. These were then spread on a slide, allowed to dry and viewed using the Veeco 2000 AFM (Zeiss).

2.9 Bio-informatic analysis

Bioinformatic analysis was carried out using a number of online tools and databases. *E. coli* DNA and protein sequences were downloaded from the Biocyc *E. coli* database (http://www.biocyc.com/ecocyc/index.shtml). Msm DNA and protein sequences were downloaded from the Ecole Polytechnique Fédérale de Lausanne Smegmalist database (http://mycobrowser.epfl.ch/smegmalist.html) and Mtb DNA and protein sequences were downloaded from the Ecole Polytechnique Fédérale de Lausanne Tuberculist database (http://tuberculist.epfl.ch/). Protein and DNA sequence BLAST searches were conducted using the NCBI Blast tool (http://blast.ncbi.nlm.nih.gov/Blast.cgi), Protein domain determination was conducted using the Sanger institute pfam tool (http://pfam.sanger.ac.uk/), determination of signal peptides was conducted using the SignalP version 4.1 online tool (http://www.cbs.dtu.dk/services/SignalP/) and protein alignment was conducted using the EMBL-EBI clustalW tool (http://www.ebi.ac.uk/Tools/msa/clustalw2/) .

2.10 Construction of knock out strains

The gene deletion system used in this study was a two-step allelic exchange system, which involves the substitution of the wild type gene with a truncated/deleted, non-functional version of the gene, a process driven by homologues recombination, Figure 2.1 (Gordhan and Parish, 2001). This system takes advantage of the cell's homologues recombination machinery. It involves the amplification of the regions directly upstream and downstream of the gene of interest with a small portion of the 5' and 3' ends of the target gene. The gene fragments are then fused together to create a truncated, non-functional form of the gene of interest. This deletion allele is inserted into a suicide plasmid, which contains resistance markers to allow for selection of single-cross over recombinants. This plasmid is then inserted into wild type cells and grown in presence of antibiotic, since it cannot replicate and is required for cell survival in the presence of antibiotic (the antibiotic resistance gene is encoded on the plasmid); the construct is incorporated into the genome by homologous recombination with either the upstream or downstream region giving rise to a single-crossover (SCO) strain, Figure 2.1. This results in the presence of both the wild type and deletion alleles; hence a recombination event in the adjacent region has to occur for the allelic exchange. The second homologous recombination event is induced by using a counter selectable marker on the plasmid, the *sacB* gene, which encodes an enzyme called Levane Sucrase that converts sucrose to a toxic metabolite, resulting in the death of bacterial cells (Reyrat *et al*., 1998). Hence, by plating the SCO strain onto sucrose containing media, the second cross is facilitated and the vector is expunged, to prevent the lethality encoded by the *sacB* gene. The second crossover can occur in the same homologous region as the first crossover, resulting in the regeneration of the wild type strain, or it can occur in the opposite homologous region, resulting in the production of a mutant strain, Figure 2.1.

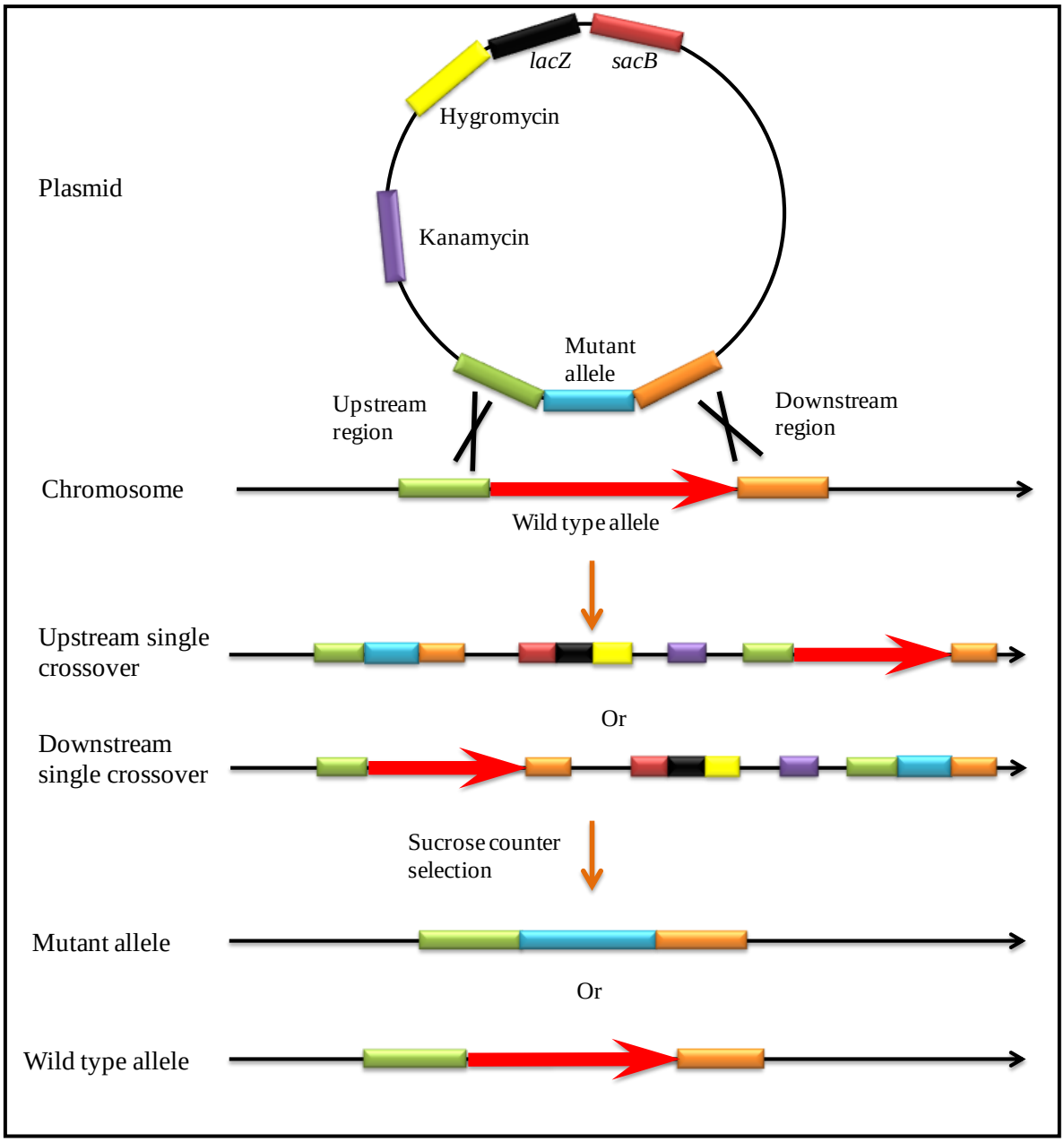


Figure 2.1: Diagrammatic representation of the allelic exchange process. Shown is the initial SCO event and the subsequent sucrose-induced second cross over resulting in the formation of either a wild type or mutant strain.

2.10.1 Construction of *ami1* and *ami2* knockout vectors

2.10.1.1 *PCR reactions*

Primers were designed using the Primer3 software to amplify the upstream and downstream regions of homology for *ami1* and *ami2* genes (Table 2.4). The *ami1* primers

amplify a 1704 bp upstream region including 31 bp of the 5' end region of the *ami1* gene and a 1674 bp downstream region including 13 bp of the 3' end region of the *ami1* gene. Fusion of these two fragments results in a truncated version containing only 5 % of the original gene. Since the deletion allele is out-of-frame, the resulting truncated allele will encode the first 10 amino acids of Ami1. The *ami2* primers amplify a 1436 bp upstream region including 98 bp of the 5' end of the *ami2* gene and a 1316 bp downstream region including 72 bp of the 3' end region of the *ami2* gene. Fusion of these two fragments results in a truncated version of the gene containing 14 % of the original gene. Since the deletion is out-of –frame, the resulting truncated allele will encode the first 32 amino acids of Ami2. We do not expect any second-site polar effects on downstream genes since neither *ami1* nor *ami2* are operonic with other downstream genes, Figure D4, appendix. The primers were tested using Roche Fast-start Taq and optimized by Phusion PCR. The upstream and downstream fragments for both genes were amplified using the optimal Phusion conditions and run on 0.8 % agarose to ensure amplification of correct fragments. The positive Phusion PCR reactions were then purified and phosphorylated using PNK.

Table 2.4: Primers used for amplification of upstream and downstream regions of the *ami1* and *ami2* genes.

Gene	Region	Primers	Amplicon properties
ami1	Upstream	GCCGCC**GGATCC**CAGGTACAGCCCGATGCT	1704 bp amplicon including 31 bp of the 5' end region of the *ami1* gene and full length MSMEG_6280 and *recR* genes
		GCCGCC**GAATTC**GCAGACAGGCTGGGACTC	
	Downstream	GCCGCC**GAATTC**TGCGTTGACCCTCGGCTA	1674 bp amplicon including 13 bp of the 3' end region of the *ami1* gene, a full length MSMEG_6282 genes and 1126 bps of MSMEG_6283
		GCCGCC**AAGCTT**CGCTGTCACGCAACCGTAG	

ami2	Upstream	GCGCGC**GGATCC**GTGTTCGAGGGCACACAGTT	1436 bp amplicon including 98 bp of the 5' end region of the *ami2* gene and full length *txr* and *txrB* genes
		GCGCGC**GAATTC**AGGTCAGTGTCGGGGTTCT	
	Downstream	GCGCGC**GAATTC**ACAGGCACTTTCACGTTCG	1316 bp amplicon including 72 bp of the 3' end region of the *ami2* gene, a full length MSMEG_6936 gene and 187 bps of MSMEG_6938
		GCGCGC**CATATG**GAACCGTGAAGGCAAGACC	

Bold: Restriction sites included to facilitate fusion of the upstream and downstream regions during cloning

2.10.1.2 *Cloning.*

The various cloning steps are shown in Figure 2.2.

2.10.1.2.1 pGEM cloning

The vector pGEM3Z(+)f was digested at the *Sma*I site located within the *lacZ* gene and dephosphorylated using AAP. Digested DNA was run on 0.8 % agarose and linear vector was excised from the gel and purified. Upstream and downstream regions were ligated separately to this vector, transformed into DH5α cells and plated on LA containing Amp and 0.004 % X-gal followed by incubation at 37 ºC overnight. Following incubation, white colonies for upstream and downstream clonings were selected, the plasmid DNA minipreped and screened by restriction digest using the following enzyme sets: (I)*Bam*HI and *Eco*RI for the upstream region of *ami1* and *ami2* (II) *Eco*RI and *Hind*III for the downstream region of *ami1* (III) and *Eco*RI and *Pst*I for the downstream region of *ami2*. These restriction digests resulted in the liberation of the cloned PCR products. A single positive clone per fragment was selected, grown up in 100 ml LB and bulk plasmid preparations were carried out on these clones. These were then digested with the same enzymes used for screening, run on agarose and the liberated insert was excised from the gel and purified.

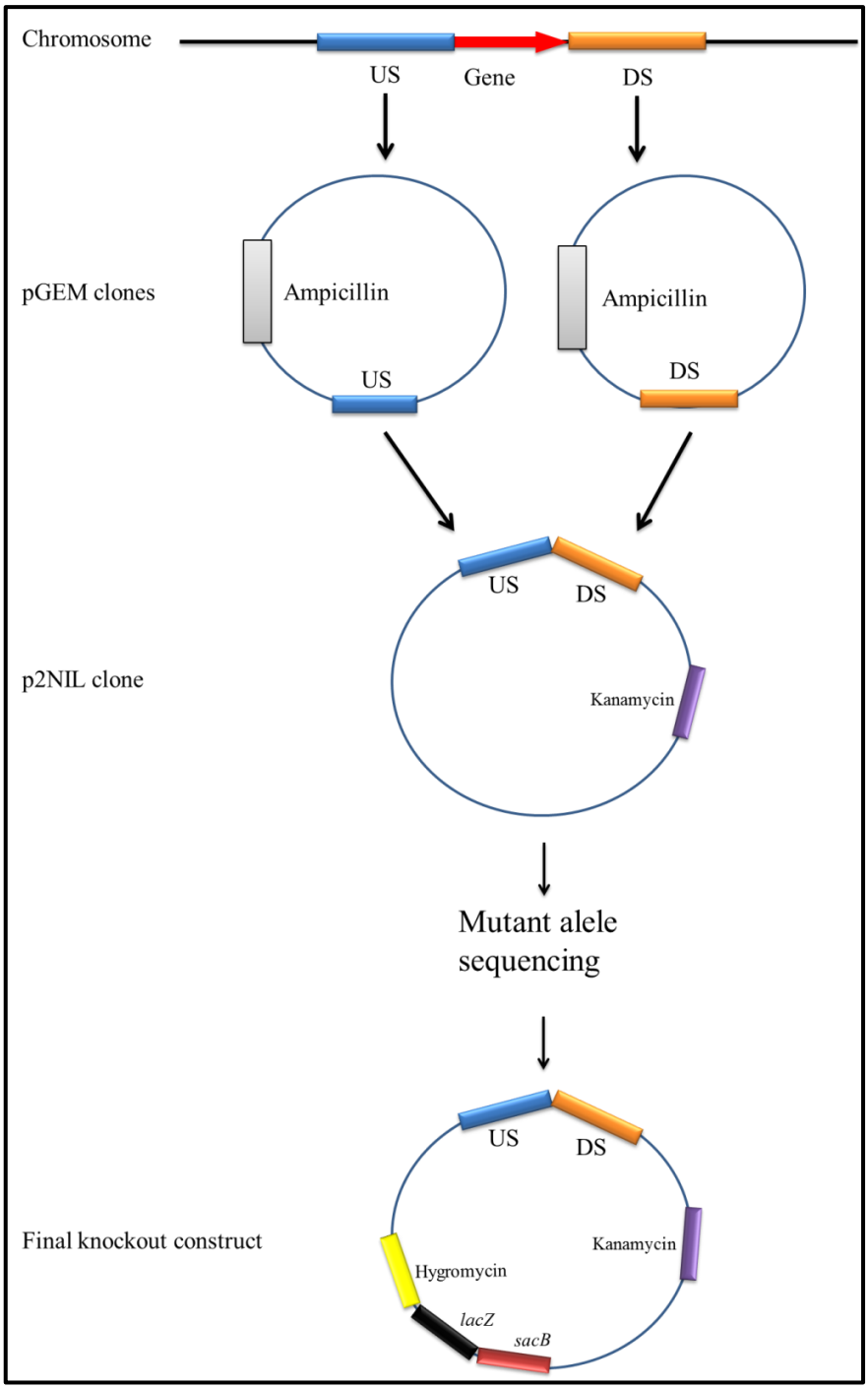


Figure 2.2: Diagrammatic representation of the construction of knockout vectors. The diagram depicts the process beginning with PCR amplification of the upstream (US) and downstream (DS) fragments followed by cloning into pGEM, p2NIL and subsequent insertion of the *Pac* cassette from pGOAL19 into the p2NIL clone.

2.10.1.2.2 Three Way cloning

The suicide vector p2NIL was restricted with *Bam*HI and *Hind*III for *ami1* cloning and

*Bam*HI and *Pst*I for *ami2* cloning, dephosphorylated and run on a 0.8 % agarose gel. The

linearized vector was excised from the gel and purified. The vector, upstream and downstream fragments were run on agarose gel to ensure that the fragments were still intact after purification and present in sufficient quantity for ligation. The upstream and downstream fragments were simultaneously ligated to the p2NIL vector in 3 way ligations using ratios of 1:1:1, 1:3:3 and 1:5:5 vector: upstream region: downstream region. These ligations were transformed into DH5α cells, plated on LA containing Kan and incubated at 30 ºC for 2 days. Colonies were then selected, the plasmid was extracted and screened for insertion by restriction digest. A single positive clone for each construct (named p2NILAmi1 and p2NILAmi2) was inoculated in 200 ml LB containing Kan and incubated at 30 °C overnight. Bulk plasmid extraction was conducted followed by extensive restriction profiling of the resulting plasmid constructs, using a range of restriction enzymes.

2.10.1.2.3 Pac cassette cloning

The plasmids pGOAL19, p2NILAmi1 and the p2NILAmi2 were digested with *Pac*I and the linearized vectors, along with the 7939 bp pGOAL19 *Pac*I cassette (containing the hygromycin resistance marker, *lacZ* and *sacB* genes), were excised from the gel and purified. The *Pac*I cassette was then ligated to the linearized p2NILAmi1 and p2NILAmi2 fragments followed by transformation into DH5α cells and plating on LA containing Kan, Hyg and 0.004 % X-gal to select for clones, which contain the kanamycin resistant marker from the p2NILAmi1 / p2NILAmi2 constructs as well as the hygromycin resistance marker and functional *lacZ* gene acquired from the *Pac*I cassette, Figure 2.2. Successful ligation between the *Pac*I cassette and p2NIL constructs was determined by the presence of blue colonies on selection plates. These transformations were incubated at 30 ºC for 2 days. Clones were selected, the plasmid was minipreped and screened by restriction digest with

*Bam*HI. A single positive clone was selected for each cloning (named p2ΔAmi1 G19 and p2ΔAmi2G19), bulk plasmid preparation was then conducted and the constructs were profiled by restriction digest with a range of enzymes to confirm the integrity of the constructs.

2.10.1.3 *Testing for acquired sucrose sensitivity*

As mentioned above, *sacB* encodes the enzyme Levane Sucrase, which degrades sucrose producing a toxic element that kills the cells, which retain the gene. The function of this enzyme is a key component in the induction of the second cross over to produce mutant strains, Figure 2.1. Thus, the activity of the *sacB* gene product, and ultimate sucrose sensitivity of bacteria carrying the knockout vector, is a critical component that requires validation before continuing with the gene knockout methodology. A spotting assay on LA containing Kan, Hyg and 0.004 % X-gal and LA containing 5 % sucrose and 0.004 % X-gal was conducted to test sucrose sensitivity in *E. coli*; the activity of Levane Sucrase would result in growth inhibition of the strain on media containing sucrose with no impact in viability on plates without sucrose.

2.10.1.4 *Two-step homologues recombination*

The p2ΔAmi1G19 and p2ΔAmi2G19 vectors were electroporated into mc^2155 cells using 1, 3 and 5 µg of DNA and plated on 7H10 containing Kan, Hyg and 0.004 % X-gal. The transformation efficiency of the electro-competent cells was determined by electroporating 1 µg of the pOLYG replicating vector and plating a serial dilution of the transformation on 7H10 supplemented with Hyg. The desired efficiency for the electroporation of mc^2155 cells is usually 10^4 CFU/µg of plasmid DNA. After electroporation, cells were plated onto solid media and incubated at 37 ºC until blue colonies emerged (SCO). A Single blue colony per construct was then cultured in 7H9 supplemented with Kan and Hyg at 37 ºC

then sub-cultured in 7H9 containing Kan and Hyg. The resulting cells were subjected to sucrose counter selection by plating 100 µl of a 10-fold serial dilution series onto media containing sucrose and X-gal. The plates were incubated for 3 - 5 days until blue and white colonies emerged. White colonies represent strains, which have undergone the second cross over event to yield either wild type again or a mutant strains and blue colonies represent and strains, which have incurred a mutation in the *sacB* to render them resistant to the toxic effects of sucrose.

2.10.1.5 *PCR Screening*

White colonies were selected and screened using a PCR method, which takes advantage of the deleted region in the truncated version of the gene. The SCO strains were also included in the PCR screen to allow differentiation between mutant strain and a SCO strain. Three primers per gene were designed, a forward primer, which binds upstream of the transcriptional start site of the target genes and two reverse primers, one, which binds downstream of the stop codon and a second, which binds within the deleted region and hence will not have a binding site in the mutant strain resulting in the amplification a fragment, which is different from the wild type fragment, Figure 2.3. The primers used are listed on Table 2.5. The PCR was run using an annealing temperature of 60 ºC and run on 2 % agarose and view using the G-Box.

2.11 Complementation of Msm Δ*ami1* strain

Genetic complementation of mutant strains is important to confirm that any phenotypic variations observed with the mutant strain is due to loss of a particular gene and not due to second-site polar effects. In this study, the complementation technique involved the use

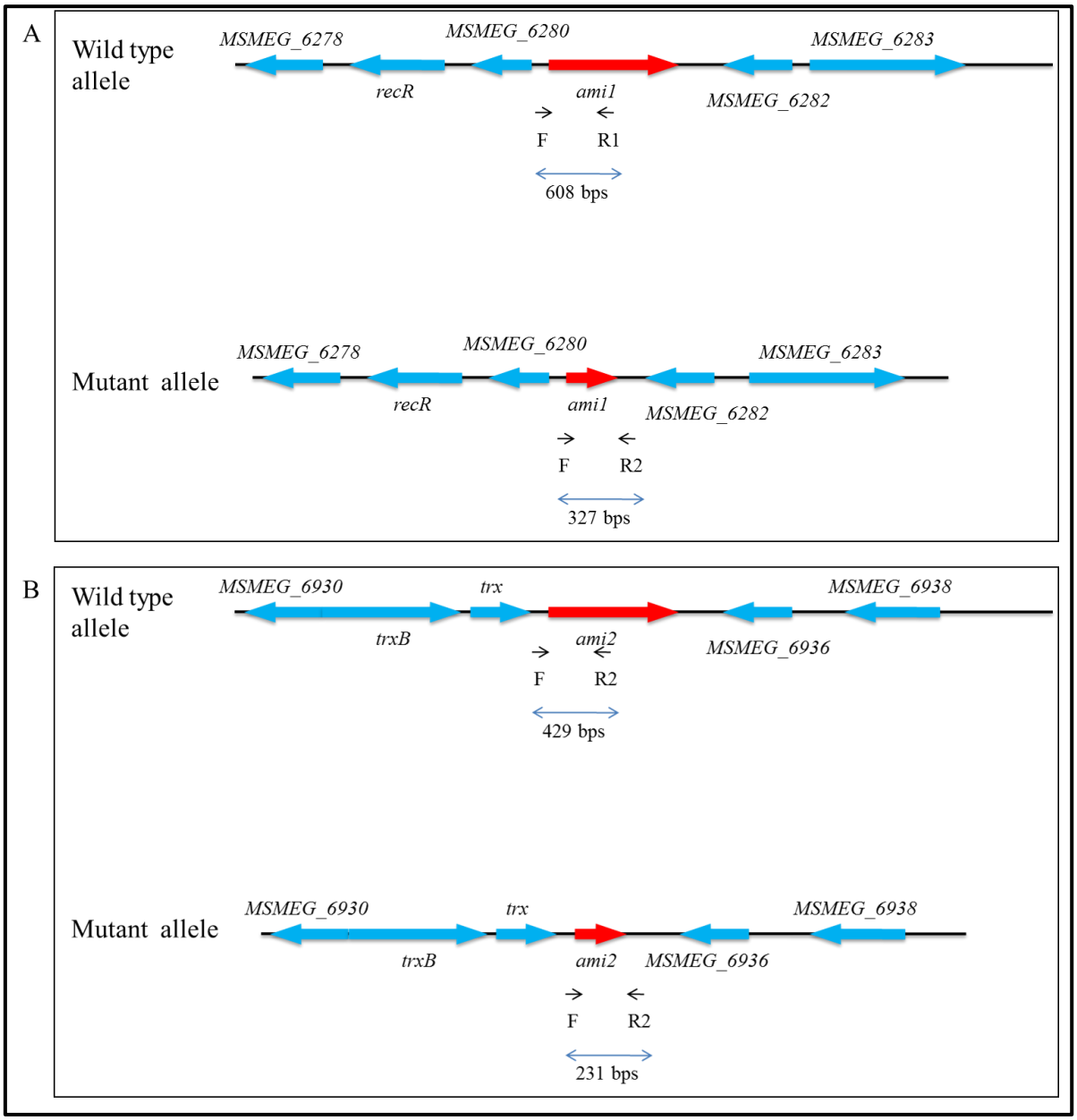


Figure 2.3: Schematic representation of the PCR screen for deletion mutants. Both reverse primers are included in the PCR reaction, resulting in amplification from the first reverse primer in strains containing the wild type allele and amplification from the second reverse primer product in strains containing the mutant allele as the binding site for the first primer is deleted. **(A)** represents the *ami1* PCR screen profiles showing both wild type and mutant alleles and **(B)** represents the *ami2* PCR screen profiles showing both wild type and mutant alleles.

Table 2.5: Double cross over screening primers

Gene	Forward	Reverse	Amplicon
ami1	TCTCGGTTGCGTCTTCTTG	R1 CGTCCCTGGTGAGCAACT	608 bp wild type *ami1* amplicon
		R2 ACGAGTACAGCACGTGGAA	327 bp Δ*ami1* amplicon
ami2	CAGGACGCGCTTGGCGTT	R1 TGCCTGTGAATTCAGGTCAG	429 bp wild type *ami2* amplicon
		R2 TGTAGAAGCCGAGGTCCTG	231 bp Δ*ami2* amplicon

of an integrating vector. Briefly, a full length functional version of *ami1*, including 400 bp of the upstream region, which encompasses the gene's native promoter region and ribosomal binding site, was cloned into an integration vector and transformed into the mutant strain. It is expected that the construct will integrate into the genome incorporating a functional gene, which will be regulated by the cell's native regulatory system.

2.11.1 Construction of the complementation vector

Primers, *ami1* comp F (GCGCGCGCGCGATATCCTGCGCCATGATCGTCACCTGCT) and the *ami1* comp R (GCGCGCGCGCGATATCGCCGAGGGTCAACGCACGGGGCT), were designed to amplify a 1203 bp DNA fragment containing the 400 bp region upstream of the *ami1* gene and the full length *ami1* gene. The PCR product was then digested with *Eco*RV, run on 0.8 % agarose gel and the 1203 bp band was excised from the gel and purified.
The plasmid, pMV306(H) was digested with *Eco*RV to linearize the vector, the 5' ends were dephosphorylated with AAP followed by running on a 0.8 % agarose gel. The linear 4271 bp vector band was excised from the gel and purified. The purified pMV306(H) fragment was ligated with the restricted *ami1* fragment using molar ratios of 1:1, 1:3 and

1:5 plasmid to insert, transformed into DH5α cells, spread on LA supplemented with Hyg and incubated at 37 °C overnight. Clones were then selected and screened by restriction digest with *Bam*HI, which would yield three bands 4507 bp, 711 bp and 262 bp (positive orientation) or 3804 bp, 965 bp and 711 bp (negative orientation) depending on the orientation of the insert in relation to the *E. coli* origin of replication (*oriE*) (data not shown). The resulting plasmid was also sent for sequencing to confirm that the cloned *ami1* region contained no mutations as a result of the Phusion PCR or subsequent cloning steps.

2.11.2 pMVAmi1 integration into Δ*ami1* strain genomic DNA

The pMVAmi1 construct was electroporated into the Msm Δ*ami1* strain. The electroporations were carried out using 1, 3 and 5 µg of DNA and a 1 µg pSE100 control was included to calculate the transformation efficiency of the electro-competent cells. The desired efficiency for the electroporation of mc^2155 cells and the derivatives thereof, in this case, is usually 10^4 CFU/µg of plasmid DNA. The pMVAmi1 transformations were plated on 7H10 supplemented with Hyg and incubated at 37 ºC for four days. Clones were selected and genomic DNA was extracted by use of colony boil and these colonies were screened for the presence of a full length *ami1* gene by conducting a PCR utilizing the primers used to amplify the *ami1* complementation fragment, as crude method of checking for plasmid retention and likely integration. The sizes expected were 1203 bp, which indicates the presence of a full length gene and approximately 418 bp indicating the truncated version of the gene. Genomic DNA from the Msm Δ*ami1* strain was also included as a negative control. The PCR products were run on 0.8 % agarose and visualized to check whether any of the clones contained the full length gene (data not shown).

A positive clone was selected and further PCR analyses were carried out to determine if the complemented vector was integrated at the correct locus. The underlying principle of this screen involved the use of 2 primers sets both consisting of a single primer, which bind plasmid DNA flanking the integration (AP) site on the plasmid and the second binding primer, which binds to genomic DNA flanking the $tRNA^{Glycine}$ locus, thus integration at the correct site will result in PCR amplification while incorrect integration will result in no amplification, Figure 3.13 A.

2.12 Construction of *ami2* knockdown strain

Targeted gene knockdown is usually used to study the function of essential genes, which cannot be deleted in vitro. The knockdown system used in this study involves the replacement of the native promoter of the gene in question with a tetracycline-regulated operator that allows for the regulation of gene expression in the presence/absence of anhydrotetracycline (ATC), outlined in Figure 2.4 (Ehrt *et al*., 2005). Briefly the tetracycline operator is fused, by PCR and cloning, to the first 350 bp of the desired gene in a non-replicating vector, which is inserted into an Msm strain that carries a plasmid, integrated at the *attB* site of the bacterial chromosome, encoding the tetracycline repressor. Insertion of the non-replicating vector carrying the ATC operator leads to a single cross over event, at the locus of interest, which results in the incorporation of the ATC operator upstream of the gene of interest, to allow for ATC regulation, and wild type promoter drives the expression of a non-functional, truncated gene, Figure 2.5.

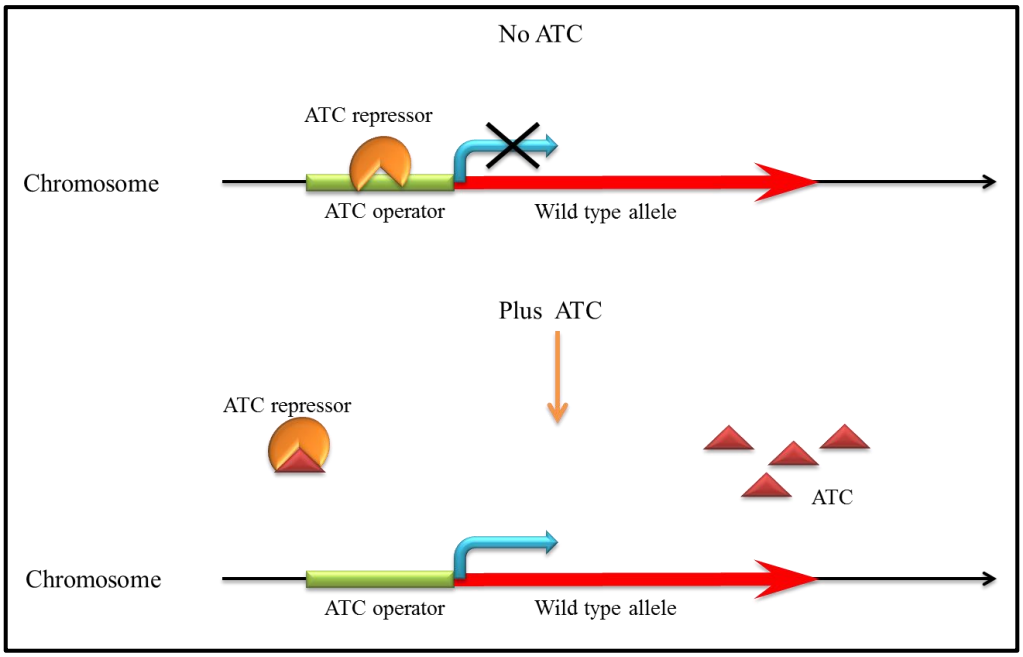


Figure 2.4: Schematic representation of the tetracycline operator knockdown system. In the absence of ATC, the ATC repressor binds the ATC operator, inhibiting gene expression. In the presence of ATC, ATC binds the repressor thus inhibiting binding to the ATC operator allowing for gene expression

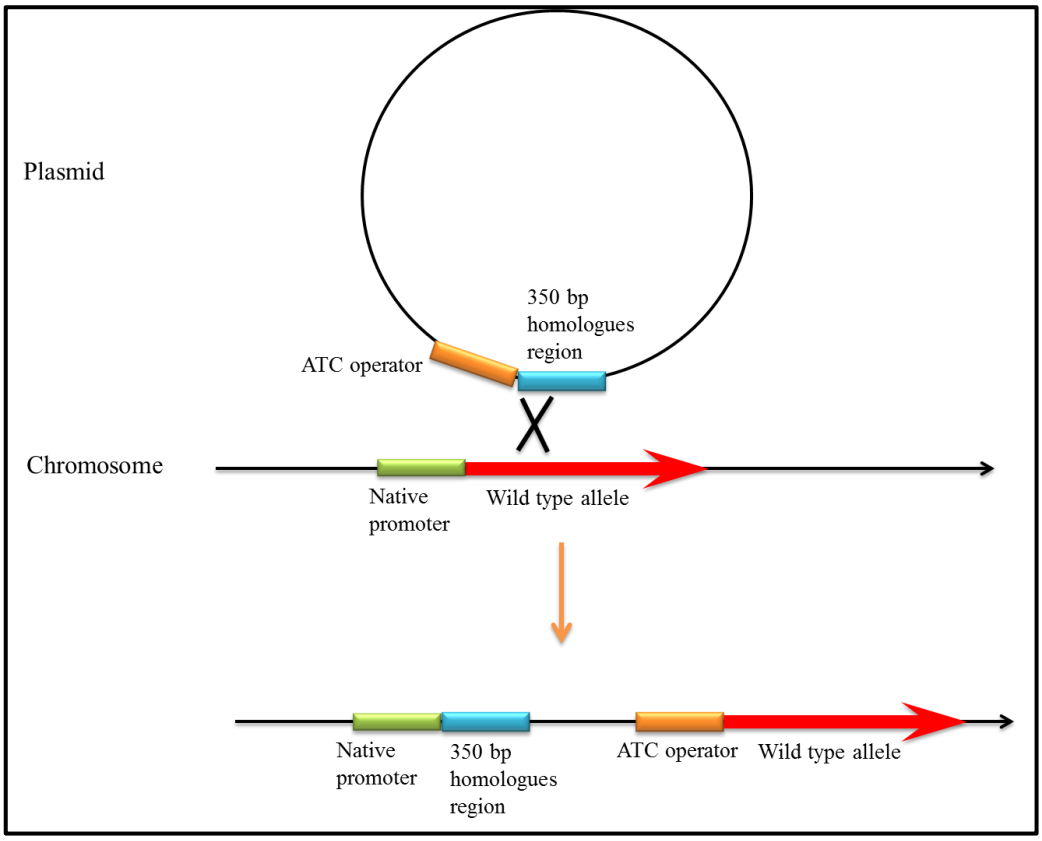


Figure 2.5: Schematic representation of the ATC-regulated knockdown strain. Shown is the method used for construction of the knockdown strain, depicting the single cross over event, which leads to replacement of the native promoter of the gene of interest with the ATC operator

2.12.1 Construction of *ami2* knockdown vector

Primers, the PanC RBS forward primer (CGCGCATGCCGTGGAGGTTTTGACGGCATGTCGAGTCTGCGTCGC) containing the *panC* ribosomal binding site (underlined) and the reverse primer (GCGCGCGGCCGCACCAGGCCGGTGTAGAAG), were designed to amplify the first 350 bp (386 bp) of the *ami2* gene. The primers included restriction sites for cloning into the desired vector and a *panC* ribosomal binding site (CGTGGAGGTTTTGACGGC). This *panC* ribosomal binding site was chosen because it displayed efficient regulation of the mycobacterial *panC* gene using the same knockdown system (Abrahams *et al*., 2012). This fragment was cloned into pSE100, a vector used for ATC-regulation in mycobacteria (Ehrt *et al*., 2005). Clones were selected and plasmid DNA screened by restriction digests with *Not*I, which would result in the liberation of a 489 bp band. A single positive clone was then selected for further analysis through more extensive restriction digest to confirm the genomic integrity of the vector, which was then further confirmed by sequencing of the cloned region.

2.13 Msm *ami2*KDP associated Phenotyping

2.13.1 Msm *ami2*KDP preculture preparation

Msm *ami2*KDP frozen culture stocks were streaked on 7H10 supplemented with Kan and Hyg containing no ATC and incubated at 37 °C until single colonies emerged. A single colony was then cultured in 10 ml 7H9 supplemented with Kan and Hyg without ATC and grown until the culture began clumping. These stages of culturing were conducted to remove any residual ATC remaining in the cell when the freezer stocks were made. The cells were then harvested and washed twice in 7H9 and incubated in 1 ml of 7H9. The

OD_{600nm} of the 1 ml culture was recorded and the culture was used to set up bulk cultures for subsequent experiments.

2.13.2 **Analysis of regulated gene expression**

A pre-culture was set up as in section 2.13.1 and using this, three 25 ml 7H9 cultures supplemented with Kan and Hyg were set up, these included: (I) No ATC added (II) Plus 0.05 ηg/ml ATC (III) Plus 50 ηg/ml ATC. These cultures were set up with a starting OD_{600nm} of 0.15 and incubated at 37 ºC. Samples were taken after 6 and 9 hours of growth and gene expression analysis was conducted as in section 2.6 using primers listed in Table 2.6. A Student's *t*-test was then conducted comparing the no ATC data to the samples containing ATC to determine significant differences. This experiment was set up 3 times using different freezer stocks.

Table 2.6: Primer used for expression analysis

Name	Primers	Region targeted
sigA Gene		
qPCR Forward primer	GGGCGTGATGTCCATCTCCT	Produces a 122 bp amplicon, which corresponds to position 367 to 488 of the *sigA* gene
qPCR and mRNA conversion primer	GTATCCCGGTGCATGGTC	
ami2 Gene		
qPCR Forward primer	GCTGTACTTCCTCGGCTCAC	Produces a 112 bp amplicon, which corresponds to position 435 to 564 of the *ami2* gene
qPCR Reverse primer	ATCGATGATGACCCGCTTAC	
mRNA conversion primer	AGGATGTCGGCCTCACTGAT	Produces a 186 bp amplicon, which corresponds to position 435 to 638 of the *ami2* gene

2.13.3 **Msm *ami2*KDP growth kinetics**

This analysis was conducted with growth curves, done in triplicate using different batches of 7H9 media and different freezers stocks. A pre-culture was set up as in section 2.13.1. Thereafter five 25 ml cultures (7H9, supplemented with Kan and Hyg) with starting OD_{600nm} of 0.025, containing the following ATC concentrations were set up: 0 ηg/ml, 0.001 ηg/ml, 0.05 ηg/ml, 1 ηg/ml and 50 ηg/ml ATC followed by incubation at 37 ºC. Cultures of mc^2155 containing no ATC and 50 ηg/ml ATC were included to evaluate the inhibitory impact of ATC on Msm growth kinetics. The mc^2155 culture containing no ATC was also included to determine the optimal level of ATC required for *ami2*KDP growth kinetics that are similar to mc^2155. OD_{600nm} readings were taken every 3 hours and the data was represented using a scatter plot.

3. Results

3.1 Bioinformatics analyses and identification of putative amidase-encoding genes in mycobacteria

Mycobacterial cell wall amidases have not been the subject of extensive study. Consequently, the genetic annotation for this group of enzymes in mycobacterial genomes is poor and subject to mis-annotation. The extensive repertoire of other amidase-encoding genes (not associated with the PG) in mycobacteria further complicates this. To identify PG-degrading amidases for subsequent analysis, extensive bioinformatic analyses were conducted. As stated earlier in section 1.6, these enzymes can be classified into two main groups namely the amidase_2 and amidase_3 domain – containing amidases. These domains also define these enzymes as PG degrading amidases since they are only found in PG associated enzymes with cell wall amidase activity (Vollmer *et al*., 2008, Shida *et al*., 2001, Mesnagi and Fouet, 2002). To identify these enzymes in Mtb and Msm, the amidase_2 and amidase_3 domains of the well-characterized *E. coli* enzymes were blasted against these mycobacterial genomes using the NCBI protein blast tool. The enzymes resulting from this search were further analyzed using the Sanger Pfam tool to identify the domains contained within these enzymes and the SignalP tool was used to determine the presence of signal peptides, which would indicate whether the enzyme is exported to the cell wall, Figure D1 and D2, Appendix. The resulting hits were aligned with the *E. coli* homologues using the EBI clustalW tool to determine the presence of conserved domains between the enzymes in *E. coli* and mycobacteria, this resulted in the identification of three PG amidase-encoding genes in Msm, MSMEG_6281, MSMEG_6406 and MSMEG_6935 and in Mtb namely, Rv3717, Rv3811 and Rv3915, Figure 3.1.

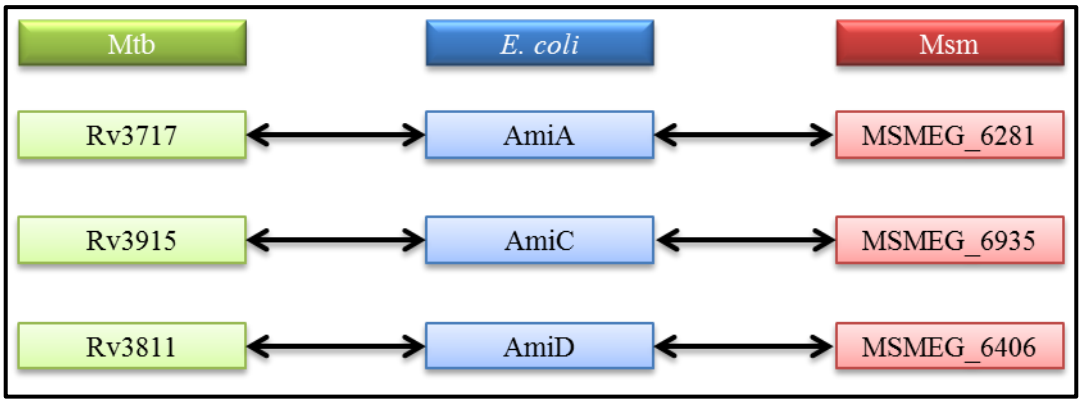


Figure 3.1: Schematic representing the mycobacterial amidases and their *E. coli* homologues. Shown are the three putative mycobacterial amidases identified through BLAST search analysis of the signature amidase domains against mycobacterial genomes, as well as the three *E. coli* amidases, which show the closest similarity to the mycobacterial amidases.

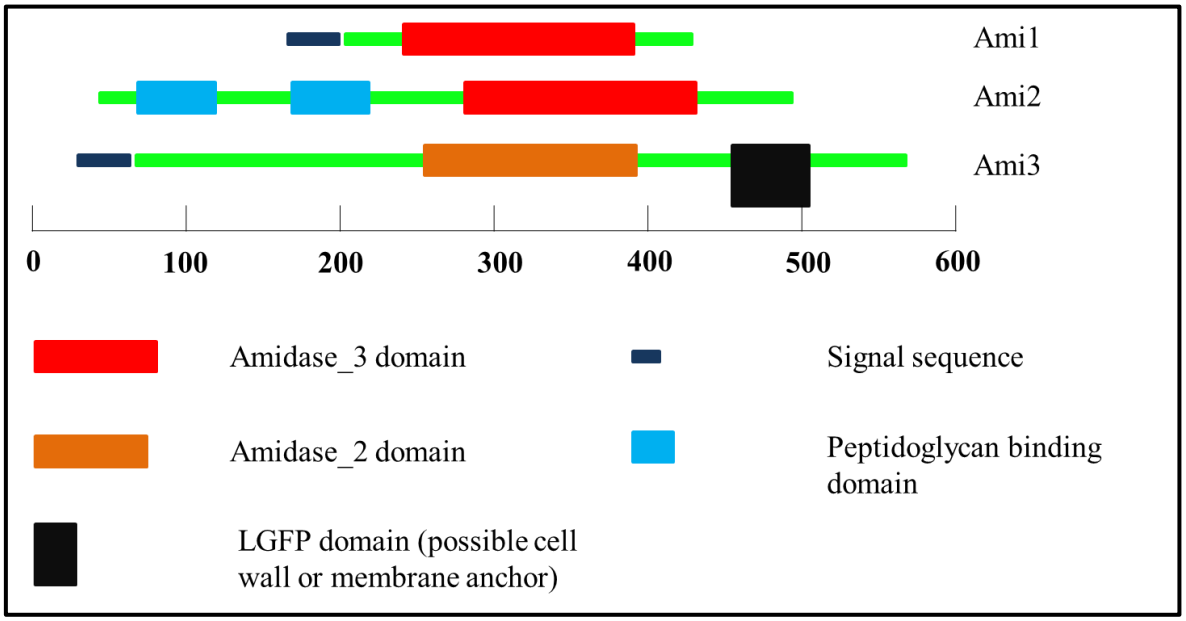


Figure 3.2: Diagrammatic representation of the Msm cell wall amidases and their respective functional domains. Shown are the amidase_3 domains found in Ami1 and Ami2 and the amidase_2 domain present in Ami3. Also shown are the additional domains such as the PG binding domains on Ami2 and the LGFP domain on Ami3.

The three genes identified in Msm were annotated as follows: MSMEG_6281 – *ami1* MSMEG_6935 – *ami2* and MSMEG_6406 – *ami3*. As shown in Figure 3.2, Ami1 and Ami2 possess an Amidase_3 domain whilst Ami3 contains an Amidase_2 domain. Ami1 and Ami3 contain a signal peptide suggesting these enzymes are most likely exported to the PG. Ami2 does not have such a motif, indicating possible localization in the cytoplasm.

Ami1 contains no PG binding domains suggesting it requires association with other enzymes in order to interact with PG. Ami2 contains two PG binding domains confirming that it retains the capacity to bind PG without the aid of additional enzymes. However, this does not preclude the possibility that Ami2 is activated in a similar way to the *E. coli* homologue [section 1.6.2 –(Yang *et al*., 2012)]. Ami3 contains a LGFP domain, the function of which is currently unknown. This domain is found in proteins, which are membrane associated, suggesting it might play a role in anchoring proteins to the cell membrane (Brand *et al*., 2003). Ami3 also does not contain any PG binding domains, which again could indicate association with other proteins for PG interaction.

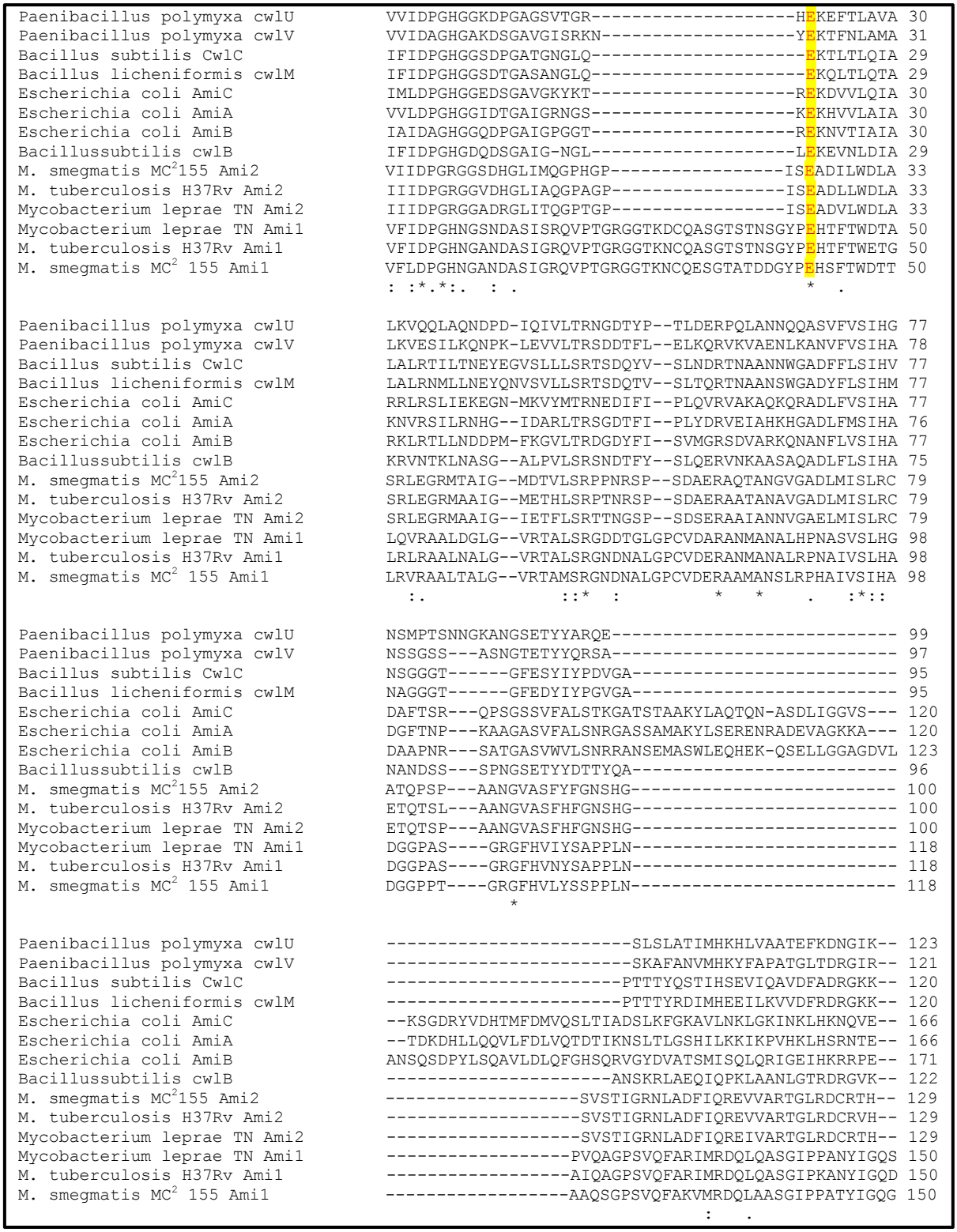
The pFAM analyses was not only conducted on all three of the Msm and Mtb amidases but also on all five of the *E. coli* homologues, Figure D1, appendix, to confirm that this analysis reliably detected PG amidases and to further differentiate domains contained within each amidase for comparison to those found in the mycobacterial homologues. The three *E. coli* homologues, which displayed the closest similarity to the mycobacterial amidases were AmiA, AmiC and AmiD. AmiA displayed high similarity to Ami1 as both were shorter amidases containing only the amidase_3 domain and no additional domains. From the five *E. coli* amidases, AmiC was highly similar to Ami2 since they both possess an amidase_3 domain, AmiC however contains a second domain called the AMIN (Amidase-N-terminal) domain, which is predicted to be involved in the localization of AmiC to the septal ring, while Ami2 contains two putative PG binding domains (PG_binding_1), which have been found to be associated with PG degrading enzymes (Foster, 1991, Joris *et al*., 1982, Krogh *et al*., 1998). AmiD displayed high similarity to Ami3, they both possess an amidase_2 domain. Ami3 also possesses a predicted membrane anchoring domain, though the pFAM analyses suggested AmiD did not display the

presence of any membrane anchoring domains. It has been shown in *E. coli* that AmiD is a membrane associated protein (Uehara and Park, 2007).

3.1.1 Conservation of catalytic residues within the Amidase 3 domain

To identify conserved catalytic residues, clustalW analysis was conducted using the signature amidase domains from each gene. The crystal structure of the amidase_3 domain has yet to be resolved however, sequence alignment of the amidase_3 domain-containing amidases from a wide range of bacterial and viral organisms has identified the residues essential for catalysis (Shida *et al*., 2001, Mesnagi and Fouet, 2002). These conserved residues were then subjected to site directed mutagenesis to identify domains essential for catalysis using the *B. subtilis* CwlC amidase as a template. Two essential residues, Glu^{21} and Glu^{138}, were identified as highly conserved and essential for catalytic activity (Shida *et al*., 2001). A clustalW alignment was conducted using the *Bacillus* amidases domains (Shida *et al*., 2001). The alignment of AmiA and AmiC domains from *E. coli* and the Ami1 and Ami2 domains of the Msm, Mtb and *M. leprea* homologues are shown in Figure 3.3.

Alignment of these proteins reveal that the Glu^{21} is conserved throughout the different organisms depicted in Figure 3.3, however the second catalytic residue is only conserved in the Ami1 homologues and not entirely conserved in the Ami2 homologues where, in some cases, the Glu^{138} is replaced by Asp, which is slightly different with respect to structure but possesses the same overall charge, Figure D3, Appendix, and could thus still function as a catalytic residue (Berg *et al*., 2007).


Paenibacillus polymyxa cwlU VVIDPGHGGKDPGAGSVTGR----------HEKEFTLAVA 30
Paenibacillus polymyxa cwlV VVIDAGHGAKDSGAVGISRKN----------YEKTFNLAMA 31
Bacillus subtilis CwlC IFIDPGHGGSDPGATGNGLQ----------EKTLTLQIA 29
Bacillus licheniformis cwlM IFIDPGHGGSDTGASANGLQ----------EKQLTLQTA 29
Escherichia coli AmiC IMLDPGHGGEDSGAVGKYKT----------REKDVVLQIA 30
Escherichia coli AmiA VVLDPGHGGIDTGAIGRNGS----------KEKHVVLAIA 30
Escherichia coli AmiB IAIDAGHGGQDPGAIGPGGT----------REKNVTIAIA 30
Bacillussubtilis cwlB IFIDPGHGDQDSGAIG-NGL----------LEKEVNLDIA 29
M. smegmatis MC2155 Ami2 VIIDPGRGGSDHGLIMQGPHGP----------ISEADILWDLA 33
M. tuberculosis H37Rv Ami2 IIIDPGRGGVDHGLIAQGPAGP----------ISEADLLWDLA 33
Mycobacterium leprae TN Ami2 IIIDPGRGGADRGLITQGPTGP----------ISEADVLWDLA 33
Mycobacterium leprae TN Ami1 VFIDPGHNGSNDASISRQVPTGRGGTKDCQASGTSTNSGYPEHTFTWDTA 50
M. tuberculosis H37Rv Ami1 VFIDPGHNGANDASIGRQVPTGRGGTKNCQASGTSTNSGYPEHTFTWETG 50
M. smegmatis MC2 155 Ami1 VFLDPGHNGANDASIGRQVPTGRGGTKNCQESGTATDDGYPEHSFTWDTT 50
LKVQQLAQNDPD-IQIVLTRNGDTYP--TLDERPQLANNQQASVFVSIHG 77
LKVESILKQNPK-LEVVLTRSDDTFL--ELKQRVKVAENLKANVFVSIHA 78
LALRTILTNEYEGVSLLLSRTSDQYV--SLNDRTNAANNWGADFFLSIHV 77
LALRNMLLNEYQNVSVLLSRTSDQTV--SLTQRTNAANSWGADYFLSIHM 77
RRLRSLIEKEGN-MKVYMTRNEDIFI--PLQVRVAKAQKQRADLFVSIHA 77
KNVRSILRNHG--IDARLTRSGDTFI--PLYDRVEIAHKHGADLFMSIHA 76
RKLRTLLNDDPM-FKGVLTRDGDYFI--SVMGRSDVARKQNANFLVSIHA 77
KRVNTKLNASG--ALPVLSRSNDTFY--SLQERVNKAASAQADLFLSIHA 75
SRLEGRMTAIG--MDTVLSRPPNRSP--SDAERAQTANGVGADLMISLRC 79
SRLEGRMAAIG--METHLSRPTNRSP--SDAERAATANAVGADLMISLRC 79
SRLEGRMAAIG--IETFLSRTTNGSP--SDSERAAIANNVGAELMISLRC 79
LQVRAALDGLG--VRTALSRGDDTGLGPCVDARANMANALHPNASVSLHG 98
LRLRAALNALG--VRTALSRGNDNALGPCVDERANMANALRPNAIVSLHA 98
LRVRAALTALG--VRTAMSRGNDNALGPCVDERAAMANSLRPHAIVSIHA 98
NSMPTSNNGKANGSETYYARQE---------- 99
NSSGSS---ASNGTETYYQRSA---------- 97
NSGGGT------GFESYIYPDVGA---------- 95
NAGGGT------GFEDYIYPGVGA---------- 95
DAFTSR---QPSGSSVFALSTKGATSTAAKYLAQTQN-ASDLIGGVS--- 120
DGFTNP---KAAGASVFALSNRGASSAMAKYLSERENRADEVAGKKA--- 120
DAAPNR---SATGASVWVLSNRRANSEMASWLEQHEK-QSELLGGAGDVL 123
NANDSS---SPNGSETYYDTTYQA---------- 96
ATQPSP---AANGVASFYFGNSHG---------- 100
ETQTSL---AANGVASFHFGNSHG---------- 100
ETQTSP---AANGVASFHFGNSHG---------- 100
DGGPAS----GRGFHVIYSAPPLN---------- 118
DGGPAS----GRGFHVNYSAPPLN---------- 118
DGGPPT----GRGFHVLYSSPPLN---------- 118
----------SLSLATIMHKHLVAATEFKDNGIK-- 123
----------SKAFANVMHKYFAPATGLTDRGIR-- 121
----------PTTTYQSTIHSEVIQAVDFADRGKK-- 120
----------PTTTYRDIMHEEILKVVDFRDRGKK-- 120
--KSGDRYVDHTMFDMVQSLTIADSLKFGKAVLNKLGKINKLHKNQVE-- 166
--TDKDHLLQQVLFDLVQTDTIKNSLTLGSHILKKIKPVHKLHSRNTE-- 166
ANSQSDPYLSQAVLDLQFGHSQRVGYDVATSMISQLQRIGEIHKRRPE-- 171
----------ANSKRLAEQIQPKLAANLGTRDRGVK-- 122
----------SVSTIGRNLADFIQREVVARTGLRDCRTH-- 129
----------SVSTIGRNLADFIQREVVARTGLRDCRVH-- 129
----------SVSTIGRNLADFIQREIVARTGLRDCRTH-- 129
----------PVQAGPSVQFARIMRDQLQASGIPPANYIGQS 150
----------AIQAGPSVQFARIMRDQLQASGIPKANYIGQD 150
----------AAQSGPSVQFAKVMRDQLAASGIPPATYIGQG 150

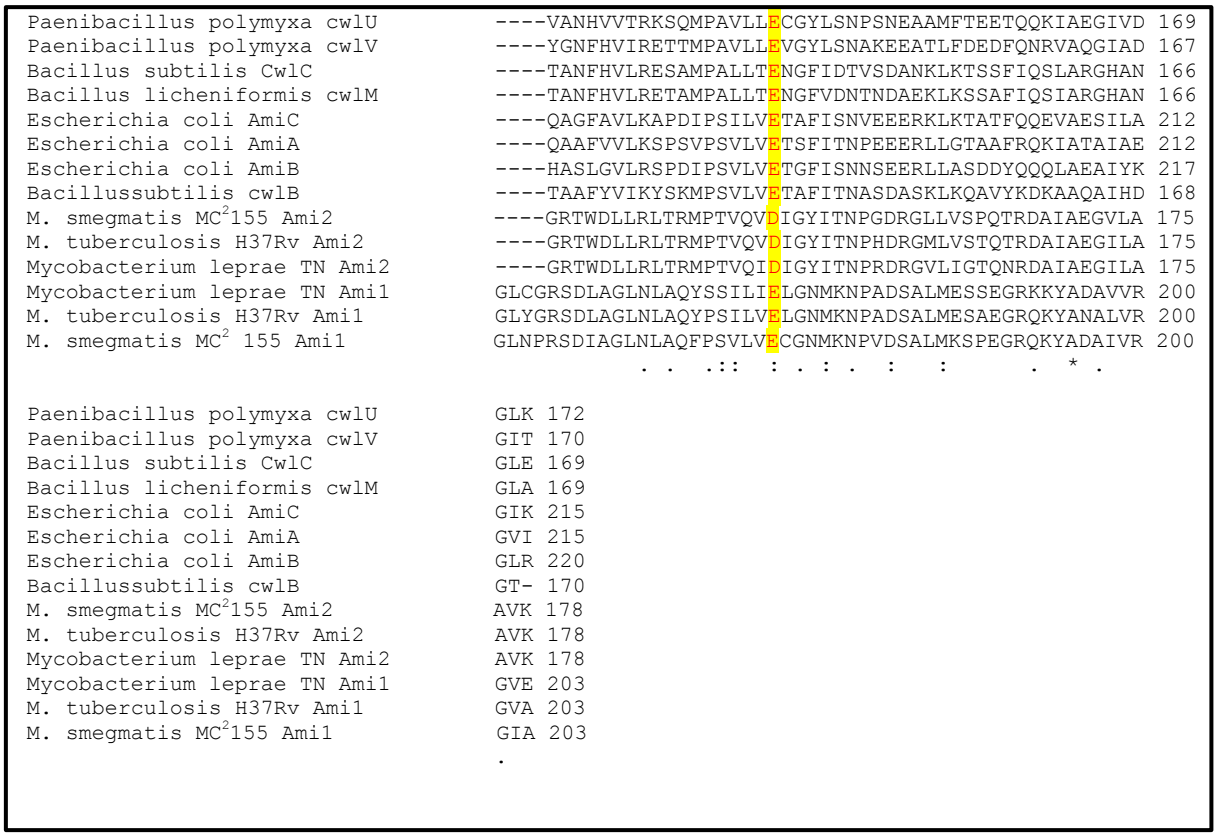


Figure 3.3: ClustalW analysis of amidase_3 domain containing amidases. Shown is the alignment of amidase_3 domains from *Bacillus*, mycobacterial species and *E. coli* and the conserved catalytic residues. Yellow highlight indicates conserved catalytic Glu^{21} and Glu^{138} residues.

3.1.2 Conservation of catalytic residues within the Amidase 2 domain

The crystal structure of AmiD has been resolved and in this case, the residue essential for catalysis is Glu^{89}, residing within the AmiD amidase_2 domain (Kerff *et al*., 2010). To further assess this in mycobacteria, the AmiD amidase domain was aligned with the Msm and Mtb homologues, retaining the amidase – 2 domain, to determine whether this residue is conserved, Figure 3.4. AmpD and amidase_2 containing amidases were included to determine whether the catalytic residue is conserved throughout different organisms.

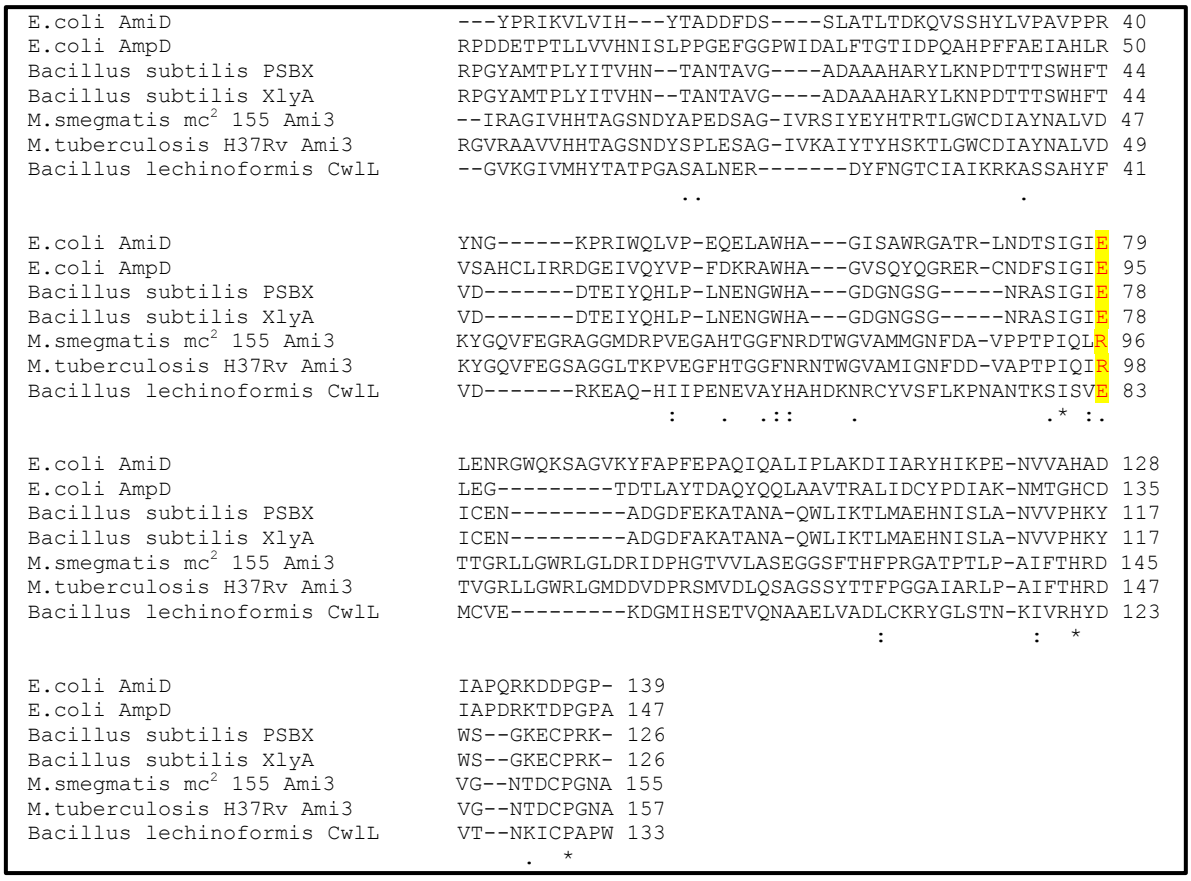


Figure 3.4: ClustalW analysis of amidase_2 amidases containing amidases. Shown is the alignment of amidase_2 domains from *Bacillus*, mycobacterial species and *E. coli* and the conserved catalytic residues. Yellow highlight indicates conserved Glu[89] catalytic residue.

Alignment of the amidase_2 domain revealed that the catalytic residue is not conserved between the mycobacterial amidases and in the organisms examined, as depicted in Figure 3.4. The Glu[79] residue in the AmiD amidase domain, which corresponds to the Glu[89] catalytic residue in AmiD from *E. coli,* was replaced by Arg in the mycobacterial Ami3, which is sterically and chemically different, Figure D3, Appendix. The implications of these changes on PG and/or cell wall hydrolytic activity are currently unknown.

3.2 Construction of deletion mutants defective in the *ami1* and *ami2* genes.

Of the three putative amidase-encoding genes identified, only *ami1* and *ami2* were targeted for deletion due to the fact that they displayed higher similarity indices to the *E. coli* amidases. In addition, time constraints necessitated that only two genes were further

evaluated. Also, the *E. coli* homologues for Ami1 and Ami2 have both been linked to cell division and septation thus making them interesting homologues to study within the context of PG degradation and remodeling. Of particular interest in this regard is the fact that the Mtb homologue of *ami2*, Rv3915, is designated as an essential gene, suggesting that it plays an important role in cell division and would hence be a likely choice for further study in Msm. The predicted essentiality of Rv3915 in Mtb makes it a possible drug target and further investigating the role of the gene product in cell growth and physiology would be important for validating this class of enzymes as possible drug targets. The gene deletion system used in this study was a two-step, allelic exchange system, which involves substitution of the wild type gene with a truncated/deleted, non-functional version of the gene by homologues recombination (Parish and Stoker 2000, Gordhan and Parish 2001), Figure 2.1).

3.2.1 Construction of vectors for deletion of *ami1* and *ami2*.

The upstream and downstream fragments of the *ami1* and *ami2* genes were amplified by PCR and each fragment was cloned into pGEM3Z(+)f. Subsequent clones were then screened by restriction as detailed in section 2.10.1.2.1 and the upstream and downstream PCR fragments from positive clones were sub-cloned into p2NIL using the 3 way cloning technique. These clones were screened by restriction digest, detailed in section 2.10.1.2.2. A single clone per gene was selected confirmed by use of extensive restriction endonuclease profiling, Figure 3.5 and Figure 3.6.

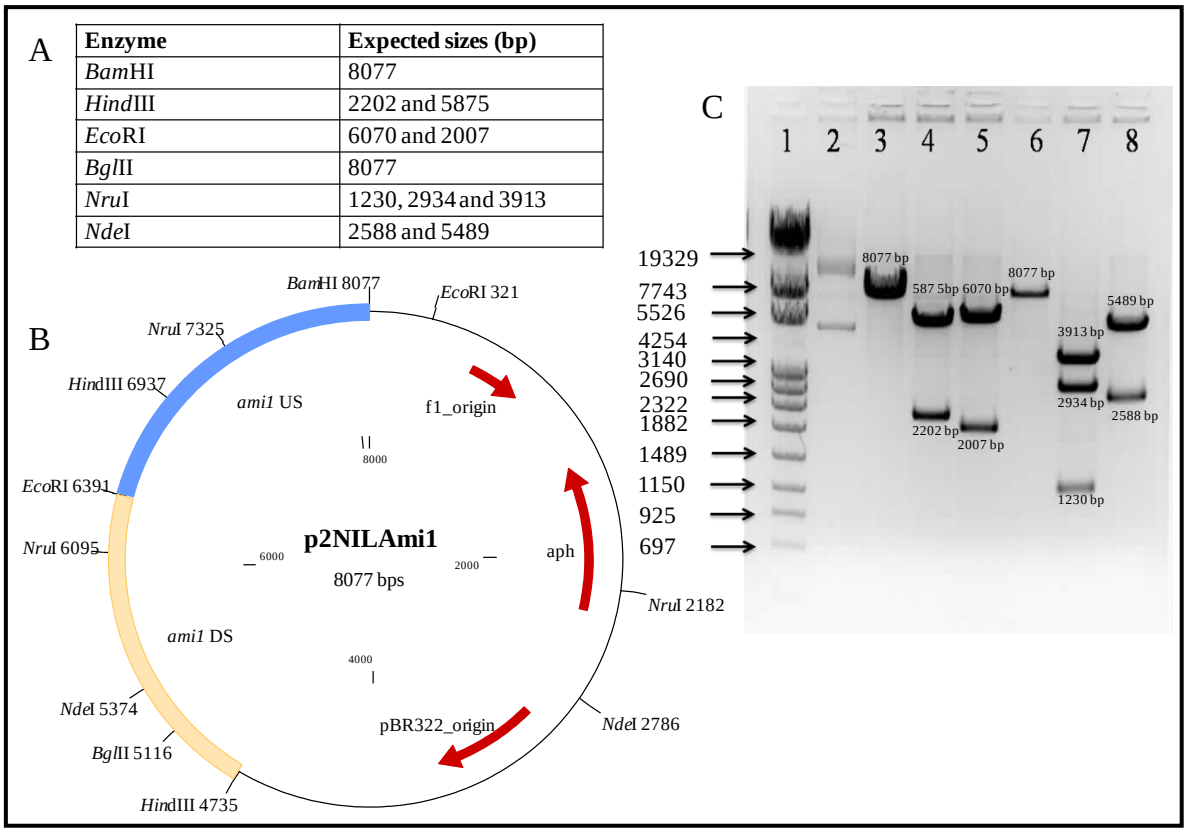


Figure 3.5: Restriction profile of p2NILAmi1. **(A)** Table displaying the different restriction endonucleases used and the expected fragment sizes, which result from restriction digest of the p2NILAmi1 construct. **(B)** Plasmid map of p2NILAmi1 showing the fused upstream and downstream fragments (blue), cloned into the p2NIL backbone. **(C)** Agarose gel showing the result of restriction enzyme profiling of p2NILAmi1.**[Lane 1]** Roche marker VI, **[Lane 2]** Uncut plasmid, **[Lane 3]** *Bam*HI, **[Lane 4]** H*ind*III, **[Lane 5]** *EcoRI*, **[Lane 6]** *Bgl*II, **[Lane 7]** *Nru*I and **[Lane 8]** *Nde*I

Restriction analysis confirmed that the clones selected displayed the expected restriction enzyme patterns predicted for the p2NILAmi1 and p2NILAmi2 constructs. Figure 3.5 and Figure 3.6 show that the restriction profiles obtained by restriction digest of the clones, with various enzymes, Figure 3.5 C and Figure 3.6 C, corresponded to the predicted plasmid map and the expected fragment banding patterns. There were no aberrant or missing bands, thus confirming the genetic integrity of the selected clones. The plasmids were then further analyzed by sequencing to ensure that the upstream-downstream fusion fragment, and deletion allele, contained no inadvertent mutations introduced during the PCR and cloning steps. Sequence data revealed that indeed, no mutations had occurred

(data not shown), which further confirmed the genetic integrity of the constructs for use in subsequent cloning and allelic exchange mutagenesis.

A

Enzyme	Expected sizes (bp)
*Bam*HI	6712
*Eco*RI	1785 and 4927
*Mlu*I	2482 and 4230
*Not*I	556 and 6156
*Pac*I	6712
*Pst*I	6712

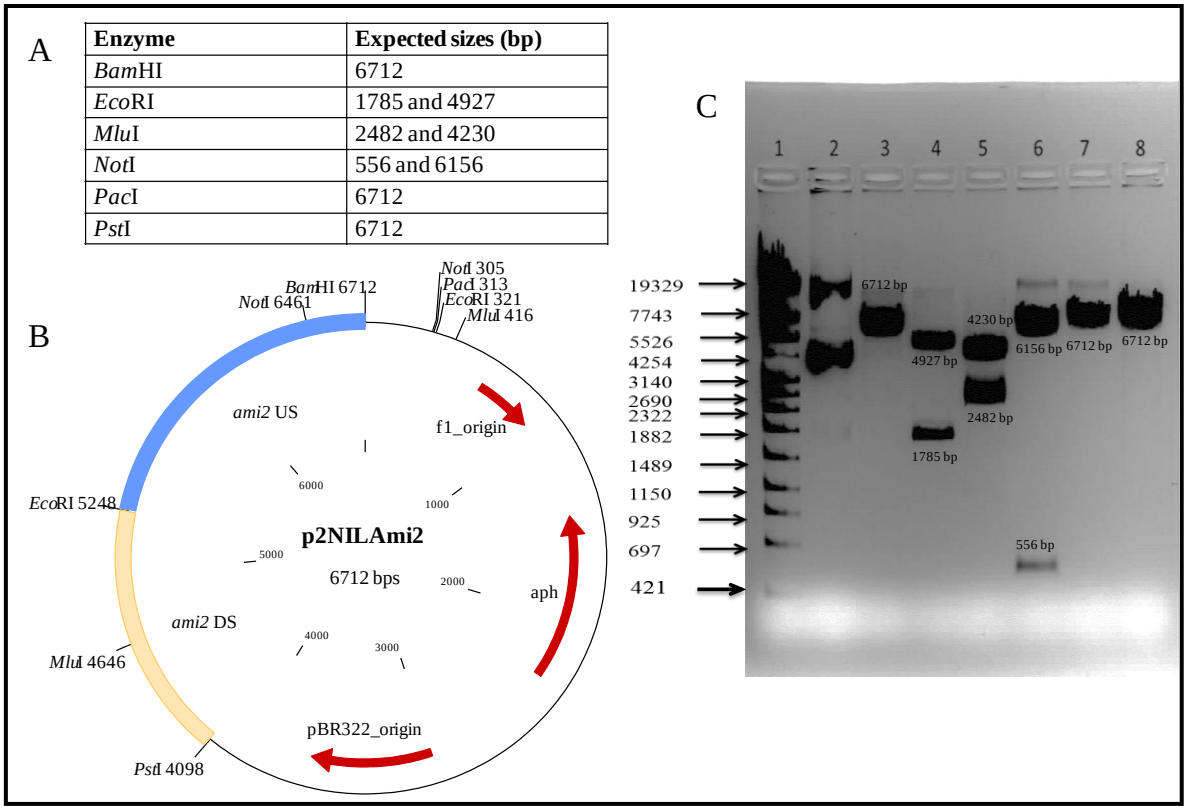


Figure 3.6: Restriction profile of p2NILAmi2. **(A)** Table displaying the different restriction endonucleases used and the expected fragment sizes, which result from restriction digestion of the p2NILAmi2 construct. **(B)** Plasmid map of p2NILAmi2 showing the fused upstream and downstream fragments (blue), cloned into the p2NIL backbone. **(C)** Agarose gel showing the result of restriction enzyme profiling of p2NILAmi2. **[Lane 1]** Roche marker VI, **[Lane 2]** Uncut plasmid, **[Lane 3]** *Bam*HI, **[Lane 4]** *Eco*RI, **[Lane 5]** *Mlu*I, **[Lane 6]** *Not*I, **[Lane 7]** *Pac*I and **[Lane 8]** *Pst*I

The pGOAL19 Pac cassette was then cloned into the p2NILAmi1 and p2NILAmi2 constructs, and screened as described in section 2.10.1.2.3, then a single positive clone per gene was selected and the genetic integrity of the final knockout constructs confirmed by extensive restriction endonuclease profiling, Figure 3.7 and Figure 3.8.

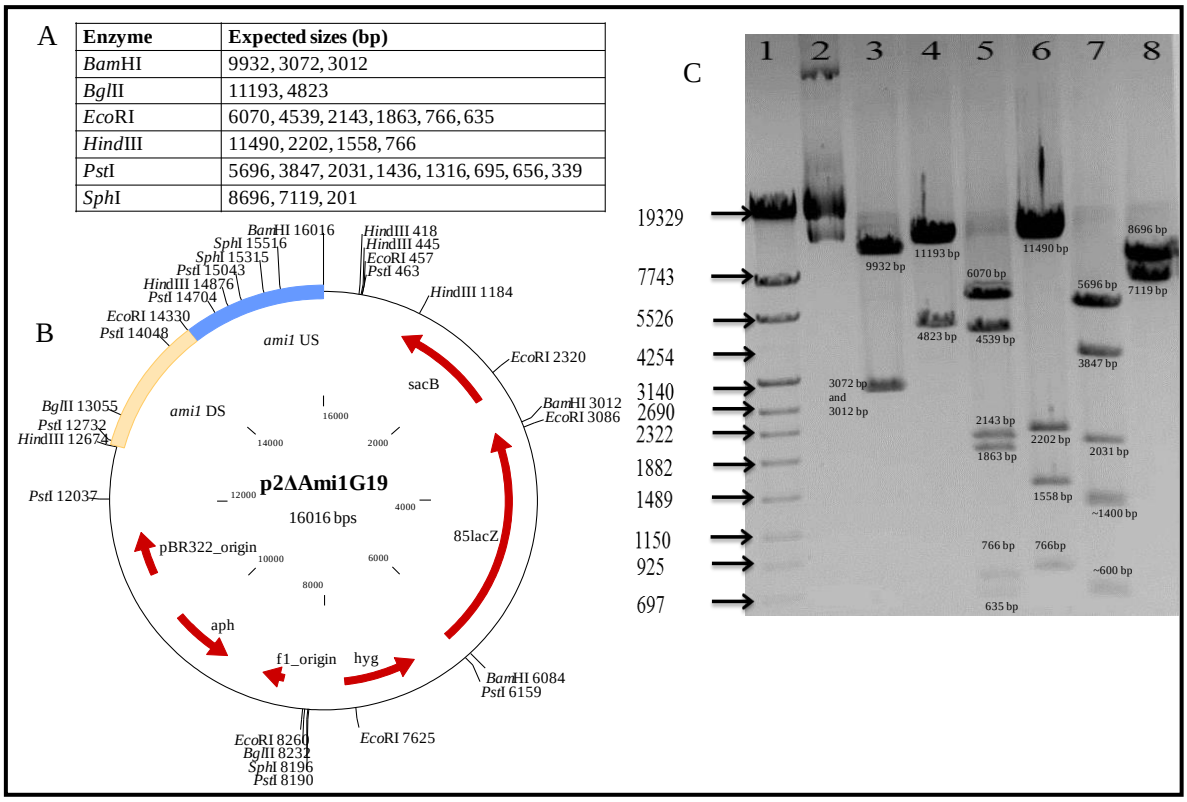


Figure 3.7: Restriction profile of p2ΔAmi1G19. **(A)** Table displaying the different restriction endonucleases used and the expected fragment sizes, which result from restriction digest of the p2ΔAmi1G19 construct. **(B)** Plasmid map of the p2ΔAmi1G19 vector. **(C)** Agarose gel of digested fragments, **[Lane 1]** Roche marker VI, **[Lane 2]** Uncut plasmid, **[Lane 3]** *Bam*HI, **[Lane 4]** *Bgl*II, **[Lane 5]** *Eco*RI, **[Lane 6]** H*ind*III, **[Lane 7]** *Pst*I and **[Lane 8]** *Sph*I

Restriction profiles of the selected clones, depicted in Figure 3.7 C and Figure 3.8 C, corresponded to the predicted plasmid map and the expected banding patterns, with the exception of the *Sph*I restriction digest p2ΔAmi2G19, which did not display the 509 bp band. This is likely due to the fact that fragments below 600 bp in size were run off the gel in an attempt to resolve the sizes of the larger bands. Though this band was absent, the profiles from all other restriction digests confirmed that both clones possess the expected p2ΔAmi1G19 and p2ΔAmi2G19 restriction patterns and were hence used for allelic exchange mutagenesis.

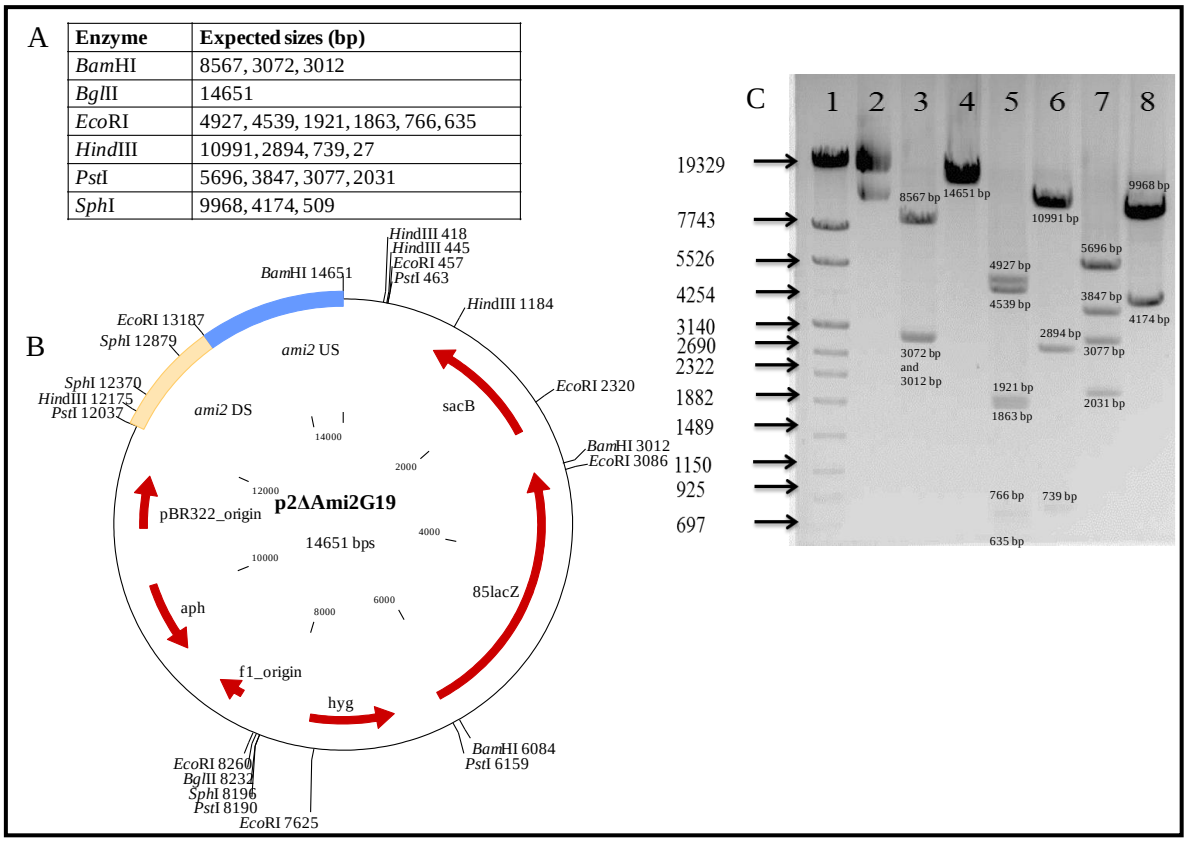


Figure 3.8: Restriction profile of p2ΔAmi2G19. **(A)**Table displaying the different restriction endonucleases used and the expected fragment sizes, which result from restriction digest of the p2ΔAmi2G19 construct. **(B)** Plasmid map of the p2ΔAmi2G19 vector. **(C)** Agarose gel of digested fragments, **[Lane 1]** Roche marker VI, **[Lane 2]** Uncut plasmid, **[Lane 3]** *Bam*HI, **[Lane 4]** *Bgl*II, **[Lane 5]** *Eco*RI, **[Lane 6]** H*ind*III, **[Lane 7]** *Pst*I and **[Lane 8]** *Sph*I

Following genetic confirmation of the final knockout constructs, the bacterial sucrose sensitivity obtained by retention of the knockout constructs, in the *E. coli* cloning host, was evaluated by way of a spotting assay (section 2.10.1.2.3). This was done to determine the level of sucrose mediated death as a result of the *sacB* gene, Figure 3.9. This would further confirm the functionality of the selectable and counter selectable markers in the knockout construct.

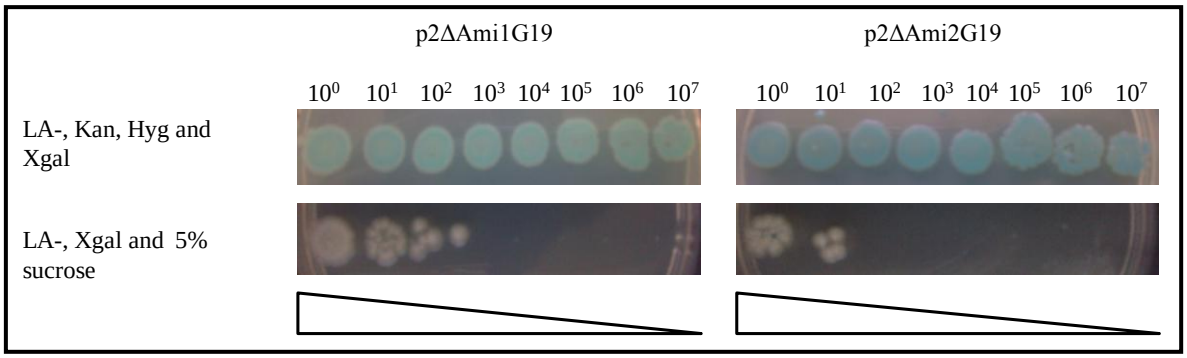


Figure 3.9: Confirmation of sucrose sensitivity in strains carrying knockout constructs. Evaluation of *E. coli* DH5α sucrose sensitivity acquired as a result of p2ΔAmi1G19 and p2ΔAmi2G19 construct retention in the cloning host. Spots represent dilution gradient of an OD = 0.5 *E. coli* culture with dilution factors of 10^0, 10^1, 10^2, 10^3, 10^4, 10^5, 10^6, 10^7.

The sucrose sensitivity assay confirmed that retention of the knockout construct leads to sucrose sensitivity and ultimately growth inhibition. This is evidenced by the reduced growth of these strains on media containing sucrose when compared to the more robust growth observed on plates without sucrose, Figure 3.9. An additional observation was the color of the bacterial colonies on the sucrose containing media; these displayed the formation of white colonies, which is likely due to plasmid loss or mutation of the *lacZ*/*sacB* gene cassette. This assay confirmed the functionality of both the *lacZ* and *sacB* genes indicating that the constructs could be used for allelic exchange mutagenesis.

3.2.2 Two-step homologues recombination and gene knockout

The p2ΔAmi1G19 and p2ΔAmi2G19 knockout vectors were electroporated into mc^2155 (section 2.10.1.4), the transformation efficiency obtained for the electro-competent cells was 3.5×10^4 CFU/µg plasmid DNA determined using the pOLYG control. The pOLYG efficiency was sufficient for efficient transformation of the knockout vectors. A single blue clone per construct (SCO strains) was cultured and subjected to sucrose counter selection (section 2.10.1.4). White colonies were then screened by PCR to identify clones, which possess only the deleted allele, Figure 3.10.

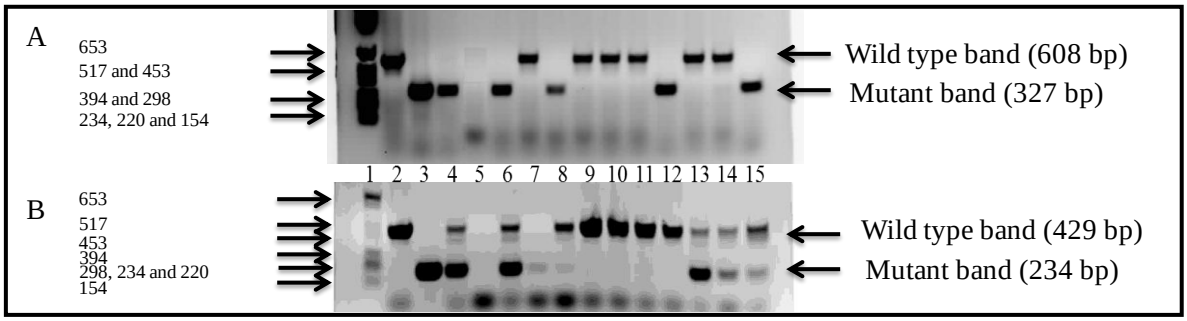


Figure 3.10: PCR screen for deletion mutants of *ami1* and *ami2*. **(A)** PCR screen for *ami1* deletion, **(B)** PCR screen for *ami2* deletion. In both cases, **[Lane 1]** Marker VI, **[Lane 2]**wild type, **[Lane 3]** Knockout construct, **[Lane 4]** SCO strain, **[Lane 5]** No DNA and **[Lane 6 to 15]** Clones 1 to 10.

PCR screening, Figure 3.10A, revealed the presence of four possible *ami1* deletion mutant strains as determined by the presence of the mutant allele only (clone 1, 3, 7 and 10). Clone 1 (designated as Δ*ami1*) was selected and used for further analysis. PCR screening for deletion of *ami2* , Figure 3.10B did show the presence of a possible mutant (clone 2) however this particular clone's ability to grow on media supplemented with Kan and Hyg proved that this clone was a SCO strain, which incurred mutations in both the *sacB* and *lacZ* genes (Data not shown). All of the remaining clones in this screen were also SCO strains, or had reverted to the wild type genotype. The presence of white SCO strains post sucrose counter selection suggested that these strains had also incurred compensatory mutants in the *lacZ* and *sacB* genes, which allowed for growth in the presence of sucrose. This is commonly seen in mycobacterial genetics and in many cases, is most likely due to the fact that the gene being targeted for deletion is essential. To test this, a further 60 additional white colonies, from multiple rounds of counter selection, were tested however, none of these displayed the mutant genotype and retained either the SCO genotype or had reverted to wild type (data not shown). These observations strongly suggest that *ami2* is essential for growth in vitro, which would be consistent with the prediction that the Mtb homologue for this gene, Rv3915, has been predicted to be essential for growth in a

genome-wide essentiality study (Sassetti *et al*., 2003). Due to the inability to generate an *ami2* deletion mutant, we further studied the function of this gene by targeted gene depletion.

Southern blot analysis was conducted to confirm the genotype of the Msm Δ*ami1* strain and to confirm site-specific integration of the deletion allele without any other inadvertent genomic rearrangements. The probe for Southern blotting was constructed by PCR and the primers used to amplify the upstream homologous region, Figure 3.11. Southern blot analysis using the restriction enzyme *Bam*HI was conducted on the mc^2155, the SCO and Δ*ami1* strains, the observed sizes were compared against the expected sizes shown on Figure 3.11. The wild type, mc^2155 strain displayed the presence of 7303 bp band in lane 1 confirming the wild type genotype. The SCO strain displayed two fragments, one, which corresponded to the mutant allele and a second band, which corresponded to the fusion of the vector with the wild type allele. As expected the mutant strain (lane 2) displayed a 10 000 bp band confirming unequivocally that this strain retains the truncated version of the *ami1*. This analysis also confirmed that no gross genomic DNA rearrangements occurred during the allelic exchange mutagenesis.

3.3 Complementation of the Msm Δ*ami1* strain

Complementation of the Δ*ami1* strain with the mc^2155 *ami1* gene was accomplished by utilizing an integrating vector. Briefly, the mc^2155 *ami1* gene and the respective promoter region was cloned into an integrating vector containing antibiotic resistance markers then electroporated into the Δ*ami1* strain. This should result in plasmid integration and re-introduction of the wild type allele into the genome (section 2.11).

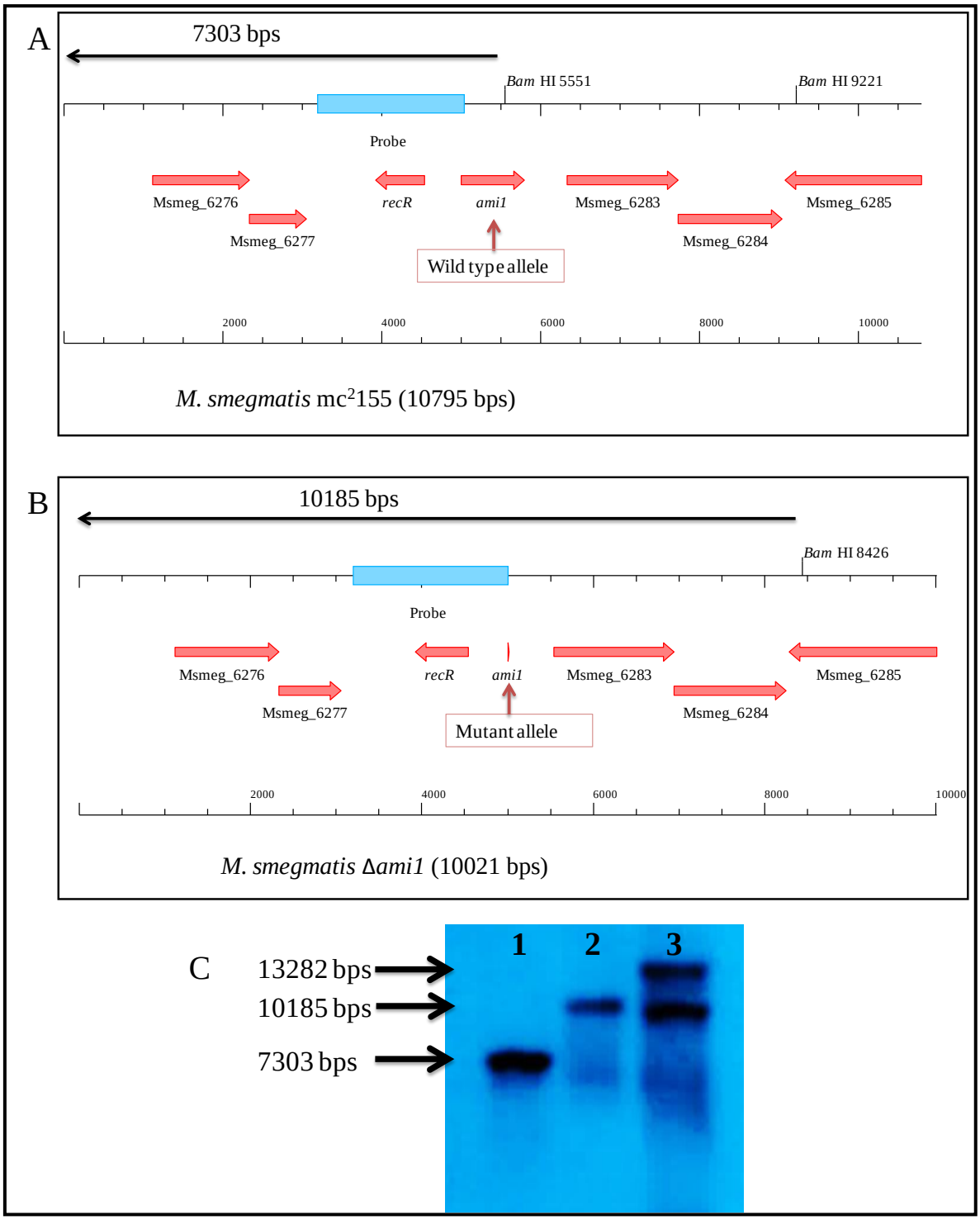
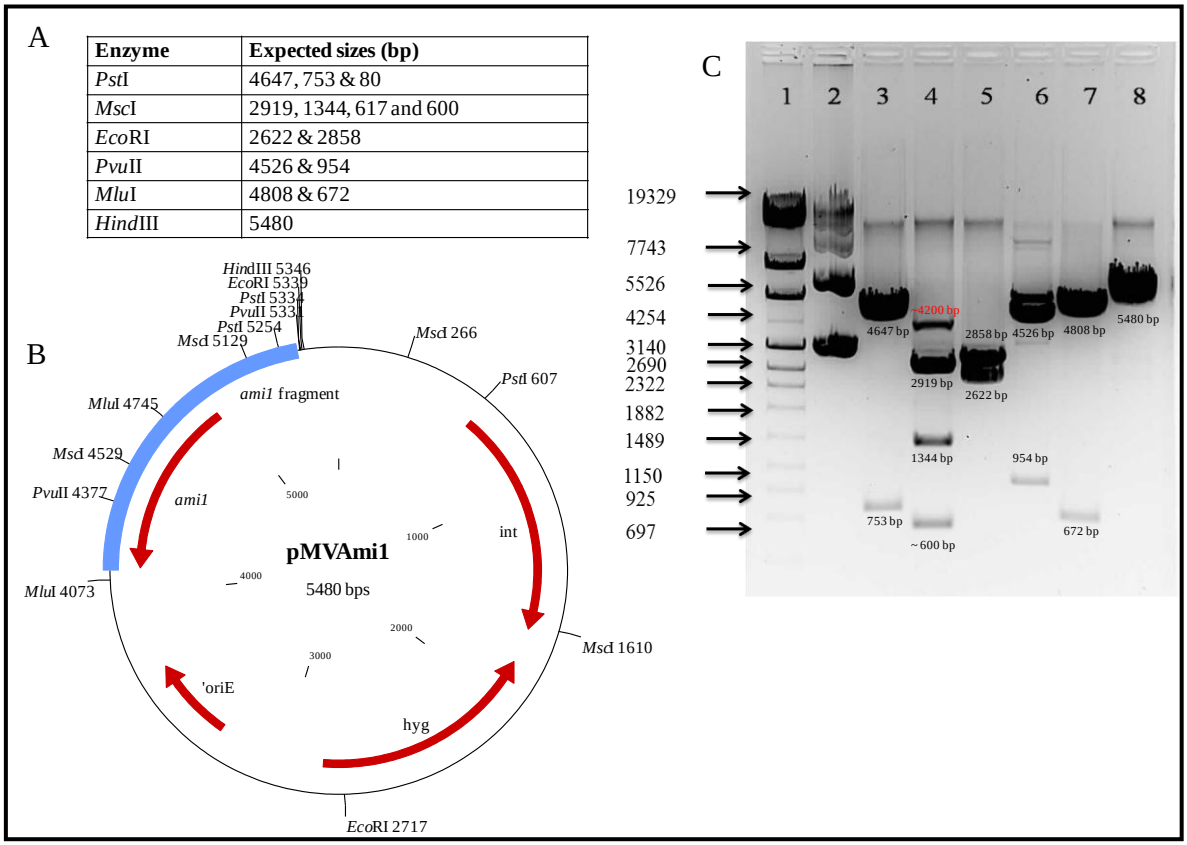


Figure 3.11: Southern Blot analysis of the Msm Δ*ami1* strain. **(A)** Genomic map of mc^{2}155 showing the expected fragment size for the wild type *ami1* allele. **(B)** Genomic map of the Δ*ami1* mutant strains showing the expected size of the deleted *ami1* allele. **(C)** Southern blot, depicting the fragments bound by the probe; **[Lane1]** mc^{2}155, **[Lane 2]** Δ*ami1* and **[Lane 3]** SCO strain.

3.3.1 Construction of the *ami1* complementation vector

The wild type allele and the native promoter region was amplified by PCR and cloned into integrating vector pMV306(H). Subsequent clones were screened by restriction digest as detailed section 2.11.1 (data not shown). Following this, a single positive clone was selected and the genetic integrity of the plasmid was confirmed by extensive restriction profiling, Figure 3.12.



Enzyme	Expected sizes (bp)
*Pst*I	4647, 753 & 80
*Msc*I	2919, 1344, 617 and 600
*Eco*RI	2622 & 2858
*Pvu*II	4526 & 954
*Mlu*I	4808 & 672
*Hind*III	5480

Figure 3.12: Restriction profile of pMVAmi1. **(A)** Table displaying the different restriction endonucleases used and the expected fragment sizes, which result from restriction digest of the pMVAmi1 plasmid. **(B)** Plasmid map of the pMVAmi1 complementation vector. **(C)** Agarose gel depicting the fragments that result from restriction digestion of the pMVAmi1 construct. **[Lane 1]** Roche marker VI, **[Lane 2]** Uncut plasmid, **[Lane 3]** *Pst*I, **[Lane 4]** *Msc*I, **[Lane 5]** *Eco*RI, **[Lane 6]** *Pvu*II, **[Lane 7]** *Mlu*I, **[Lane 8]** H*ind*III

As shown on Figure 3.12, the fragment sizes observed after restriction digest of pMVAmi1 corresponded to expected sizes from the restriction map, confirming that the clone selected

for analysis was correct. There was one exception, the *Msc*1 restriction digest displayed an aberrant approximately 4200 bp band (red), our analysis of the map suggested that this is a consequence of partial digestion by the restriction enzyme. For further confirmation, the *ami1* -encoding region cloned into pMVAmi1 was also sequenced to ensure the *ami1* fragment contained no inadvertent second-site mutations as a result of the PCR and cloning steps. The sequence data confirmed that the *ami1* fragment was identical to the published sequence and contained no mutations (data not shown). This vector was then used for the complementation of the Msm Δ*ami1* strain

3.3.2 pMVAmi1 integration into Δ*ami1* strain genomic DNA

The pMVAmi1 construct was electroporated into the Δ*ami1 s*train (section 2.11.2), the transformation efficiency obtained from the electro-competent cells was 9.8×10^3 CFU/µg plasmid DNA (determined using the pSE100 control vector), which was sufficient for efficient transformation of the complementation vector. Clones were selected and screened by PCR then a single positive clone was selected and screened further by PCR to confirm correct site-specific integration of the complementing vector (section 2.11.2), Figure 3.13.

The PCR products observed for this screen were as expected, shown in Figure 3.13, confirming site-specific integration of the complementation vector.

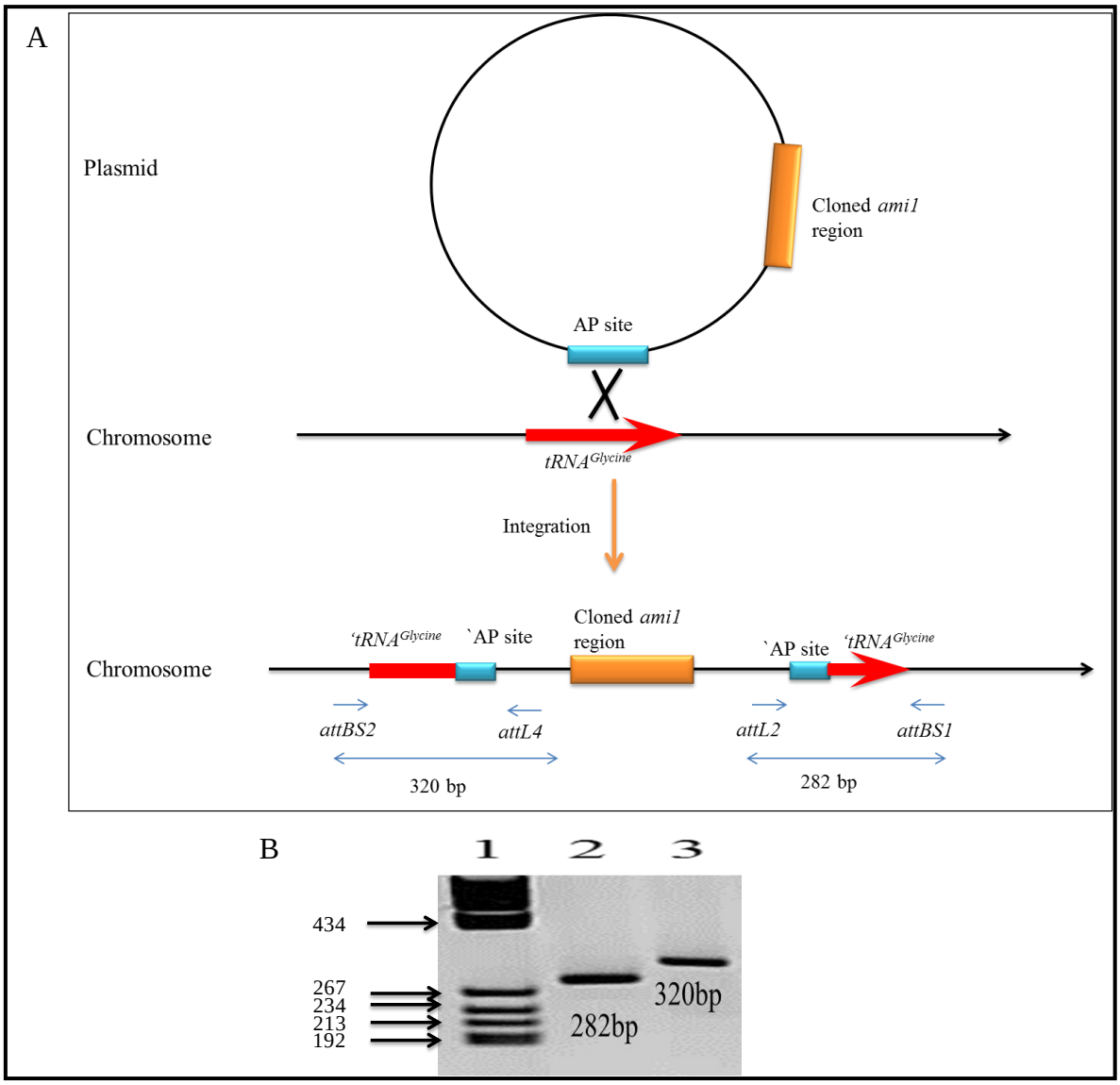


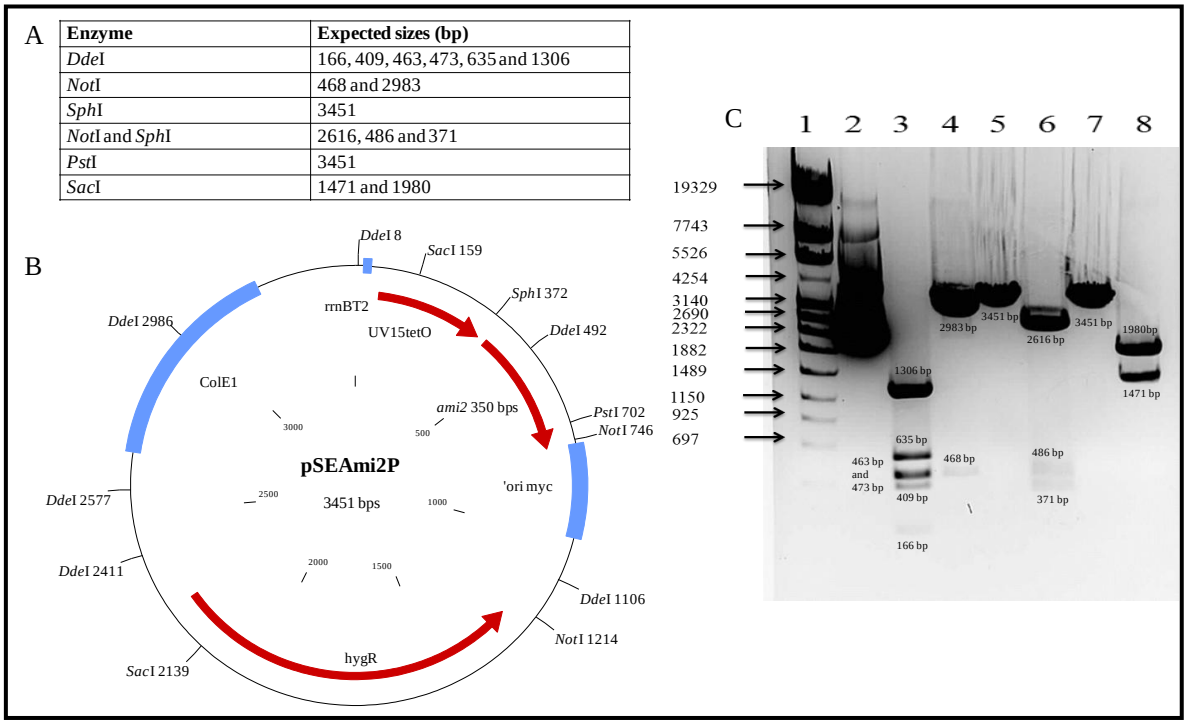
Figure 3.13: PCR Screen for integration of pMVAmi1. **(A)** Schematic representation of the PCR screen principle. Shown is the integration of the plasmid into the *tRNA*^{Glycine} site of the chromosome resulting in integration of the plasmid into the genome. **(B)** PCR screen for pMVAmi1 integration. **[Lane 1]** Roche marker V, **[Lane 2]** *attL2*, *attBS1* PCR reaction and **[Lane 3]** *attBS2*, *attL4* PCR reaction.

3.4 Construction of an *ami2* knockdown strain

Following continuous, unsuccessful attempts at knocking out the *ami2* gene, a gene knockdown system was adopted to evaluate the role of this gene product in Msm physiology. The knockdown system used was a ATC regulated system, which leads to down-regulated expression of the targeted gene in the absence of ATC (Ehrt *et al*., 2005), Figure 2.4.

3.4.1 Construction of *ami2* knockdown vector

PCR amplification was conducted to amplify a fragment consisting of 386 bp from the 5' region of the *ami2* gene fused to the *panC* ribosomal binding site. The fragment was then cloned into pSE100 and clones were screened by restriction with *Not*I. A single positive clone was then selected and the genetic integrity of the construct was confirmed by extensive restriction profiling, Figure 3.14.



Enzyme	Expected sizes (bp)
*Dde*I	166, 409, 463, 473, 635 and 1306
*Not*I	468 and 2983
*Sph*I	3451
*Not*I and *Sph*I	2616, 486 and 371
*Pst*I	3451
*Sac*I	1471 and 1980

Figure 3.14: Restriction profile of pSEAmi2P. **(A)** Table displaying the different restriction endonucleases used and the expected fragment sizes, which result from restriction digest of the pSEAmi2P plasmid. **(B)** Predicted plasmid map of pSEAmi2P vector. **(C)** Agarose gel depicting the products of restriction digest of pSEAmi2P. **[Lane 1]** Roche marker IV, **[Lane 2]** Uncut, **[Lane 3]** *Dde*I, **[Lane 4]** *Not*I, **[Lane 5]** *Sph*I, **[Lane 6]** *Not*I and *Sph*I, **[Lane 7]** *Pst*I and **[Lane 8]** *Sac*I.

In all cases, all the fragment sizes observed corresponded to the plasmid map and expected sizes, confirming the genetic integrity of the vector, Figure 3.14. The genomic integrity of the vector was then further confirmed by sequencing of the cloned region, which revealed

that no mutations had occurred during PCR and cloning processes (data not shown). This construct was then used for construction of an *ami2* knockdown strain.

3.4.2 Incorporation of pSEAmi2P into Msm to create a gene knockdown strain

The pSEAmi2P construct was electroporated into the SRS strain and the transformation efficiency, which was calculated using the pSE100 electroporation control, was determined to be 2.6×10^4 CFU/µg plasmid DNA. This was sufficient for efficient transformation of the knockdown vector (section 2.11.2). Clones were then selected and screened for site specific recombination of the pSEAmi2P into the *ami2* gene locus by Southern blot analysis using genomic DNA digested with *Pvu*I, Figure 3.15. As depicted in Figure 3.15, clones 2 and 3 displayed the expected hybridization pattern for a knockdown strain, confirming that they were the product of site-specific recombination of the vector. Clones 1, 4, 5 and 6 displayed the incorrect banding pattern suggesting that the recombination event did not occur at the correct site, these clones were discarded. Clone 2 was selected and used for further phenotypic analysis.

3.5 The Role of Ami1 in cell division and structural maintenance

A variety of assays were carried out on the Msm Δ*ami1* strain to evaluate the implications of deleting the *ami1* gene in the growth and development of Msm. These included analysis of growth kinetics, motility assays and single cell analysis utilizing different forms of microscopy. The outcome of these experiments is summarized below.

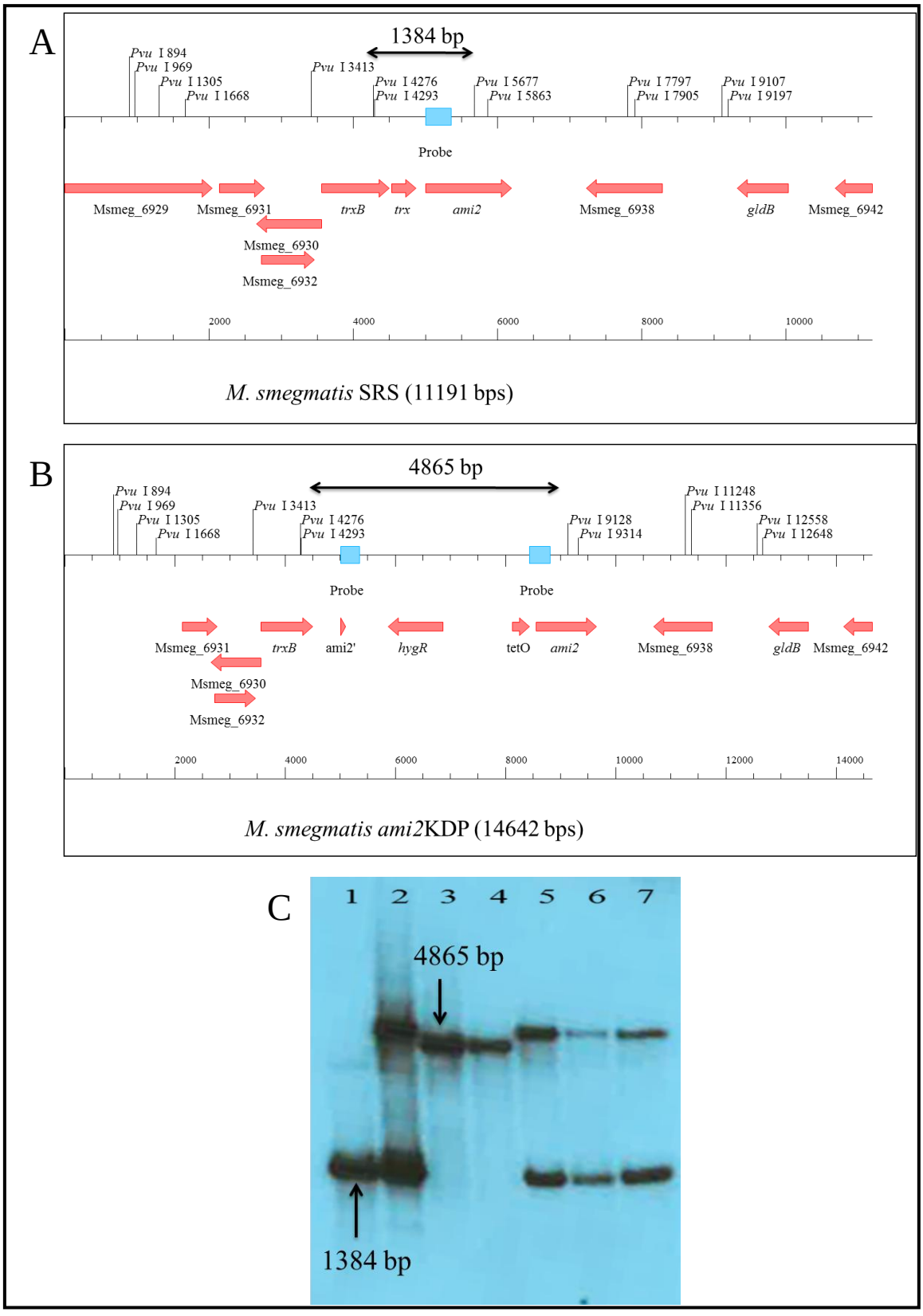


Figure 3.15: Southern Blot analysis of the Msm *ami2*KDP knockdown strain. **(A)** Genomic map of the wild type (carrying the ATC repressor – SRS) showing the expected wild type SRS hybridization pattern. **(B)** Genomic map of *ami2*KDP showing the expected mutant hybridization pattern. **(C)** Southern blot showing the hybridization pattern detected with the Probe; **[Lane 1]** SRS, **[Lane 2 to 7]** *ami2*KDP clone 1 to 6.

3.5.1 Ami1 does not play a significant role in determining growth rate

Growth analysis was carried out on the mc^{2}155 and Msm Δ*ami1* strains to evaluate the impact of Ami1 in regulating growth kinetics. This analysis was carried out using growth curves, conducted in triplicate with different batches of 7H9 media and different freezer stocks of the strain. This was done to ensure that the experimental results reflected three independent experiments. Growth assays were set up as detailed in section 2.7.1 and OD_{600nm} readings were taken every 3 hours as a measure of growth. The data was represented using a scatter plot, Figure 3.16.

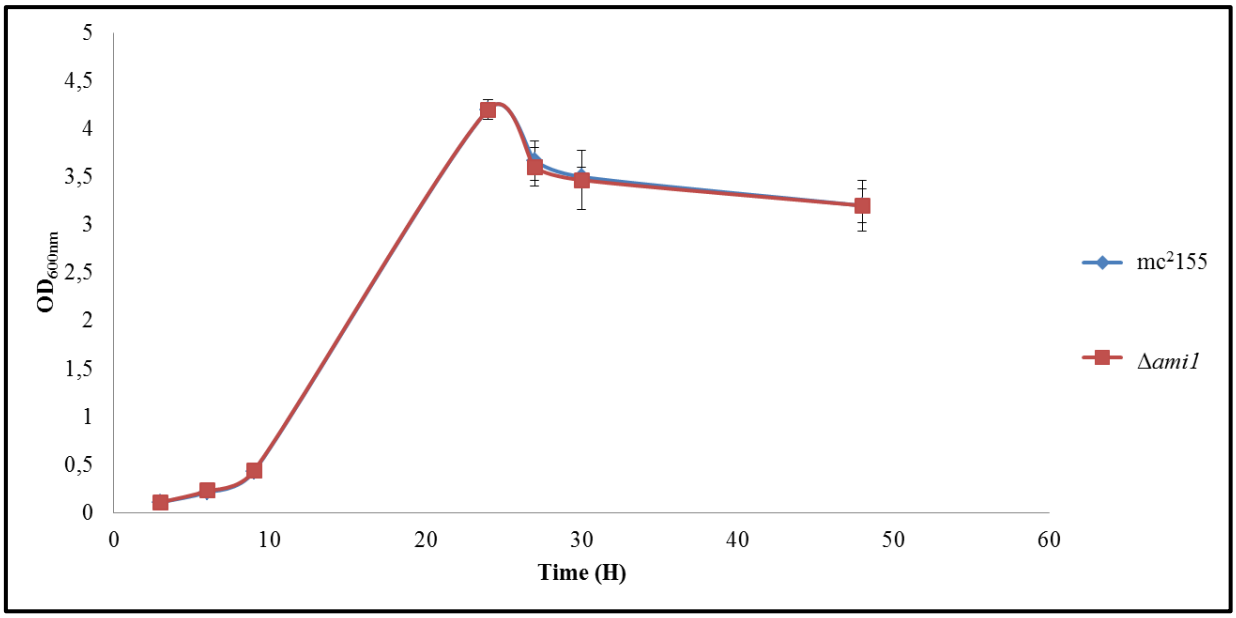


Figure 3.16: Growth kinetics of the Δ*ami1* strain. Shown is the increase in OD_{600nm} over a period of 48 hours. Error bars were determined using the standard deviation of the triplicate cultures and plotted on the graph as Y-axis error bars.

As shown in Figure 3.16, no significant difference was observed between the growth kinetics of the mc^{2}155 and Δ*ami1* strains suggesting that Ami1 does not play a significant role in the regulation of growth kinetics in Msm. There was, however, some difference in

the overall appearance of the culture as the Δ*ami1* strain began to form bacterial clumps after 30 hours of growth and the mc^{2}155 strain did not (data not shown). Since no significant effects were observed, these experiments did not include the complemented derivative.

3.5.2 Ami1 does not play a significant role in biofilm formation

Biofilm analysis was conducted on the mc^{2}155 and Δ*ami1* strains to investigate the impact of deleting *ami1* on the ability to form biofilms. Biofilm analysis was conducted as detailed in section 2.7.2. The initial CFUs for both strains were 2.31 × 10^6 CFU/ml for the mc^{2}155 and 2.17 × 10^6 CFU/ml for the Δ*ami1* strain.

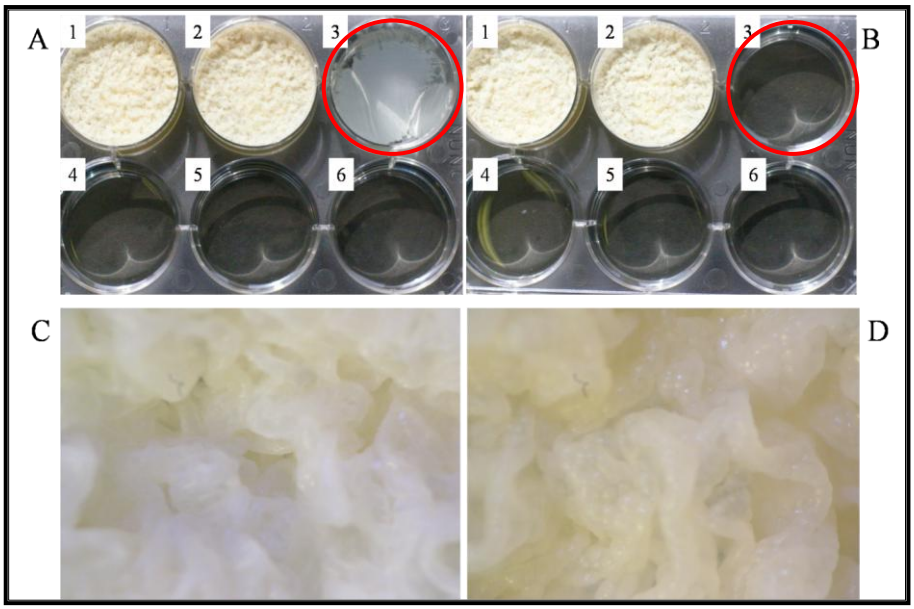


Figure 3.17: Biofilm formation with Δ*ami1* strain. **(A)** Biofilm formation in the mc^{2}155 strain at 1× magnification and **(C)** Biofilm formation in the mc^{2}155 strain at 45× magnification. **(B)** Biofilm formation of the Δ*ami1* strain at 1× magnification and **(D)** Biofilm formation of the Δ*ami1* strain at 45× magnification. 1 to 6 represents a ten-fold serial dilution of the starting inoculums, **[1]** 10^0 (undiluted), **[2]**10^1, **[3]**10^2, **[4]**10^3, **[5]**10^4 and **[6]**10^5. Red circle represents a marginal difference in the biofilm formation at the 10^3 dilution after incubation for 5 days.

Biofilm formation in these strains is shown in Figure 3.17. Biofilm formation is measured as a pellicle on the surface of a liquid culture in 6-well tissue culture plates. The biofilm does not form at inoculum concentrations below the 10^3 dilution as these wells did not

show pellicle formation and displayed only planktonic growth, Figure 3.17 A and B. At day five it can also be seen that biofilm formation has initiated in the10^3 dilution in mc^2155 and has not yet started in the corresponding Δ*ami1* well (red circle). In this case, the biofilm does however form by day 8 in the Δ*ami1* strain, indicating that there is a slight delay in formation of biofilms with the mutant, which was not statistically meaningful (data not shown). These data confirm that deletion of the *ami1* does not affect the capacity of Msm to form a biofilm. Figure 3.17 C and D depict the surface structure of the two biofilms, no significant structural differences between biofilms from the two strains were noted. This result suggests that *ami1* gene product does play a significant role in determining the overall structure of the biofilm.

3.5.3 Ami1 does not play a significant role in sliding motility

Mycobacteria have the ability to move on semi-solid media due to the presence of certain macromolecules and lipids on the outer surface of the cell (Recht *et al*., 2001). We reasoned that deletion of *ami1* may result in changes in the composition or structure of the cell wall, which would affect the organism's ability to slide. We tested sliding motility, on two types of agar, for both the mc^2155 and Δ*ami1* strains to determine whether Ami1 plays a role in sliding motility (section 2.7.3).

Mycobacterial sliding of both the mc^2155 and Δ*ami1 s*trains on two different semi solid media is depicted in Figure 3.18. There was no significant difference between sliding phenotypes of the mc^2155 and Δ*ami1* strains on both media suggesting that Ami1 does not play a significant role in the sliding motility. Bacterial sliding motility appears to be different when using different types of media supports as seen in Figure 3.18. On 7H9 media, the cells exhibit a branch-like sliding phenotype where the strain forms radiating

branches from the inoculation point moving away towards the edge. However, the same strains display a different, more diffuse sliding morphology on M63 media. The basis for these differences is currently unknown.

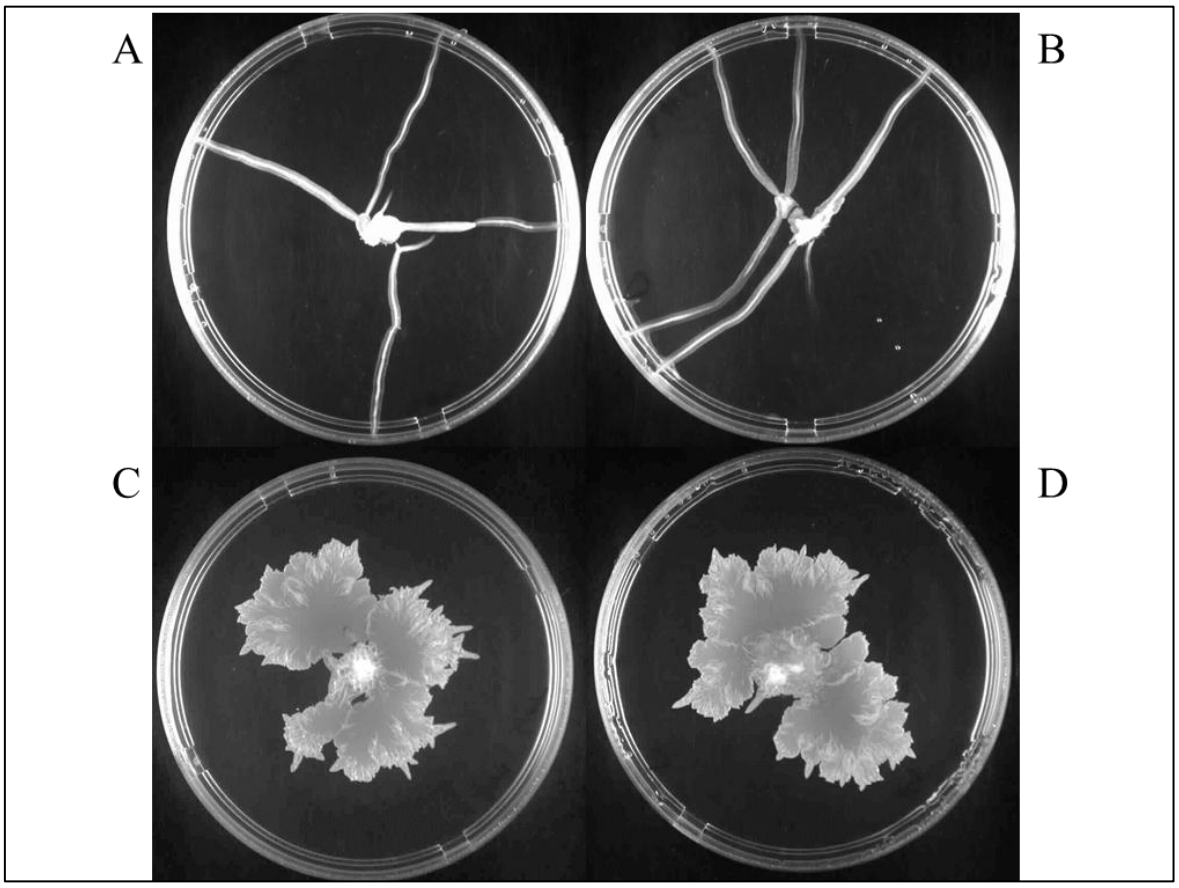


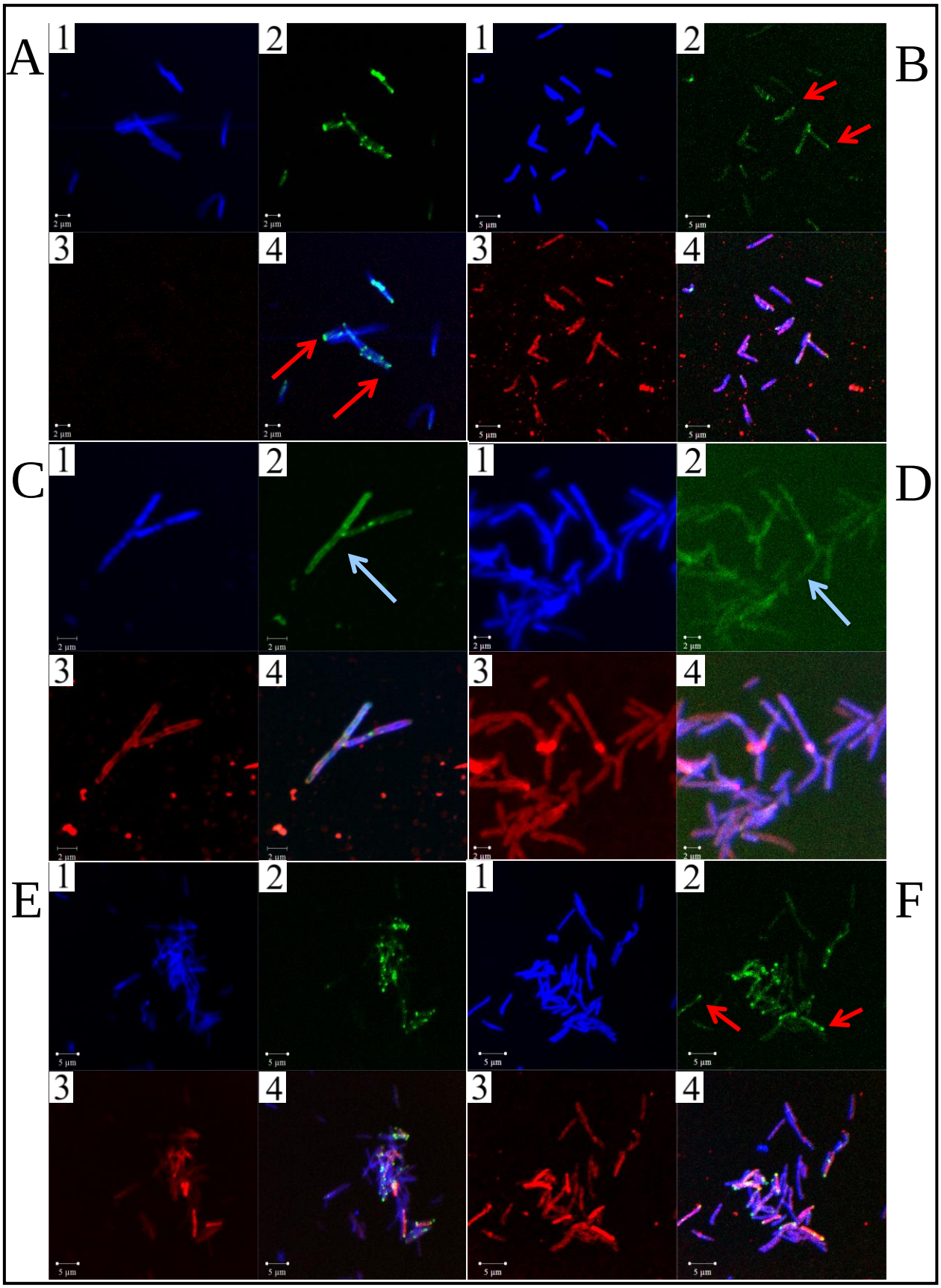
Figure 3.18: Sliding motility of the mc^{2}155 and Δ*ami1 s*trains on 7H9 and M63 agar. **(A)** and **(B)** 7H9 media containing 0.3 % agar, **(C)** and **(D)** M63 media containing 0.3 % agar. **(A)** and **(C)** mc^{2}155 strains sliding plates, **(B)** and **(D)** Δ*ami1* strains.

3.5.4 Ami1 plays an important role in cell division, cell growth and cell shape maintenance

The overall structure of individual cells was evaluated using a variety of microscopic techniques. These were carried out to evaluate the possible role Ami1 plays in cell growth and division by observing the structural defects caused by the removal of the *ami1* gene.

One of the microscopic techniques employed was confocal microscopy. This was conducted to evaluate two main aspects, (I) The localization of new PG synthesis by assessing localization of fluorescent vancomycin and (II) Assessment of cell size and shape. Localization of fluorescent vancomycin is an important and interesting component because it gives one an indication of possible sites for active PG remodeling and insertion of new PG units since vancomycin will bind new, unlinked PG (Hett and Rubin, 2008). Two additional stains used were DAPI-which stains nucleic acids and Cellmask™ orange - , which stains the phospholipid bilayer. The inclusion of multiple stains was done to allow the acquisition of composite images. Confocal microscopy was conducted on the mc^2155, Δ*ami1* and Δ*ami1::*pMVami1 strains, Figure 3.19.

Confocal microscopy on the mc^2155, *ami1* deletion mutant and complemented derivative is shown in Figure 3.19. Polar localization of vancomycin on all three strains is depicted by the bright green spots at the cellular poles (red arrow), the Δ*ami1* strain appears to have reduced polar vancomycin staining, Figure 3.19 G [II] and G [IV] (blue arrows), when compared to both the mc^2155 and Δ*ami1::*pMVami1 strains, Figure 3.19 G [I] and G [III]. It has been demonstrated that mycobacteria as well as other actimomycetes grow by extension of and incorporation of new PG at the poles (Thanky *et al*., 2006). Polar localization of fluorescent vancomycin was expected due to the active nature of the mycobacterial poles resulting in an abundance of unlinked PG (Thanky *et al*., 2006). The data showing polar localization of fluorescent vancomycin on the mc^2155 strain confirms previous observations that mycobacteria grow by incorporating new PG at the poles. The diffused vancomycin staining observed on the Δ*ami1* strain suggests a defect in polar localization of new peptidoglycan and a possible role in the establishment of an active growth pole. Of note is the observation that there was a difference in size between mc^2155


A
1
2
3
4
B
1
2
3
4
C
1
2
3
4
D
1
2
3
4
E
1
2
3
4
F
1
2
3
4

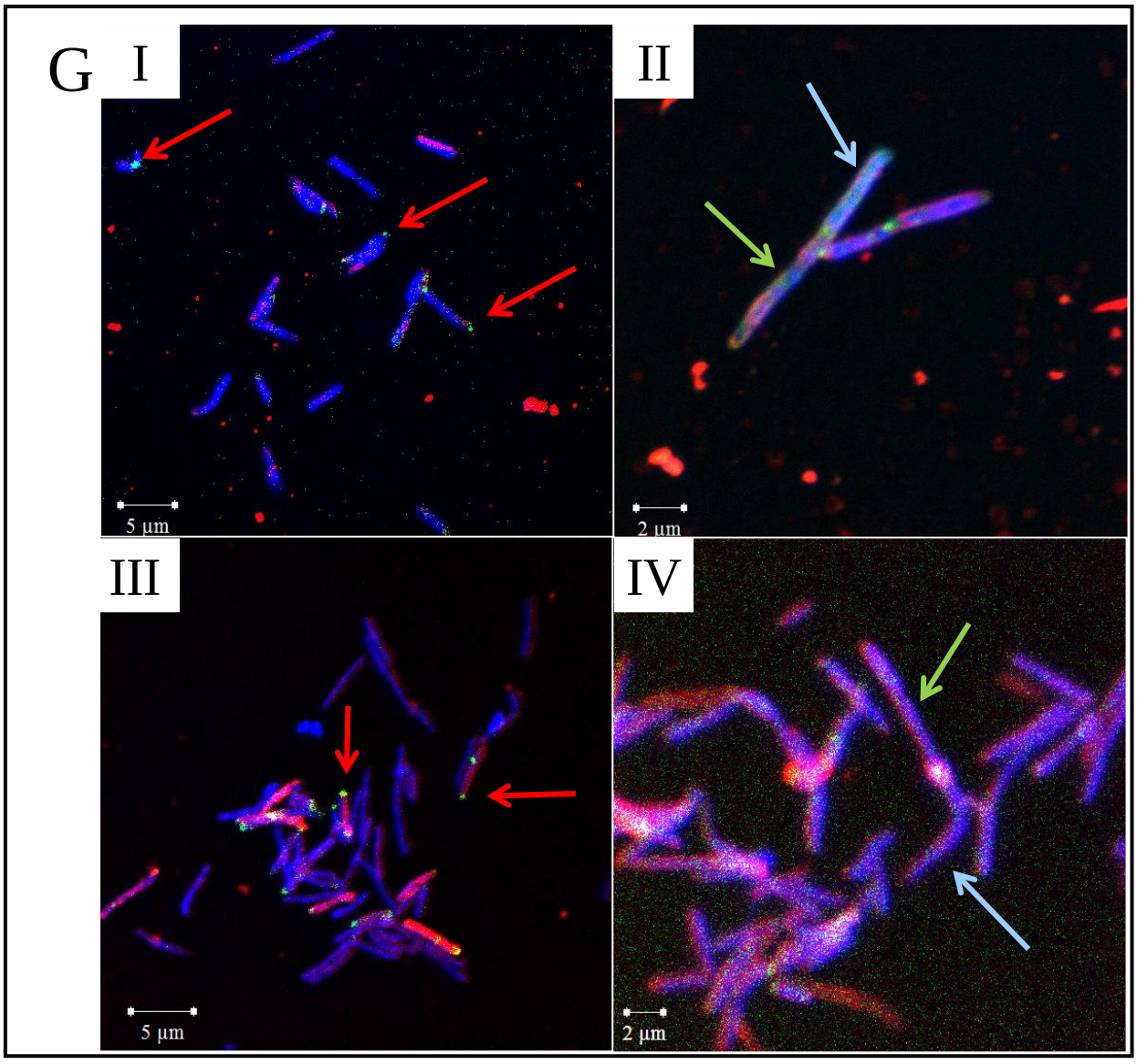


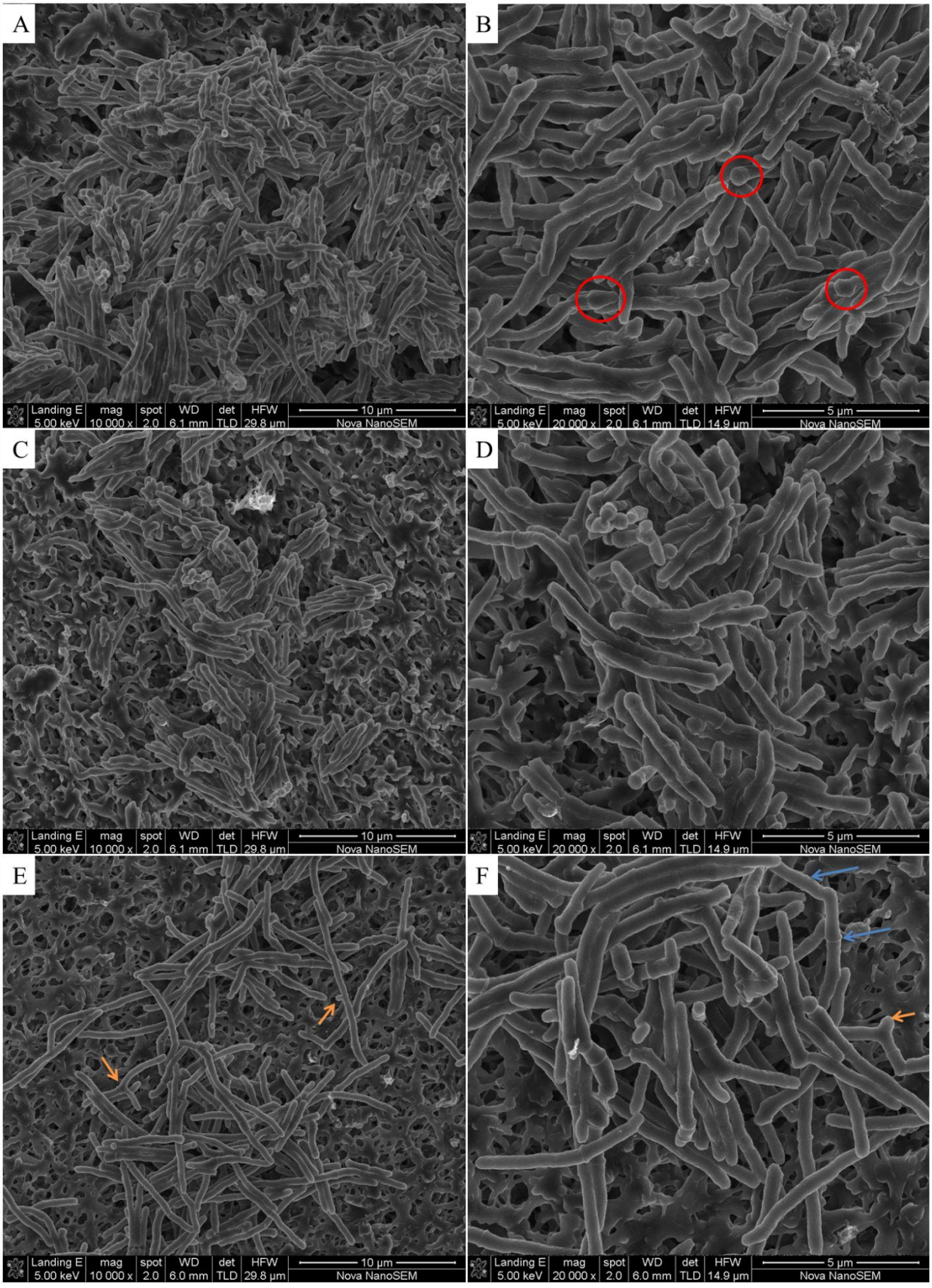
Figure 3.19: Confocal microscopy comparing mc^{2}155, Δ*ami1* and Δ*ami1::*pMVami1. **(1)** DAPI staining, **(2)** fluorescent vancomycin, **(3)** Cellmask™ Orange and **(4)** overlay of all three stains. **(A)** and **(B)** mc^{2}155, **(C)** and **(D)** Δ*ami1* and **(E)** and **(F)** Δ*ami1::*pMVami1. **(G)** Higher magnification view of the images shown in **(B) [I]**, **(C) [II], (F) [III]** and **(D) [IV]** overlays showing the polar vancomycin staining observed on the mc^{2}155 and Δ*ami1::*pMVami1 strains and the defused vancomycin staining observed on the Δ*ami1* strain. Red arrows indicated vancomycin polar localization. Blue arrows: diffused vancomycin staining Green arrow indicates a long cell. Scale for **(A)**, **(C)** and **(D)** 2 µm and **(B)**, **(E)** and **(F)** 5 µm.

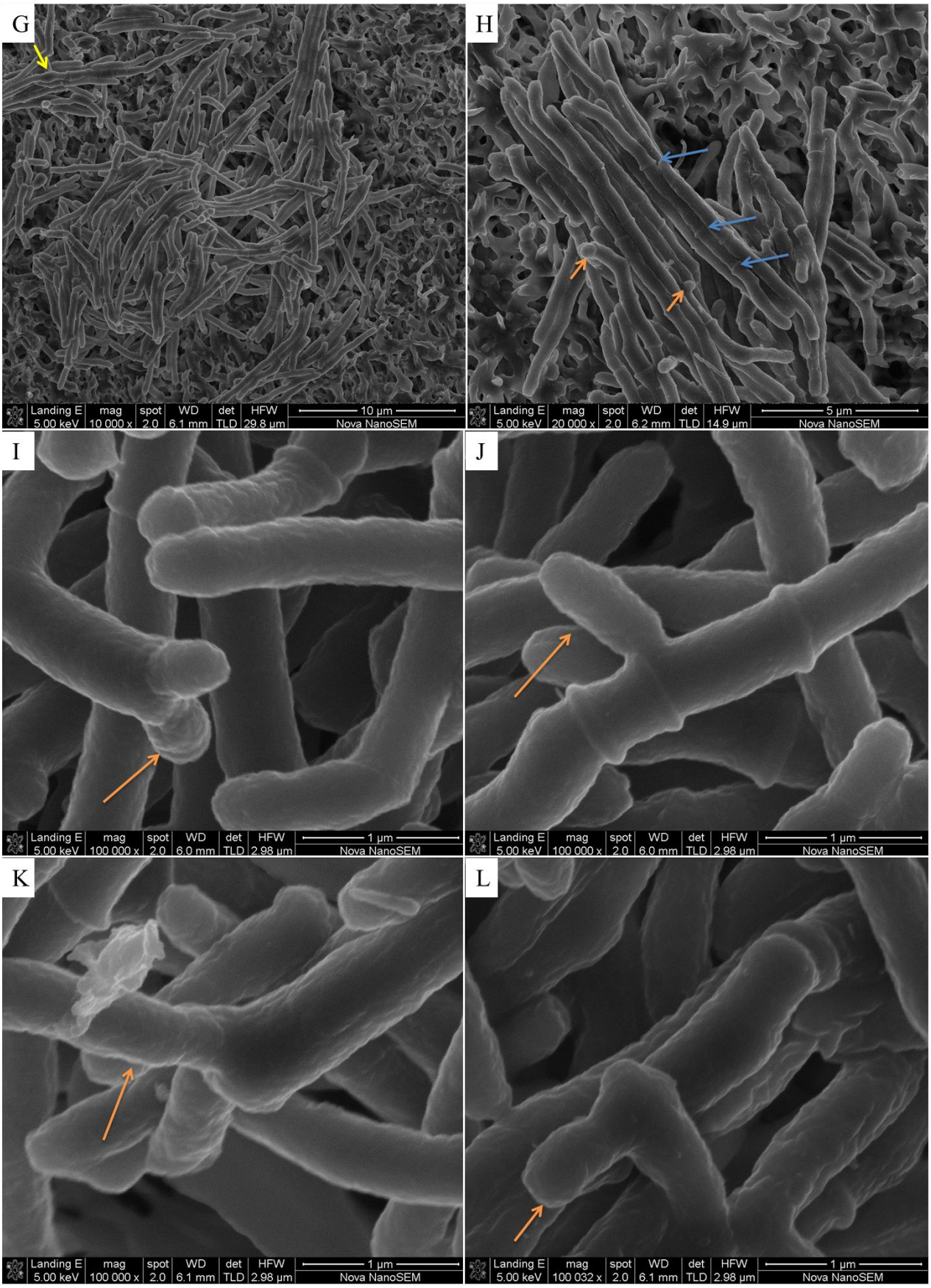
and the Δ*ami1* strains. Cells from the mc^{2}155 strain are approximately 4 to 8 µm in length while cells from the Δ*ami1* strain range between 6 to 12 µm in length, Figure 3.19D, G [II] and G [IV], green arrow. Importantly this phenotype in the Δ*ami1* mutant does revert back to that seen in the mc^{2}155 strain when the *ami1* gene is reintroduced as illustrated by the Δ*ami1::*pMVami1 confocal images, which appear more similar to the mc^{2}155 strain than

the Δ*ami1* strain. This confirms that the observed increase in cell length was due to deletion of *ami1*.These data reveal two possible roles for Ami1 in Msm namely, the determination of cell size and correct localization of new PG synthesis.

In addition to confocal microscopy, SEM was also conducted on these strains to acquire a high resolution image of the cell surface and to confirm the elongated phenotype of the Δ*ami1* cells. In addition, all three strains mentioned above were also subjected to imipenem exposure before cells were prepared for SEM (section 2.8.2). Imipenem is a β-lactam antibiotic, which is impervious to β-lactamase degradation (Livermore and Woodford, 2000). This antibiotic acts by binding to the terminal D-alanine residues thus preventing crosslinking leading to inhibition of PG crosslinking and growth (Livermore and Woodford, 2000). A recent study demonstrated that the addition of sub-lethal levels of meropenem (β-lactam antibiotic belonging to the same group as imipenem) to Mtb cultures resulted in polar bulging of cells as a result of inhibited peptide crosslinking (Kumar *et al.*, 2012). Given the phenotypes observed with confocal microscopy, we reasoned that this assay would help confirm the role of *ami1* in polar PG synthesis in Msm.

SEM revealed a number of robust phenotypes, the first being chaining or filamentation of cells in the Δ*ami1* strain, see Figure 3.20 E-H, where a number of the cells display filamentous growth, depicted by long filament consisting of cells joined together by incomplete division septa, indicated by the blue arrows. These filaments consist of 3 to 8 cells and range from 5 to 20 μm in length. Non-polar bulging, or branching, was also observed, depicted by the yellow arrow in Figure 3.20 G. Interestingly, there was a


A
Landing E 5.00 keV | mag 10 000 x | spot 2.0 | WD 6.1 mm | det TLD | HFW 29.8 µm | 10 µm | Nova NanoSEM
B
Landing E 5.00 keV | mag 20 000 x | spot 2.0 | WD 6.1 mm | det TLD | HFW 14.9 µm | 5 µm | Nova NanoSEM
C
Landing E 5.00 keV | mag 10 000 x | spot 2.0 | WD 6.1 mm | det TLD | HFW 29.8 µm | 10 µm | Nova NanoSEM
D
Landing E 5.00 keV | mag 20 000 x | spot 2.0 | WD 6.1 mm | det TLD | HFW 14.9 µm | 5 µm | Nova NanoSEM
E
Landing E 5.00 keV | mag 10 000 x | spot 2.0 | WD 6.0 mm | det TLD | HFW 29.8 µm | 10 µm | Nova NanoSEM
F
Landing E 5.00 keV | mag 20 000 x | spot 2.0 | WD 6.0 mm | det TLD | HFW 14.9 µm | 5 µm | Nova NanoSEM


G
Landing E 5.00 keV | mag 10 000 x | spot 2.0 | WD 6.1 mm | det TLD | HFW 29.8 µm | 10 µm | Nova NanoSEM
H
Landing E 5.00 keV | mag 20 000 x | spot 2.0 | WD 6.2 mm | det TLD | HFW 14.9 µm | 5 µm | Nova NanoSEM
I
Landing E 5.00 keV | mag 100 000 x | spot 2.0 | WD 6.0 mm | det TLD | HFW 2.98 µm | 1 µm | Nova NanoSEM
J
Landing E 5.00 keV | mag 100 000 x | spot 2.0 | WD 6.0 mm | det TLD | HFW 2.98 µm | 1 µm | Nova NanoSEM
K
Landing E 5.00 keV | mag 100 000 x | spot 2.0 | WD 6.1 mm | det TLD | HFW 2.98 µm | 1 µm | Nova NanoSEM
L
Landing E 5.00 keV | mag 100 032 x | spot 2.0 | WD 6.1 mm | det TLD | HFW 2.98 µm | 1 µm | Nova NanoSEM

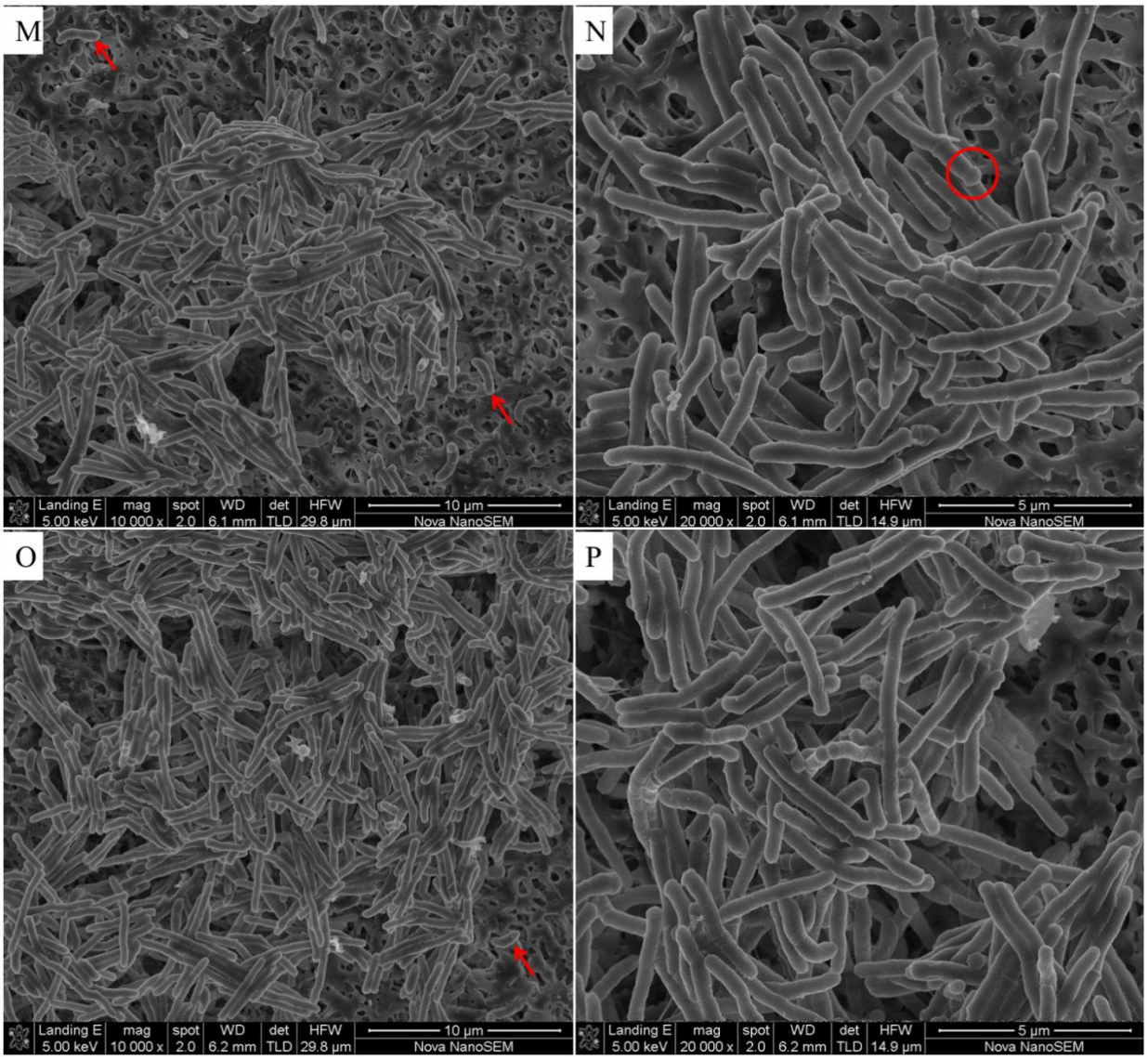


Figure 3.20: SEM images of mc^{2}155, Δ*ami1* and Δ*ami1::*pMVami1 strains. Cells were grown to an OD_{600nm} of 0.3, the cultures were split in half and one was grown in media contain 2.5 ηg/ml imipenem (Sigma) and the second in media without imipenem for 1.5 hours. The cells were then harvested, prepared for SEM as in section 2.8.2 followed by image capture. **(A)** and **(B)** mc^{2}155 treated with 2.5 ηg/ml imipenem, **(C)** and **(D)** mc^{2}155, no antibiotic treatment (**E)** and **(F)** Δ*ami1* treated with 2.5 ηg/ml imipenem, **(G)** and **(H)** no antibiotic treatment Δ*ami1* , **(I)** and **(J)** High magnification images of the lateral growth seen in the Δ*ami1* strain treated with 2.5 ηg/ml imipenem, **(K)** and **(L)** High magnification images of the lateral growth from untreated Δ*ami1*, **(M)** and **(N)** Δ*ami1::*pMVami1 treated with 2.5 ηg/ml imipenem, **(O)** and **(P)** Untreated Δ*ami1::*pMVami1. Red circles: polar bulging, Blue arrows: division septa, Orange arrows: Lateral growth, Yellow arrow: non polar bulging and Red arrows: miniature cells.

reduction of the chaining phenotype when the cells were treated with imipenem, considerably fewer cells formed chains when treated with imipenem, Figure 3.20 E and F, compared to untreated cells, Figure 3.20 G and H. Polar bulging was also observed in both

the wild type and Δ*ami1*::pMVami1 strains when subjected to imipenem exposure, depicted by Figure 3.20B and D, consistent with the result observed by Kumar et. al. (2012) this phenotype however was not evident in the Δ*ami1* strains shown by the lack of polar bulging depicted in Figure 3.20E and F. A striking phenotype observed in the *Δami1* treated and untreated samples was the formation of lateral buds that eventually form lateral cells shown by the orange arrow in Figure 3.20 E to L. This lateral growth occurs both at the poles and along the cell suggesting that there is some mis-regulation of cell growth and placement of active polar growth in the *ami1* mutant. All these observed phenotypes revert back to that seen in the wild type strain when the *ami1* gene is reintroduced as illustrated by the Δ*ami1::*pMVami1 phenotype, Figure 3.20 M to P, confirming that these defects were due to deletion of *ami1*. Of note, however, is the fact that the complemented strain displayed the presence of miniature cells depicted by the red arrows, presumably through aberrant expression or the fact that the complemented *ami1* gene was not integrated at the native locus.

To get better insight into the nature of the chaining phenotype TEM was conducted on these strains. The main objective for employing this technique was to obtain cross-sectional images of the cells and the septa. Upon observing the chaining phenotype with SEM, we reasoned that this may be a result of the inability to form a full septum or degrade the fully formed septum hence resulting in two distinct cells, which are unable to detach from each other. Unlike SEM the cells were not subjected to imipenem exposure, they were grown and prepared for TEM as in section 2.8.3 and images were taken, Figure 3.21.

Similar to that observed in the SEM images, the TEM data revealed the presence of filamentous growth exhibited by the Δ*ami1* strain, Figure 3.21 C and D, these cells appear

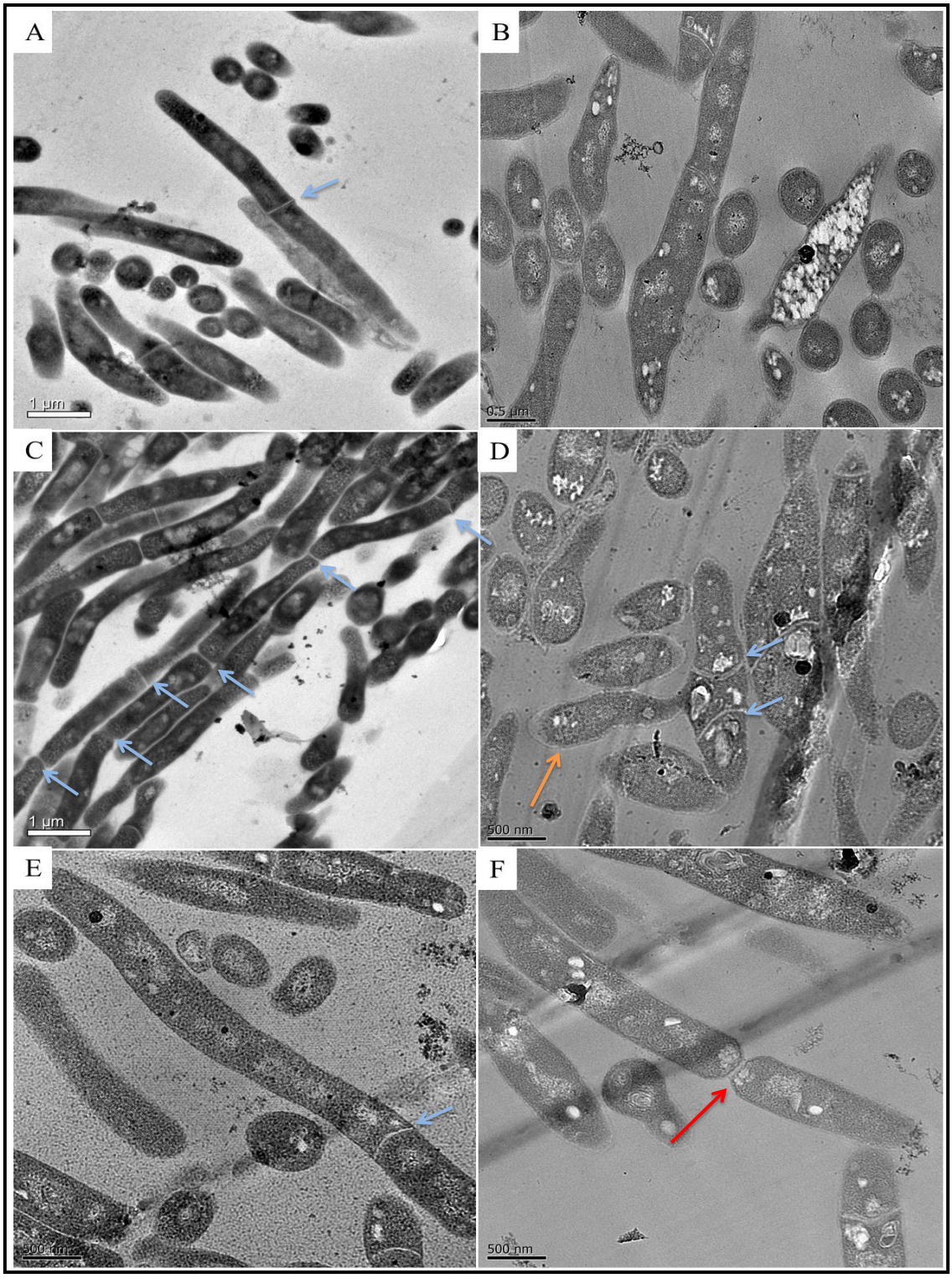


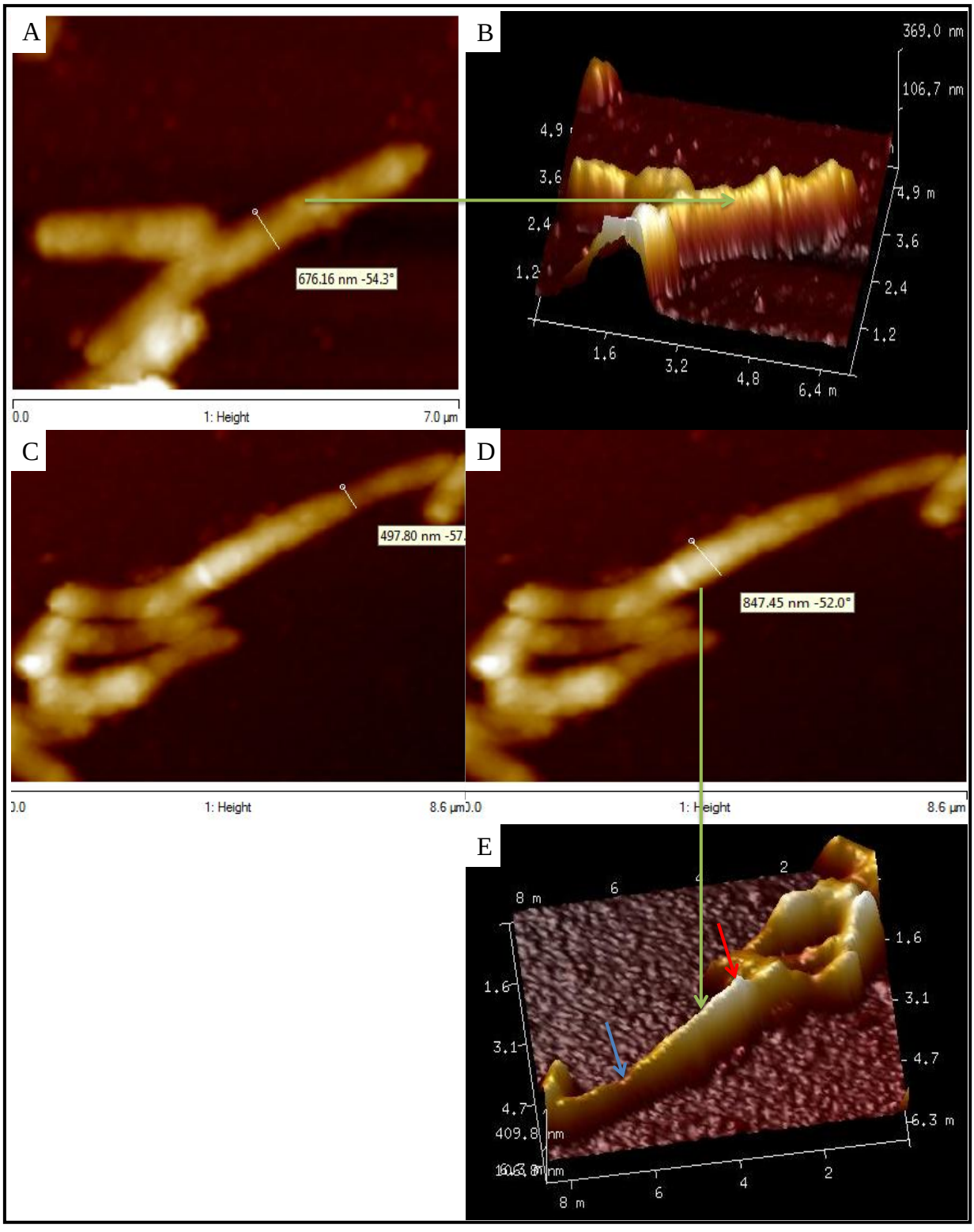
Figure 3.21: TEM images of the mc^{2}155, Δ*ami1* and Δ*ami1::*pMVami1 strains. **(A)** and **(B)** mc^{2}155, **(C)** and **(D)** Δ*ami1*, **(E)** and **(F)** Δ*ami1::*pMVami1. Blue arrows: Division septum, Orange arrows: Lateral growth, and Red arrows: septation.

to contain fully formed septa and display the presence of lateral growth, which appears to be a result of pressure applied by adjacent cells, preventing longitudinal extension, Figure 3.21 D. These phenotypes revert back to the mc^2155 morphology when the *ami1* gene is reintroduced illustrated by the Δ*ami1::*pMVami1 phenotype, Figure 3.21 E to F. The Δ*ami1::*pMVami1 strain also appears to divide properly as depicted by the septation event illustrated by the red arrow, Figure 3.21F. The reversion of the phenotype in the wild type strain confirms that these effects are due to loss of *ami1*.

Finally, these strains were also analyzed using AFM. This was conducted to determine possible variations in surface structure between the strains.

AFM data revealed the surface Δ*ami1* strain was irregular in nature, Figure 3.22 C, D and E, showing variation in the width of a single cell ranging from 497 nm to 847 nm, a phenomenon also represented by high peaks and low troughs in the 3 dimensional image. Both the mc^2155 and Δ*ami1::*pMVami1 strains are approximately 600 nm to 700 nm in width, and unlike the mutant strain, the cell width of the cells appears to be the same along the entire cell, Figure 3.22 A and F.

Collectively, these microscopic data reveal three major phenotypes, (I) Deletion of *ami1* led to the formation of long filamentous cells consisting of 3 to 8 cells attached to each other. (II) Deletion of *ami1* resulted in the formation of lateral growth at both the internal poles possibly as a result of the cell's inability to grow in a longitudinal manner and at the extreme poles. (III) Deletion of *ami1* resulted in irregular cell width as depicted by AFM data. In all cases the phenotypes reverted back to that seen in the mc^2155 wild type strain upon reintroduction of the *ami1* gene in the complemented derivative. This confirms that the defects observed, were due to loss of the *ami1* gene.


A
676.16 nm -54.3°
0.0
1: Height
7.0 µm
B
369.0 nm
106.7 nm
4.9 m
3.6
2.4
1.2
1.6
3.2
4.8
6.4 m
C
497.80 nm -57.
0.0
1: Height
8.6 µm
D
847.45 nm -52.0°
0.0
1: Height
8.6 µm
E
8 m
6
4
2
1.6
3.1
4.7
6.3 m
409.8 nm

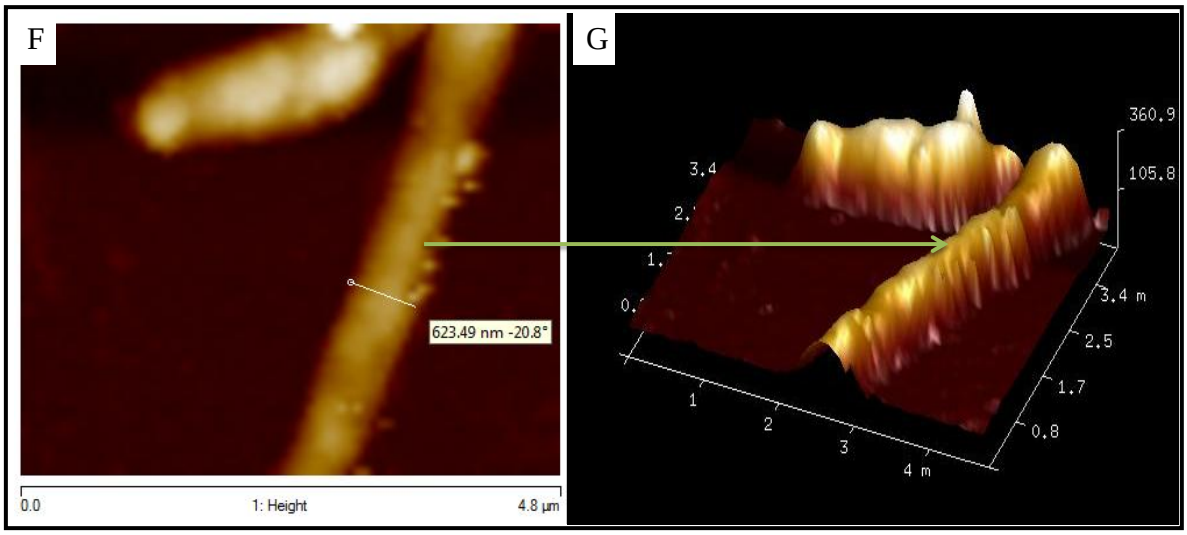


Figure 3.22: AFM images of the mc^{2}155, Δ*ami1* and Δ*ami1::*pMVami1 strains. **(A)**, **(C)**, **(D)** and **(F)** 2 dimensional AFM height images, **(B)**, **(E)** and **(G)** 3 dimensional AFM height images. **(A)** and **(B)** mc^{2}155 strain. **(C)**, **(D)** and **(E)** Δ*ami1*, **(F)** and **(G)** Δ*ami1::*pMVami1. Green arrows: Indicate the orientation of the 3 dimensional image, Blue arrows: low region, and Red arrows: high peak.

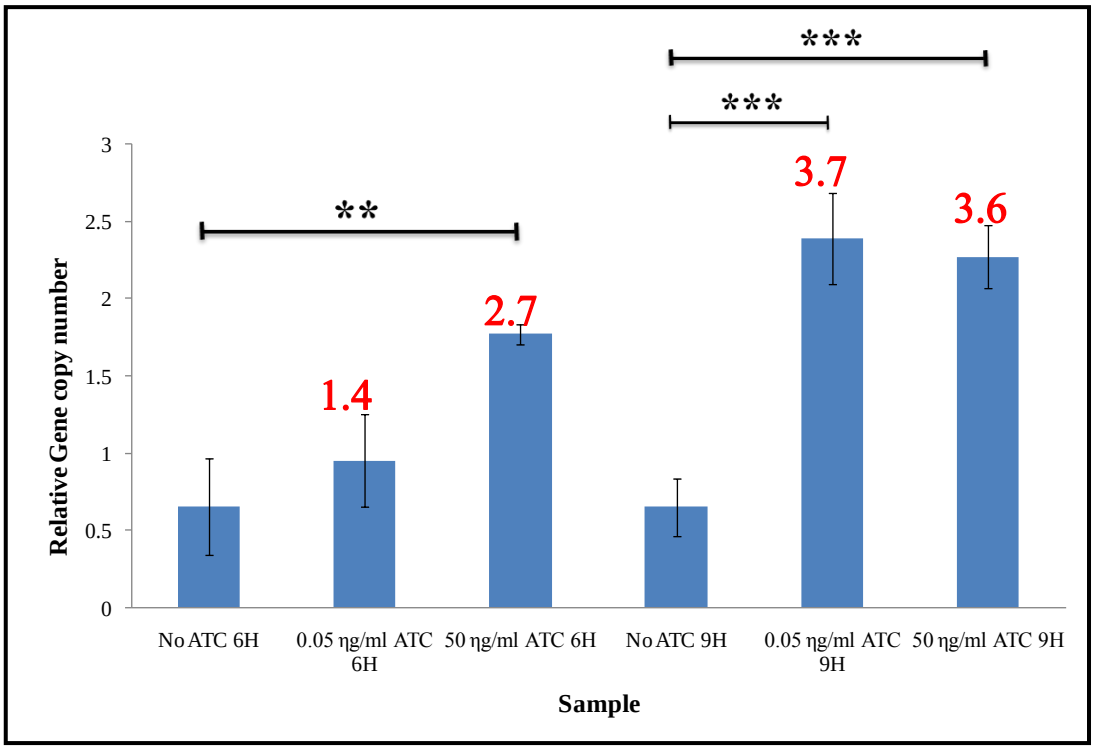
3.6 The Role of Ami2 in cell growth

The second cell wall amidase evaluated in this study was *ami2.* Attempts to delete this gene were not successful, suggesting that it was essential for growth. Hence we studied the function of Ami2 through targeted gene depletion by creating a strain that allowed for regulated *ami2* expression in response to ATC.

3.6.1 Confirmation of regulated gene expression in the *ami2* knockdown strain

Gene expression analysis was conducted to evaluate the responsiveness of the *ami2* depletion strain to the ATC inducer. This was done to determine whether the absence or presence of ATC led to significantly depleted or elevated levels of *ami2* gene transcription.

The data revealed low level, stable expression of the *ami2* gene, in the uninduced state when the culture contained no ATC, Figure 3. 22. The culture containing 0.05 ηg/ml ATC contained slightly higher levels of *ami2* mRNA, which increased significantly after 9 hours.



p<99 %

Figure 3.23: Expression analysis of ATC regulated gene expression. Shown is a bar graph depicting the level of cellular *ami2* mRNA (in relation to the *sigA* standard level) in the absence and presence of ATC at 6 and 9 hours post induction. Error bars were determined using standard deviation and student's *t*-test was conducted using a confidence level of 99 % to determine significance. Red text indicates mRNA fold increase from the respective uninduced state

The culture containing 50 ηg/ml ATC – that is with a higher concentration of inducer - contained significantly higher *ami2* mRNA levels at both 6 and 9 hours after induction, Figure 3.23. These data confirm that the knockdown strain does allow for regulated gene expression of *ami2* in response to ATC. These data also show that the *ami2* mRNA levels are not completely abolished in the absence of ATC thus basal level expression does occur, Figure 3.23, and this needs to be considered when assessing the phenotypes. The data also shows that *ami2* expression, 6 hours post induction, responds to ATC concentration depicted by the *ami2* mRNA fold increase relative to the uninduced state, Figure 3.23 (red text). This regulatory effect appears to be lost 9 hours post induction as both the culture containing 0.05 ηg/ml and 50 ηg/ml ATC appear to express *ami2* mRNA at the same level, Figure 3.23 (red text), suggesting escape from ATC regulation.

3.6.2 Ami2 plays a role in determining growth rate

Growth analysis was carried out on the *ami2*KDP and mc^{2}155 strains to evaluate the impact of depleting Ami2 on growth of Msm, Figure 3.24.

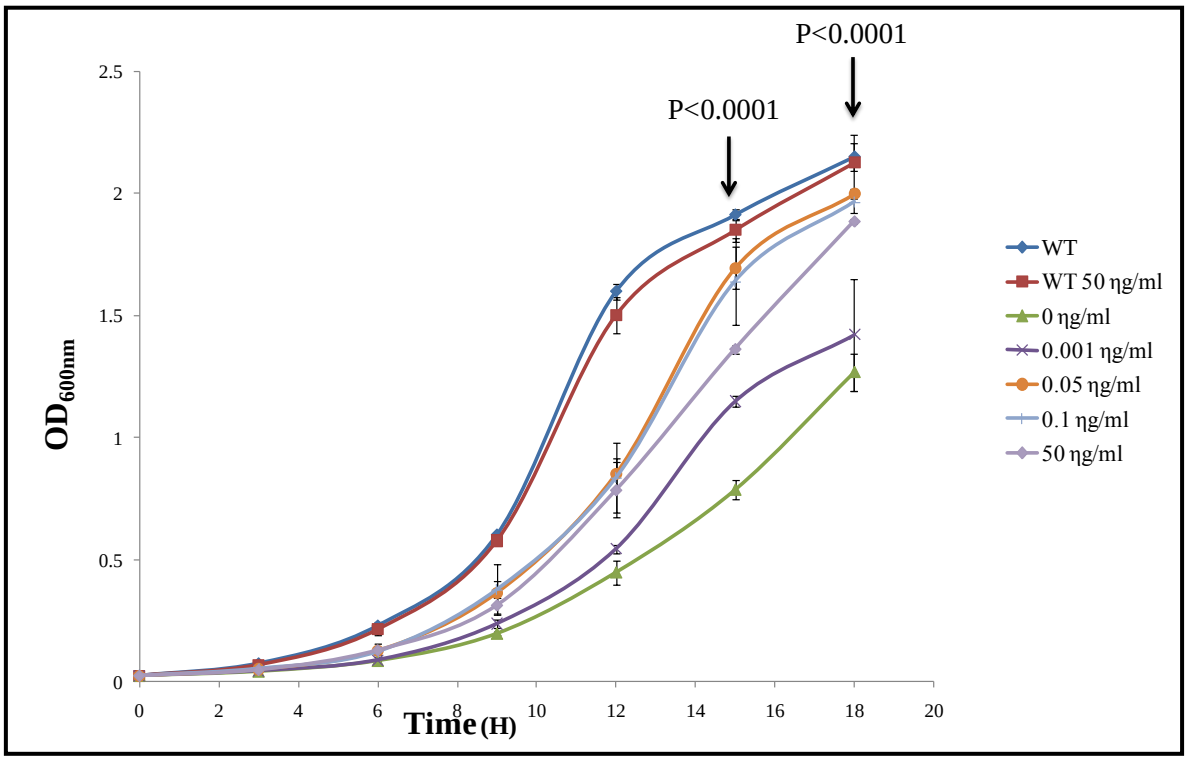


Figure 3.24: Depletion of *ami2* results in reduced growth of Msm. Growth curve showing the growth kinetics of the *ami2*KDP strains in response to different concentrations of ATC. Error bars were determined using the standard deviation of the triplicate cultures and plotted on the graph.

The two mc^{2}155 cultures (one grown in the presence of ATC and the second grown in the absence of ATC) grew at a similar rate. The culture containing ATC appears to grow at a slightly slower rate suggesting ATC possesses a very low, insignificant, growth inhibitory effect against mc^{2}155, Figure 3.24. This is an important control as it confirms that the inducer has no effect on cell growth. The *ami2*KDP culture, which contained no ATC grew the slowest, confirming that *ami2* is important for growth, Figure 3. 23. The strain grown in the absence of ATC does eventually catch up with the induced strains (data not shown) suggesting escape from ATC dependent *ami2* expression, this data correlates with the diminished regulation seen in the RT data. The growth rate of *ami2*KDP increased with

increasing ATC levels until a concentration of 0.05 ηg/ml following, which, the growth rate decreased as more ATC was added to the culture. The *ami2*KDP strain did not show growth comparable to the wild type with any of the ATC concentrations used, presumably due to the fact that the regulated expression was not similar to the native expression levels that would be seen in mc^2155 under the different growth phases. The concentration of ATC that resulted in optimal growth was 0.05 ηg/ml. To determine whether the growth retardation of the strain, in the absence of ATC was significant a student's *t*-test was conducted comparing the 2 cultures, i.e the no ATC culture and the culture containing 0.05 ηg/ml. Two time points were taken, 15 and 18 hours post induction and the P values were determined. Figure 3.24 shows that the difference between these two cultures at these two time points is significant up to a confidence level of greater than 99.99%, confirming that depletion of *ami2* gene expression results in significant growth arrest.

3.6.3 Ami2 plays role in sliding motility

To evaluate the role of Ami2 in cellular motility, the sliding motility assay was conducted on both the mc^2155 and *ami2*KDP strains on plates containing different amounts of the inducer, ATC, Figure 3.25.

Interestingly, the wild type mc^2155 displayed progressively more sliding as ATC concentration was increased on both the M63 and 7H9 media, Figure 3.25. The *ami2*KDP strains did not slide in the absence of ATC when grown in 7H9 media; however the sliding progressively increased with the addition of ATC, suggesting that depletion of Ami2 results in reduced sliding motility, Figure 3.25. The structure of the sliding colony mass appears different with the *ami2*KDP strain, which shows a branch structure that is distinct from that seen in mc^2155 strain, Figure 3.25 B. With regard to the M63 media assay, the

*ami2*KDP strain displayed sliding in the absence of ATC however the sliding appeared to be unstructured. At an ATC concentration of 0.05 ηg/ml the bacterial mass gains structural integrity but does not slide significantly and at an ATC concentration of 50 ηg/ml the sliding mass retains both structure and it also slides, Figure 3.25 A, confirming that *ami2* gene expression is required for sliding motility.

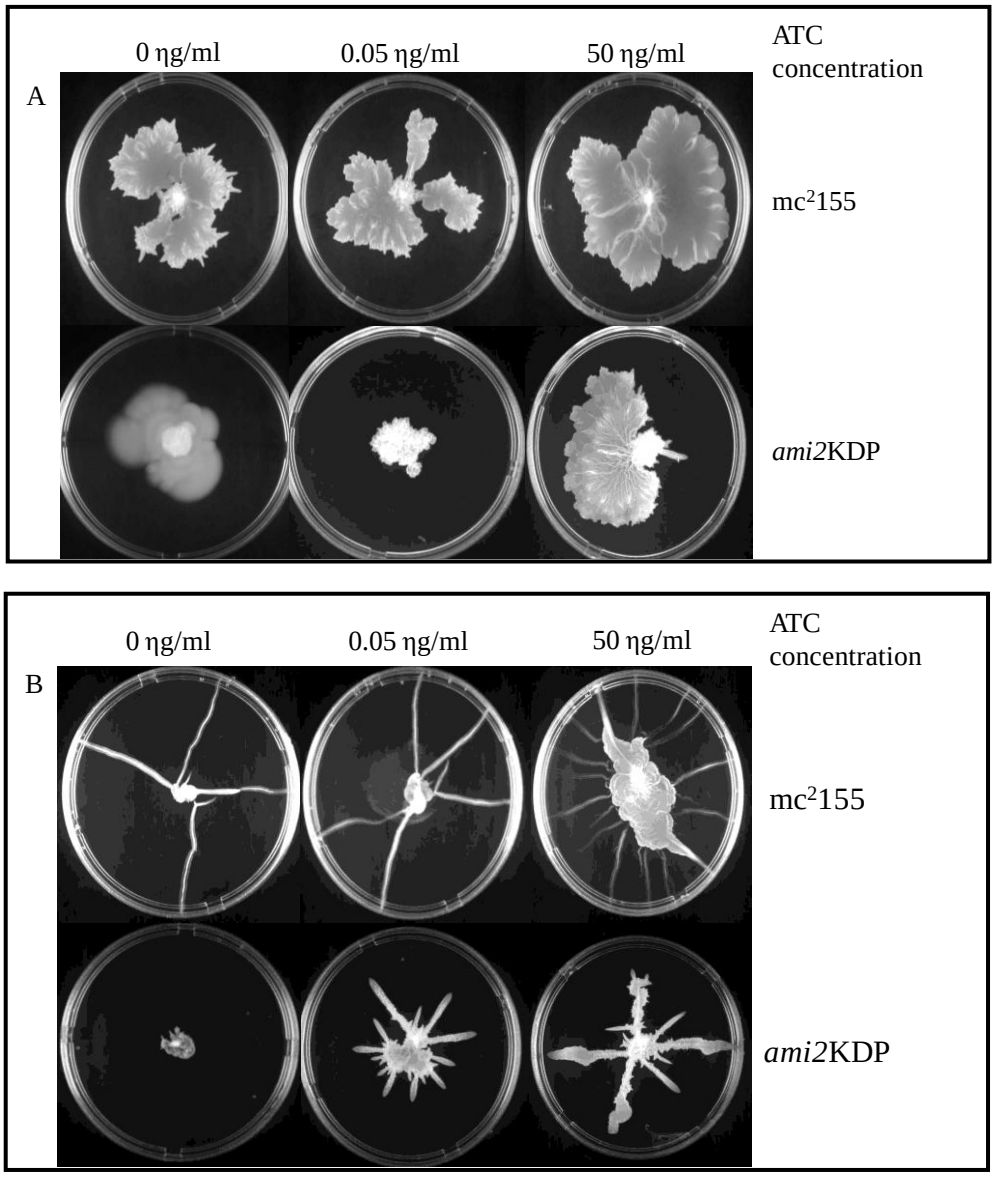


Figure 3.25: Sliding motility assays with the *ami2* depletion strains. Images show mc^2155 and *ami2*KDP strains sliding motility on 7H9 and M63 agar. **(A)** M63 media containing 0.3 % agar and **(B)** 7H9 media containing 0.3 % agar.

3.6.4 Ami2 plays role in determining colony morphology

Cultures of the *ami2* depleted strain were spotted onto solid media to determine if *ami2* plays a role in colony morphology; the data are shown in Figure 3.26.

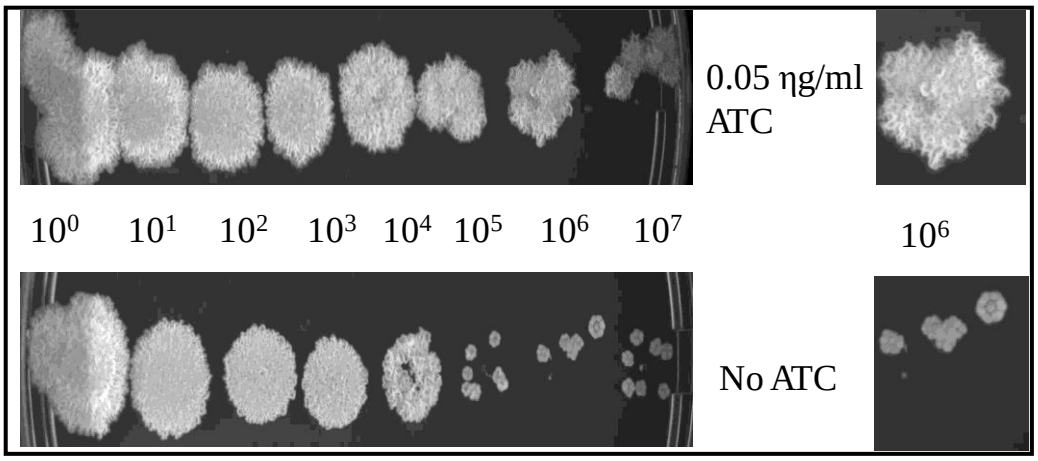


Figure 3.26: The impact of *ami2* depletion on colony morphology. Images show *ami2*KDP spotting assay on 7H10 agar. Top depicts *ami2*KDP colony morphology on agar supplemented with 0.05 ηg/ml ATC and bottom shows *ami2*KDP colony morphology on agar without ATC. Spots represent dilution gradient of an OD = 0.8 Msm *ami2*KDP culture with dilution factors of 10^0, 10^1, 10^2, 10^3, 10^4, 10^5, 10^6, 10^7.

On solid media, the *ami2*KDP strain displayed two distinct morphologies in the presence and absence of ATC. When ATC was removed, resulting in reduced *ami2* expression, the presence of miniature colonies, which appear to lack cording were observed, Figure 3.26. These colonies were not observed in the presence of ATC and cording was substantially increased suggesting that *ami2* plays an important role in colony formation.

3.6.5 A role for Ami2 in determining cell morphology

SEM was conducted to get high-resolution images of the individual cells and bacterial cell surface to evaluate the single cell impact of Ami2 depletion on bacterial growth. Cells were prepared for SEM as in section 2.13.6, Figure 3.27. Reduced *ami2* expression in the absence of inducer resulted in the formation of miniature cells depicted by the blue arrows in Figure 3.27D, the size range of these cells was between 2 µm and 7 µm as oppose to the mc^2155 cells, which were 4 µm to 8 µm in length. Cells grown in 0.05 ηg/ml (inducer

concentration, which should relieve these phenotypes) were 3.5 µm to 8 µm long. Depletion of *ami2* (no ATC) results in the presence of large cellular bulges depicted by the red arrows, Figure 3.27 C, these bulges were also observed in the culture containing 0.05 ηg/ml ATC, however the frequency was lower.

Further microscopic analysis was conducted on the *ami2*KDP strain utilizing confocal microscopy, Figure 3.28.

Confocal microscopy with the *ami2*KDP strain confirmed the formation of miniature cells in the absence of ATC indicated by the blue arrows on Figure 3.28, which correlates with the SEM data. When grown in the presence of 50 ηg/ml ATC the strain exhibits the presence of cells longer than the wild type mc^2155 strains depicted by the orange arrows suggesting that increased expression of *ami2* in the presence of high concentrations of inducer results in aberrant growth. Additionally, elevated expression of *ami2* resulted in loss of polar vancomycin staining, depicted in Figure 3.28 E and F (blue arrow), when compared to both the wild type and the depleted strains, Figure 3.28 A, B, D and G [II] (red arrow), which both retained polar vancomycin staining. This data implicates Ami2 in the localization of new PG units to the growth poles and a possible role in the determination of an active growth pole.

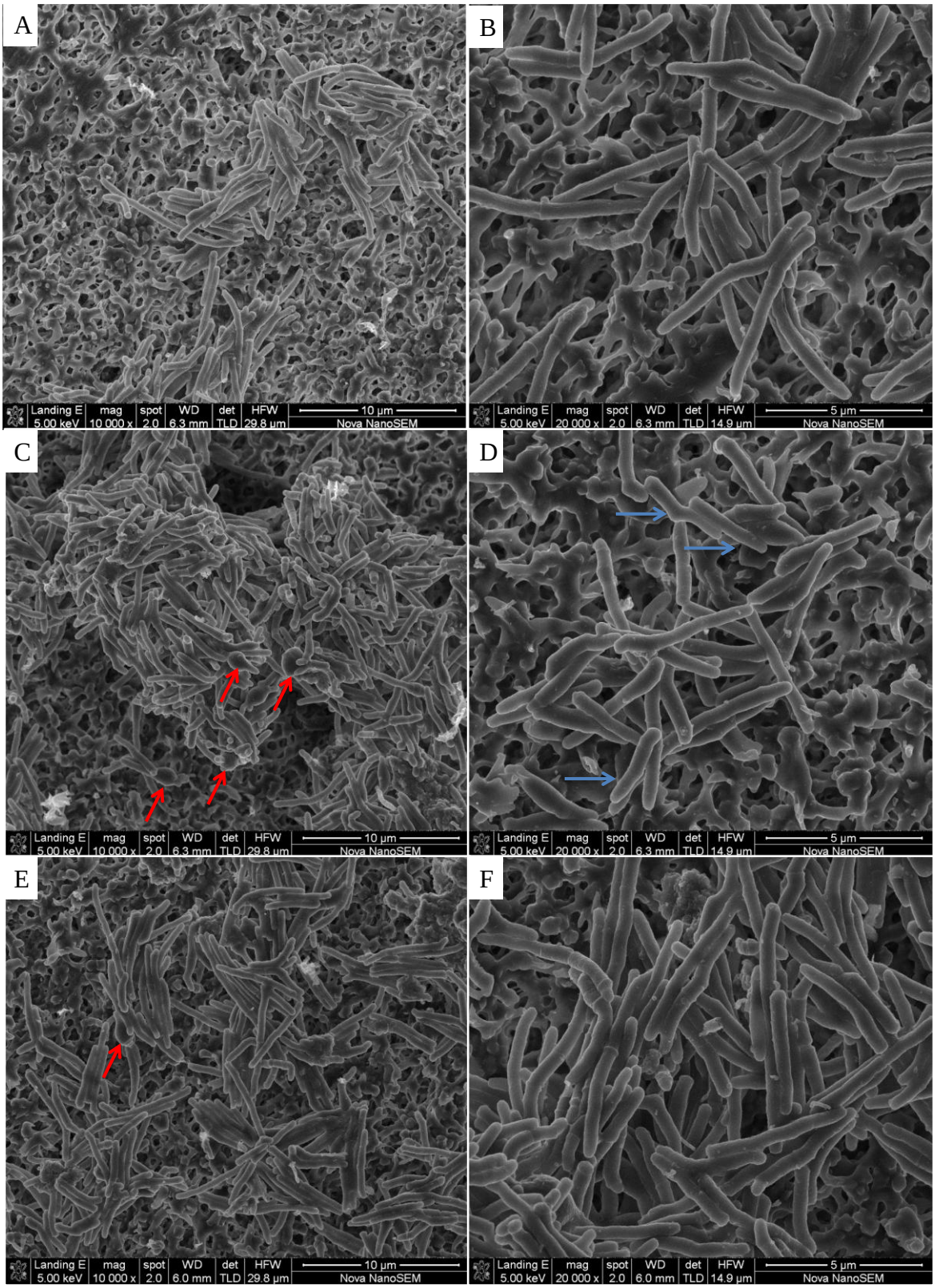
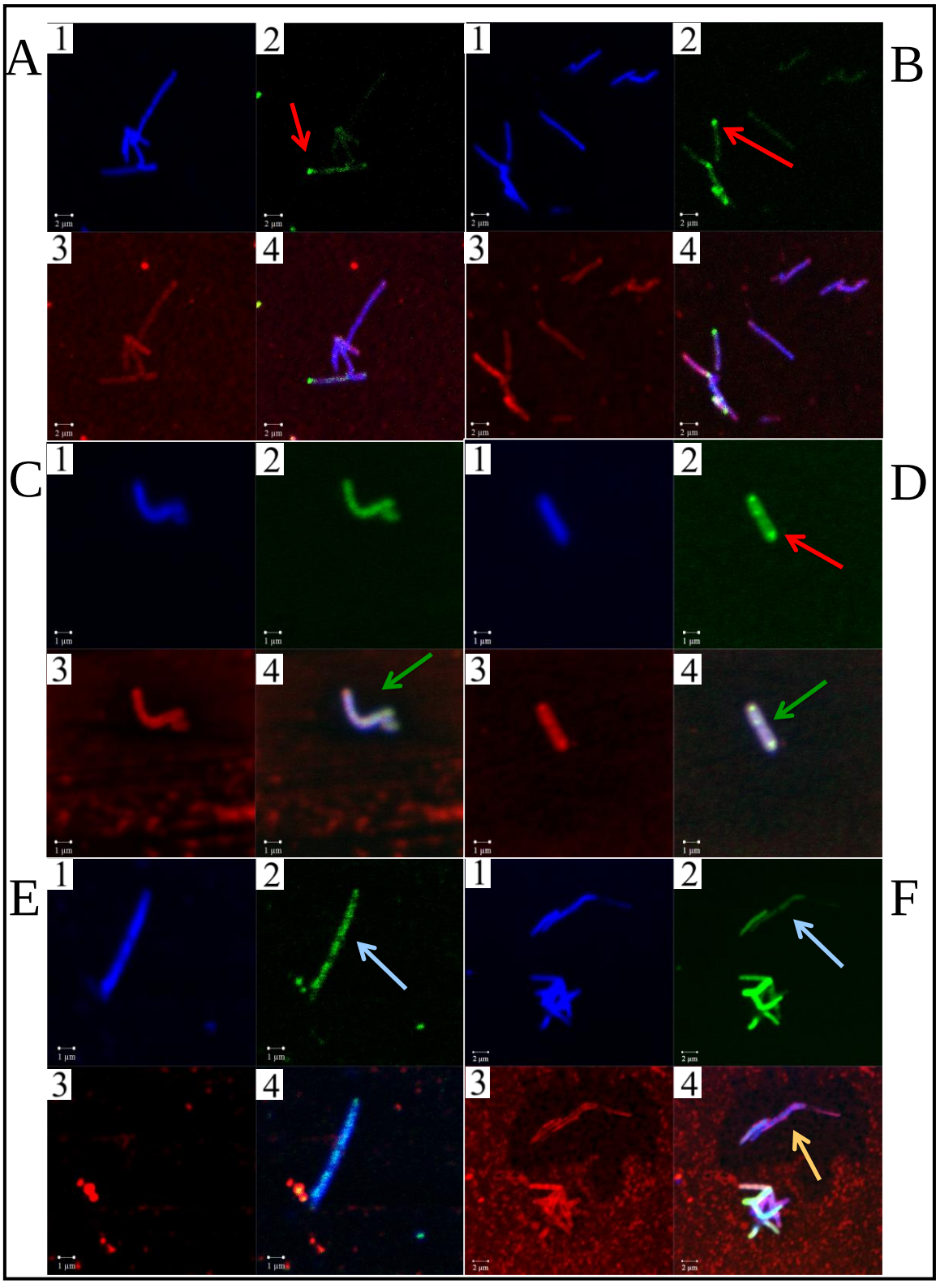


Figure 3.27: SEM images of the mc^{2}155 and *ami2*KDP strains. **(A)** and **(B)** show the mc^{2}155 strain, (**C)** and **(D)** show the *ami2*KDP strain grown in the absence of ATC, **(E)** and **(F)** show the *ami2*KDP strain grown in the presence of 0.05 ηg/ml ATC. Blue arrows: miniature cell, green arrows: thick cells and Red arrows: cellular bulging.


A
B
C
D
E
F
1
2
3
4

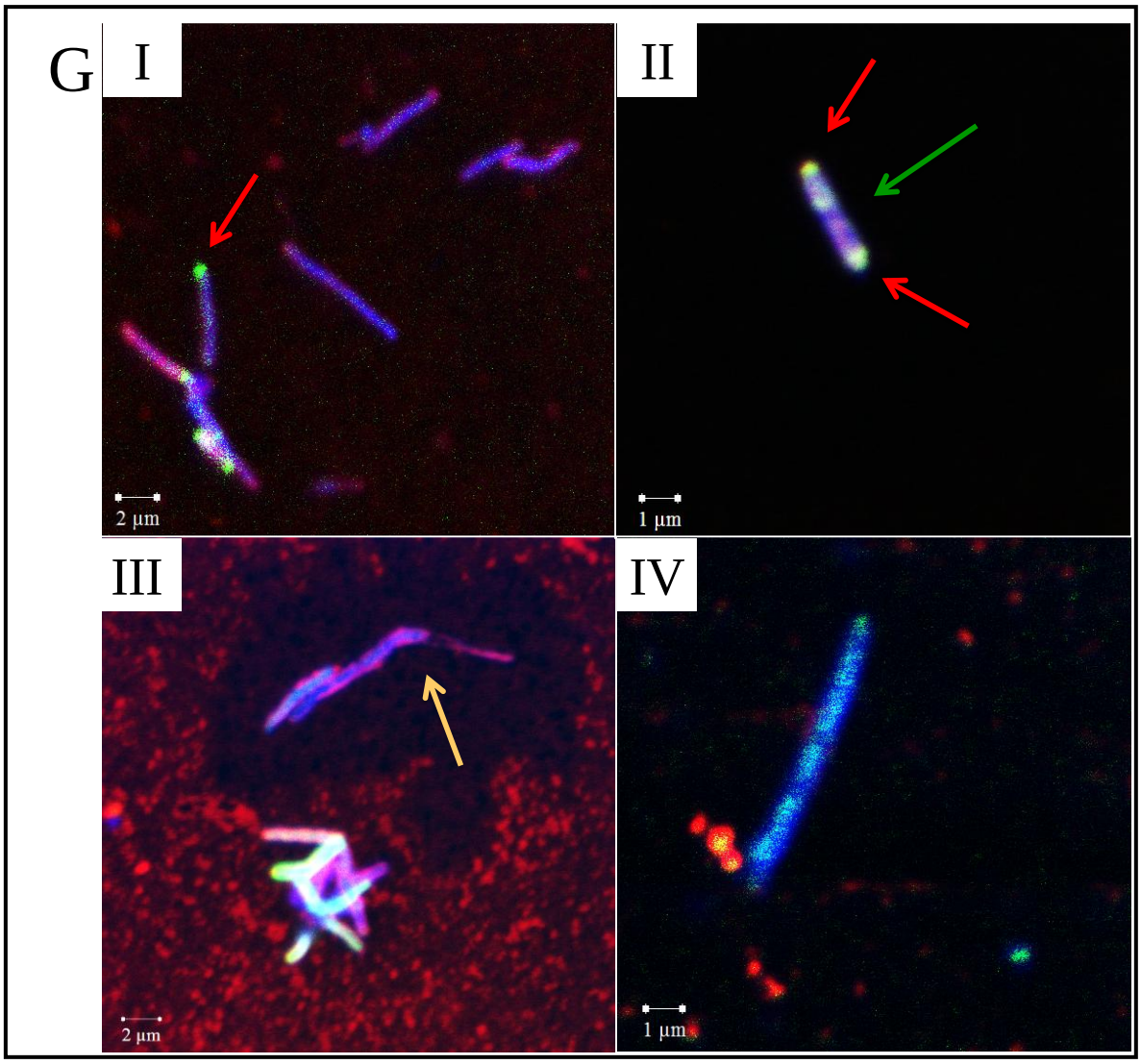


Figure 3.28: Confocal microscopy of the mc^{2}155 and *ami2*KDP strains. Cultures were grown in the absence of ATC and *ami2*KDP grown in media containing 50 ηg/ml ATC. **(1)** DAPI staining, **(2)** fluorescent vancomycin, **(3)** Cellmask™ Orange and **(4)** overlay of all three stains. **(A)** and **(B)** show the mc^{2}155 strain, **(C)** and **(D)** show the *ami2*KDP strain grown in the absence of ATC and **(E)** and **(F)** show the *ami2*KDP strain grown in media containing 50 ηg/ml. **(G)** High magnification view of the images shown in **(B) [I]**, **(D) [II], (E) [IV]** and **(F) [III]** overlay showing reduction in cell size in the absence of ATC and the presence of longer cells when ATC is reintroduced. Green arrows indicate miniature cells. Orange arrows indicate extended cells. Red arrows indicate polar vancomycin staining. Blue arrows indicate defused Vancomycin staining. Scale (**A)**, **(B)** and **(F)** 2 µm, **(C)**, **(D)** and **(E)** 1 µm

4. Discussion

TB continues to threaten global health and has been a consistent source of human mortality over the past century (Zhang, 2005). Rather than a decline in numbers, we are currently faced with a staggering epidemic where one third of the world's population harbours Mtb, the majority of, which carry LTBI (Chao and Rubin, 2010, Barry *et al*., 2009). No other disease today can boast this level of infiltration into its host population. The large reservoir of latently infected individual stands as a clear and present threat to the future eradication of TB (WHO, 2011).

Following the isolation of Mtb in the late 1800 s, a plethora of drugs have been evaluated for anti-tubercular activity however, the highly impervious nature of the cell envelope coupled with the inherent requirement for cytoplasmic entrance has limited the range of antimicrobials that can be used against the tubercle bacillus (WHO, 2011, Hett and Rubin, 2008). Despite these restrictions, a number of anti-tubercular drugs were discovered and used successfully for decades until the emergence of drug resistant Mtb strains (WHO, 2011). These troubling factors have regressed human kind to a point where effective treatment of TB is an enigma (WHO, 2011).

Under these circumstances, there is a dire need for new TB drugs with novel modes of action. In this context, mycobacterial PG holds promise for numerous reasons; (I) It is a bacterial specific structure, which could reduce drug toxicity, (II) It is required for bacterial survival and disruption of this structure will lead to cell death or increased bacterial permeability, (III) There are a large number of enzymes associated with PG synthesis and degradation, which provides a fertile mining ground for drug discovery and (IV) PG is a periplasmic structure thus drugs that target this structure do not need to traverse an

additional layer of the cell wall (Tripathi *et al*., 2005, Vollmer *et al*., 2008, Hett and Rubin, 2008). However, like many aspects of Mtb physiology that have potential for drug development, very little is known about PG synthesis and remodelling. The cytoplasmic components of PG synthesis have reduced potential for drug development since chemical agents would still need to traverse the entire cell wall to achieve significant target vulnerability. The potential of the PG hydrolysing enzymes as possible drug targets is yet to be thoroughly investigated. This gap in mycobacterial research forms part of the underlying theme of this MSc, which is aimed at characterizing cell wall amidases in an attempt to not only understand the importance of these enzymes to mycobacterial dormancy and physiology, but also to validate them as a legitimate target for drug discovery.

In this MSc study, we report the characterization of two mycobacterial cell wall amidases in Msm by assessing the phenotypic variations observed in Msm growth and cell division, derived from assessing either amidase gene deletion or gene depletion strains. Both Msm and Mtb encode three cell wall amidases designated Ami1, Ami2 and Ami3.Ami1 and Ami2 are both amidase_3 domain containing amidases, which show structural homology to the *E. coli* AmiA and AmiC respectively. Both these *E. coli* counterparts are periplasmic enzymes, exported from the cytoplasm through the use of the Twin-Arginine Translocation (tat) system (Bernhardt and de Boer, 2003). In Msm, we hypothesize a similar mechanism of translocation exists since the genome encodes a tat-like transporter system and Ami1 possesses a signal peptide at the N-terminus, suggesting possible translocation of the enzyme from the cytoplasm to the mycobacterial periplasmic region (McDonough *et al*., 2005, McDonough *et al*., 2008). Ami2 does not possess a signal peptide suggesting its localization is cytoplasmic in nature. Mycobacteria however, contain multiple exported

proteins, which do not have the classic signal peptide sequences, suggesting the presence of alternate translocation mechanisms, which have not been fully characterized as yet (de Souza *et al*., 2011). These data indicate that Ami2 could still function as a periplasmic amidase. Ami1 and Ami2 both retain the conserved residues shown to be essential for catalytic activity in the *B. subtilis* CwlC. This suggests they have the capacity to function as cell wall amidases (Mesnagi and Fouet, 2002). Furthermore, our bioinformatics analysis confirms that these two mycobacterial amidases possess all the structural traits necessary for cell wall amidase activity. Ami3 is an amidase_2 domain containing enzyme, which shares homology to AmiD. Ami3 also possesses the necessary secondary structures required for cell wall amidase activity however; our sequence alignments reveal a substitution of the catalytic residue to an amino acid with different structural and chemical properties. This calls into question the functionality of Ami3 in PG degradation and based on this, we did not evaluate Ami3 further in this study and focused our efforts on characterizing Ami1 and Ami2.

Loss of Ami1 resulted in no significant defects in bacterial growth rate or survival confirming that this amidase was not essential for bacterial growth and survival *in vitro*. This corroborated previous findings from a forward genetic screen that demonstrated that the Mtb homologue of Ami1 was not essential for growth in vitro (Sassetti *et al*., 2003). However, the formation of filamentous/chaining growth indicates a possible role for Ami1 during septation, a role that cannot be substituted by the remaining amidase-gene complement in the organism. Research conducted in multiple organisms including both rod and coccus shaped organisms have pointed to the importance of cell wall amidases in bacterial cell division depicted by the inability to degrade the septum resulting in the formation of filaments consisting of multiple cells. Deletion of *amiA*, *amiB* and *amiC* in

E. coli resulted in the formation of filaments consisting of 6 to 20 cells (Heidrich *et al*., 2001). Deletion of one amidase from *B. subtilis* (which generally forms chains) resulted in even longer chains (Blackman et al., 1998). The deletion of a single amidase in *Neisseria gonorrhoeae*, a coccus shaped organisms, resulted in the formation of bacterial masses consisting of multiple cells attached to each other by the cell wall due to the inability to complete septation (Garcia and Dillard, 2006). We observed similar phenotypes with our *ami1* deletion mutant, confirming that just like the other counterparts, Ami1 plays a crucial role in bacterial cell division. Saturating transposon mutagenesis in Mtb has confirmed that whilst being dispensable for growth *in vitro*, Ami1 plays an essential role in Mtb survival during infection as depicted by the inability of a *rv3717* mutant of Mtb to establish an infection in C57BL_6J mice (Sassetti and Rubin, 2003).

Despite numerous attempts and screening 70 putative knockout clones, an *ami2* deletion strain could not be generated by allelic exchange, suggesting that this gene is essential for *in vitro* growth. This result is consistent with the observation that the Mtb *ami2* counterpart (Rv3915) is predicted to be essential for bacterial growth in vitro as determined by saturating transposon gene disruption (Sassetti *et al*., 2003). Thus a knockdown strain was generated to evaluate the effects of *ami2* gene depletion on bacterial physiology.

Depletion of *ami2* expression resulted in retarded growth rate but this effect is progressively lost over time in culture, presumably through second-site mutations that alleviate the repression of the *ami2*. This phenotype was unanticipated; one would expect growth inhibition with the repressed strains, which would be consistent with the apparent essentiality of *ami2* for growth *in vitro*. Most certainly, gene knockdown of other essential genes studied in our laboratory results in almost complete inhibition of growth such as the

effects observed with *panC* depletion (Abrahams *et al*., 2012). There are two possible reasons for these observations: (I) Compensatory mutations in the ATC operator resulting in abrogation of ATC regulation or (II) Our use of a perfect prokaryotic RBS in depletion construct, which would result in leaky translation even with a reduced level of transcript. With regards to the first possibility, it is noteworthy that whilst expression analysis of the knockdown strain confirmed reduced transcription at 6 hours, this inhibitory effect on transcription of *ami2* was partially abrogated after a further three hours (9 hours post inoculation). This is shown by the fact that the levels of *ami2* mRNA 6 hours post induction were responsive to the concentration of the inducer. Addition of 50 ηg/ml ATC resulted in higher levels of mRNA when compared to the 0.05 ηg/ml ATC sample however, this regulatory effect was lost 9 hours post induction whereby both the 50 ηg/ml and 0.05 ηg/ml samples contained roughly the same amount of *ami2* mRNA suggesting the strain is no longer responding the level of ATC but rather the presence of ATC, Figure 3.23. This suggests a progressive escape from the ATC regulation over time and may explain the growth observed with the repressed strain. These data provide further confirmation of the essentiality of *ami2* since reduction in expression levels is not tolerated well and rapid compensatory mutants occur to alleviate this.

In our study, we used a similar RBS as that used by (Abrahams *et al*., 2012) since this RBS provided for efficient knockdown and subsequent depression of the *panC* gene – hence we term this the *panC* RBS. However, if this RBS is significantly more efficient that the native *ami2* RBS, the resulting leaky translation could lead to higher levels of protein synthesis than that obtained from the wild type level of mRNA transcription, without ATC regulation. One way to avoid this problem would be to use the native *ami2* RBS however, the RBS is currently unknown and taking a mandatory number of nucleotides upstream the

transcriptional start site would not guarantee the inclusion of the native RBS. The native RBS needs to be determined first. We are currently in the process of doing this.
Other knockdown systems may also be used to bypass the RBS limitation including a system of mRNA silencing. This involves cloning an antisense copy of the gene of interest downstream of an inducible transcriptional operator such as the ATC operator, resulting in the expression of complementary RNA, which would bind to mRNA inhibiting ribosome binding resulting in inhibition of mRNA translation (Good and Stach, 2011). Another system recently reported is a merodiploid system, which involves introducing a second copy of the gene of interest. This not only results in stable knockdown strains but also conclusively proves gene essentiality (Pecsi *et al*., 2012).

Microscopic analysis of the Ami2 depletion strain revealed the presence of short, broad cells, which contained globular bulges, Figure 3.26 and Figure 3.27. This amidase associated phenotype was not anticipated mainly because amidase deletion in various organisms lead to the formation of long filaments, this suggests that Ami2 might not be crucial for cell division but plays an important role in the development of the cell and correct placement of the pole. Of particular interest in this regard is the report of the depletion of Wag31 in mycobacteria, which results in the formation of short, broad cells, that contained globular bulges (Kang *et al*., 2008).

Wag31 is an essential protein shown to play a role in determining the growth of cell poles and structural maintenance (Kang *et al*., 2008, Nguyen *et al*., 2007). Depletion of this protein results in the formation of short cells, which contain globular bulges (similar to the Ami2 depletion phenotype). Over expression lead to the formation of long, branched filaments, similar to the Δ*ami1* strain phenotype (Kang *et al*., 2008, Nguyen *et al*., 2007).

The resemblance between the two phenotypes suggests a possible interaction between these two cell division proteins during growth and implicates Ami2 in structural maintenance and possibly growth of the cell pole. A similar phenotype has been observed in the *Cyanobacterium glutamicum* as a result of DivIVA (a Wag31 homologue) depletion, in, which case the phenotype was rescued by the introduction of Wag31 (Hempel *et al.*, 2008).

Depletion of *ami2* also resulted in defects in sliding motility and colony morphology. Sliding motility is a form of passive bacterial motility, which involves pushing of cells at the extremities as the bacterial population grows on solid media (Harshey, 2003). Though passive, sliding motility is thought to be an essential part of tissue invasion in some organisms (Harshey, 2003). Both sliding motility and colony morphology require a level of communication between bacteria to form complex structures (Harshey, 2003, Ben Jacob *et al.*, 2004). The *ami2* depletion strains displayed sliding in the absence of the inducer however the morphology was characterized by weak structural integrity, and was very distinct from that seen with the wild type strain suggesting that the cells could be moving individually by simple diffusion through the media. Elevated expression of *ami2* lead to the formation of a sliding mass with structural integrity and efficient sliding on the surface of the media. Colony defects noted with *ami2* depletion included the formation of miniature colonies devoid of any serpentine cording in the absence of the inducer, the cording phenotype was observed when gene repression was relieved. Research done on the nature of bacterial communities has shown the importance of regulated bacterial communication in the formation of complex structures, thus it is worth exploring the possibility that these phenotypes could be a result of miscommunication between bacteria rather than bacterial structural defects (Ben Jacob *et al.*, 2004). In this context, the bacterial

communication mechanisms discussed in section 1.5.4.1 are worthy of consideration as amidase would play an important role in these phenomena. This is discussed further below.

PknA and PknB are eukaryotic like membrane associated Ser/Thr kinases, which have been implicated in a number of bacterial processes. PknA is responsible for the phosphorylation of a wide range of enzymes including: FtsZ -, which is essential for cell division, MurC -, which is a D-alanine- D-alanine ligase required for PG synthesis and Wag31 -, which is essential for cell shape maintenance and correct placement of cell poles (Kang *et al*., 2005, Kang *et al*., 2008, Fiuza *et al*., 2008, Sureka *et al*., 2010, Nguyen *et al*., 2007). PknB has been shown to play an essential role in the reactivation of dormant *Bacillus* spores as a result of muropeptide binding to the outer membrane PASTA domains leading to activation of the cytoplasmic kinase domain resulting in germination (Kang *et al*., 2005, Shah *et al*., 2008). Overexpression of PknA and PknB result in morphological defects that resemble the *ami1* deletion and *ami2* depletion phenotypes respectively (Kang *et al*., 2005). Overexpression of the Mtb PknA results in the formation of long filaments, which consist of multiple cells attached to each other, some of, which possess lateral branches, whilst overexpression of PknB resulted in the formation of thick cells, which contain bulges (Kang *et al*., 2005). However, the link between these related phenotypes with Ami1 /Ami2 and PknA/PknB has yet to be fully unravelled. It has been shown that a muropeptide (disaccharide tripeptide) is required PknB-mediated signalling (Shah *et al*., 2008). It has also been shown that hydrolysis of the stem peptide results in abolished signalling capacity (Shah *et al*., 2008). Consequently, cell wall amidases could act as regulators of the PknB signalling pathway by hydrolysis of the stem peptide from the muropeptide resulting in a defective signalling molecule (Shah *et al*., 2008).

Research conducted on the physiological role and activity of muropeptides has revealed the importance of these molecules in the resuscitation of dormant Msm and Mtb cells (Nikitushkin *et al*., 2013). A recent study confirmed that muropeptides have the capacity to interact with the mycobacterial PknB through the periplasmic PASTA domain likely resulting in the activation of PknB mediated signalling pathways (Mir *et al*., 2011). These data indicate similarities between the *Bacillus* spore germination initiation mechanism and resuscitation of dormant mycobacteria. The study conducted by Nikitushkin *et al*., (2013) also showed the importance of environmental muropeptide concentration in resuscitation of dormant mycobacteria, too little or too much muropeptide resulted in inhibition of growth resumption. This was also observed in another study where excessive amounts of synthetic muropeptide resulted in significantly less resuscitation of dormant Mtb when compared to resuscitation of cells incubated in specialized conditioned media (Mir *et al*., 2011). The importance of regulating the levels of environmental muropeptides suggests an important role played by cell wall amidases in the efficient resuscitation of dormant mycobacteria through the hydrolysis of excess signalling molecules.

Concluding remarks

The study reported in this MSc represents the first extensive characterization of two mycobacterial cell wall amidases with the purpose of identifying the possible role of these enzymes in bacterial growth. This study reveals an important role for Ami1 in bacterial cell division, the determination of cell pole morphology and cell shape maintenance. We further confirm the essentiality of Ami2 as well as a possible role for this enzyme in bacterial growth and cell shape maintenance. Our knockdown studies are limited by the fact that our gene depletion strain displayed notable growth in the absence of inducer,

suggesting that the essentiality of *ami2* drives the emergence of mutants that have escaped the gene regulation mechanism.

Future work involves studying these genes in Mtb. This would involve deletion of the *ami1* gene in Mtb, proving the essentiality of *ami2* and subsequent depletion of *ami2* in Mtb either by use of a different knockdown system or use of the native ribosomal binding site. The phenotypic analyses conducted in this study will be applied to the Mtb strains to determine whether the phenotypes remain the same, furthermore the necessity of *ami1* for the establishment of TB infection will be investigated by the infection of mice using the Mtb Δ*ami1* strain. The role of cell wall amidases in resuscitation of dormant Mtb will be investigated by subjecting the mutant strain to a dormancy model followed by resuscitation using different concentrations of muropeptides. Furthermore the purification and crystallization of these amidases will be helpful to confirm their biochemical functions and will allow for the rational development of new drugs. The essential nature of Ami2 for growth and the importance of Ami1 for bacterial cell division identified in this study introduces a previously unexplored class of mycobacterial enzymes as legitimate targets for drug development. Furthermore their uncharacterized role in bacterial signalling and communication offers a field of study, which could offer insight into mechanisms involved the development of and reactivation from LTBI.

5. Appendices

5.1 Appendix A: Culture media

Luria-Bertani Agar (LA)

5g yeast extract, 10g tryptone, 10g NaCl, 1.5g agar, 1000 ml sdH2O

Luria-Bertani Broth (LB)

5g yeast extract, 10g tryptone, 10g NaCl, 1000 ml sdH20

2 × TY

10g yeast extract, 16g tryptone, 5g NaCl, 1000 ml sdH2O

M63

100 mM KH_2PO_4, 15 mM $(NH_4)_2SO_4$, 1.7 µM $FeSO_4.7H_2O$, pH to 7.0 with KOH

Middlebrook 7H9

4.7 g Difco Middlebrook 7H9 powder, 2 ml glycerol, 900 ml dH2O, 10 ml 100X glucose-salt, 2 ml Tween80

Middlebrook 7H10

19 g Difco Middlebrook 7H10 powder, 5 ml glycerol, 900 ml dH2O, 10 ml 100X glucose-salt

Sauton's minimal media (pH 7.2)

4 g asparagine, 0.5 g magnesium sulphate, 2 g citric acid, 0.5 g potassium dihydrogenorthophosphate, 0.05 g ammonium ferric citrate, 48ml glycerol then sterilized by filtration.

100 × Glucose-salt

Glucose salt 10 g glucose, 4.25 g NaCl, 500 ml dH2O

Tween80 (25 %)

10 ml Tween80 dissolved in 40 ml dH2O then sterilized by filtration

Sucrose (75 %)

75 g sucrose in 100 ml dH2O (autoclaved)

X-gal (2 %)

1 g X-gal in 50 ml deionised DMF

Media was sterilized by autoclaving at 121 °C for 20 min

5.2 Appendix B: Solutions

DNA manipulation solutions

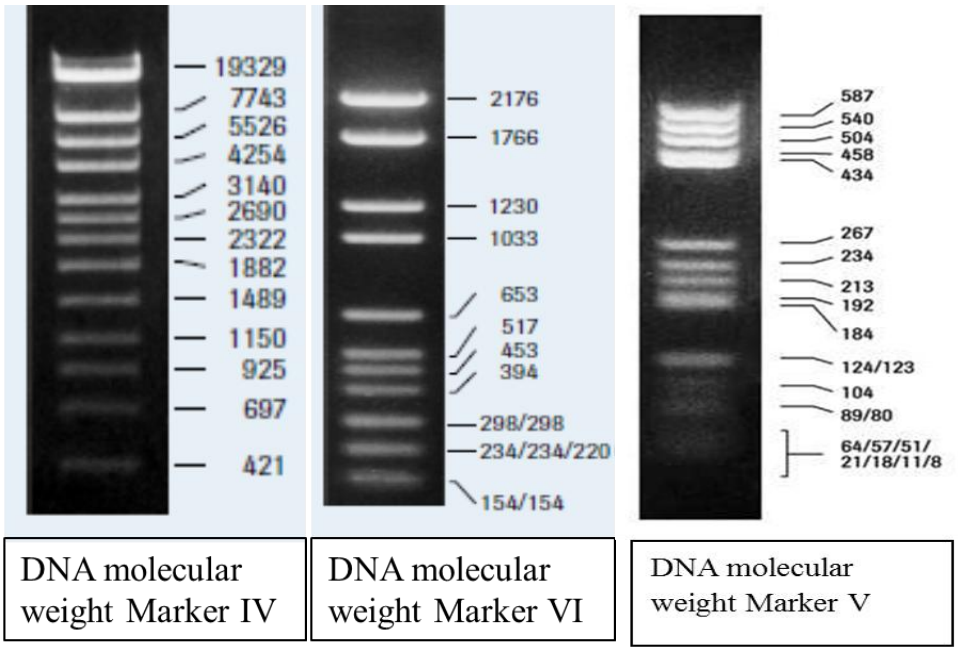
1 M Tris-HCl	60.56 g Tris, pH 8.0 with HCl, 500 ml dH2O final volume
0.5 M EDTA	18.6 g powder, pH 8.0 with NaOH, dH2O
Soln I	50 nM glucose, 25 mM Tris-HCl, 10 mM EDTA, pH 8.0
Soln II	0.2 M NaOH, 1.0 % SDS
Soln III	5 M potassium acetate, 11.5 ml glacial acetic acid, 88.5 dH20, pH 4.8
TE buffer	1 ml 1 M Tris-HCl, 2 ml 0.5 M EDTA
TAE buffer	242 g Tris base, 100 ml 0.5 M EDTA, 57.1 ml glacial acetic acid, pH 8.0, 1000 ml final volume dH2O
Chloroform: Isoamyl alcohol	24 ml chloroform, 1 ml isoamyl alcohol
Phenol: chloroform	1 ml phenol, 1 ml chloroform
Sodium acetate	3M sodium acetate dissolved in dH2O (autoclaved)
CTAB/NaCl	4.1 % NaCl, 10 % N-cetyl-N, N, N-trimethyl ammonium bromide dissolved in dH2O (filter sterilized)

Southern Blotting solutions

Denaturation solution	0.5 M NaOH, 1.5 M NaCl in dH2O
Depurination solution	0.25M HCl in dH2O
TBE (5 ×)	Tris-Borate-EDTA powder (Sigma) dissolved in 2l dH2O

SSC (20 ×)	3M NaCl, 0.3M sodium citrate in dH2O
Soln I	10 ml 20X SSC, 1 ml 10 % SDS, 89 ml dH2O
Soln II	2.5 ml 20X SSC, 1 ml 10 % SDS, 96.5 ml
10 % SDS	10 g powder, 100 ml sdH20
Maleic acid buffer	116.1 g maleic acid powder, 87. 66 g NaCl, pH 7.5 withNaOH pellets, make 1000 ml final volume with dH2O
Wash buffer	0.1M Maleic acid buffer, 0.3 % Tween20
Blocking solution (Roche)	1 × blocking solution in maleic acid buffer
Detection buffer	0.1M Tris-HCl, 0.1M NaCl in dH2O (pH 9.5)
Antibody solution (Roche)	Dilute 1 in 10 000 in blocking solution
CSPD (Roche)	Disodium 2-chloro-5-(4-methoxyspiro (2-dioxetane-3,2 (2-dioxetane-3,2'-(5'-chloro)-tricyclo[3.3.1.1. 3, 7.]decan)-. 4-yl)-1-phenyl phosphate

5.3 Appendix C: Molecular weight markers



DNA molecular weight Marker IV | DNA molecular weight Marker VI | DNA molecular weight Marker V

5.4 Appendix D: Bioinformatic analysis

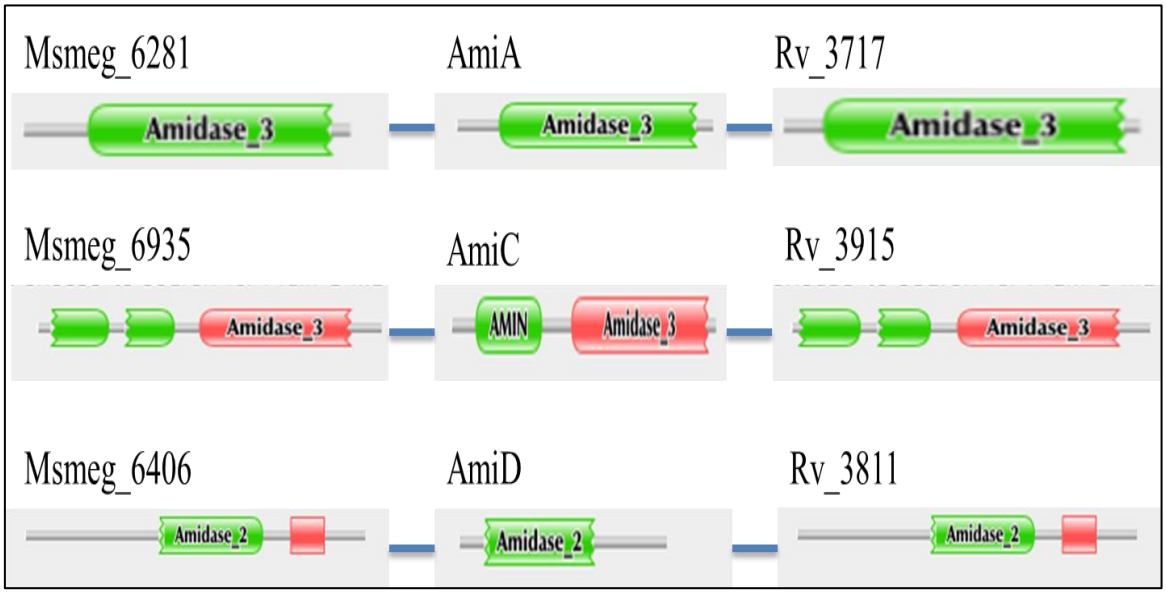
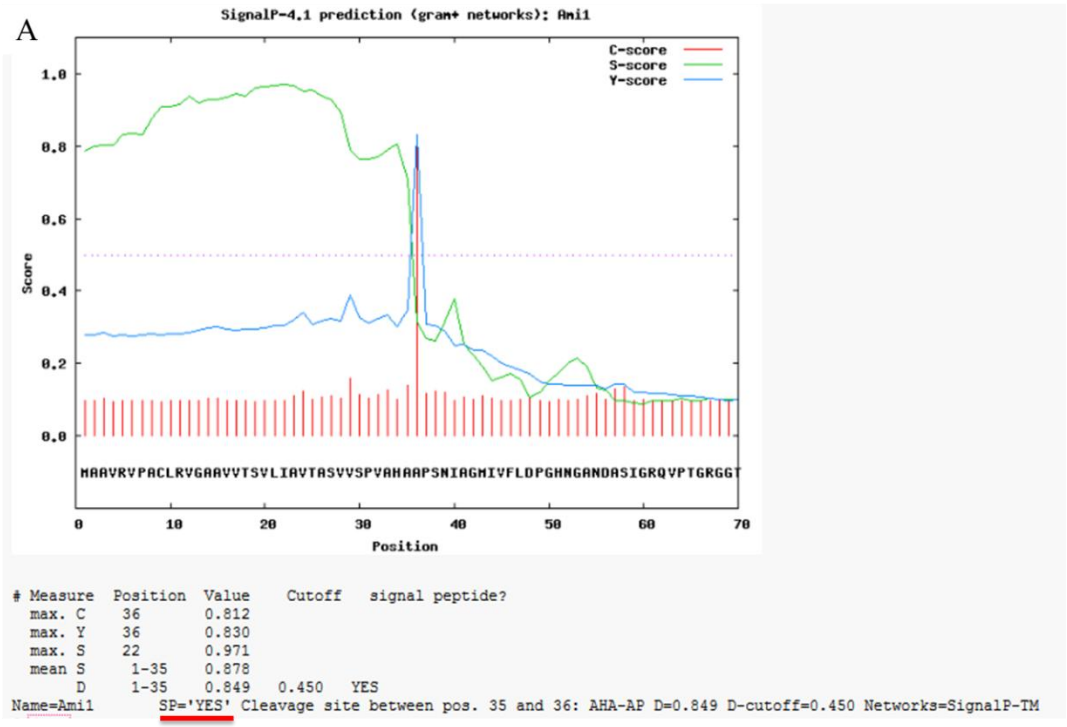


Figure D1: Pfam analysis of the three Mycobacterial amidases and their prospective *E. coli* homologues



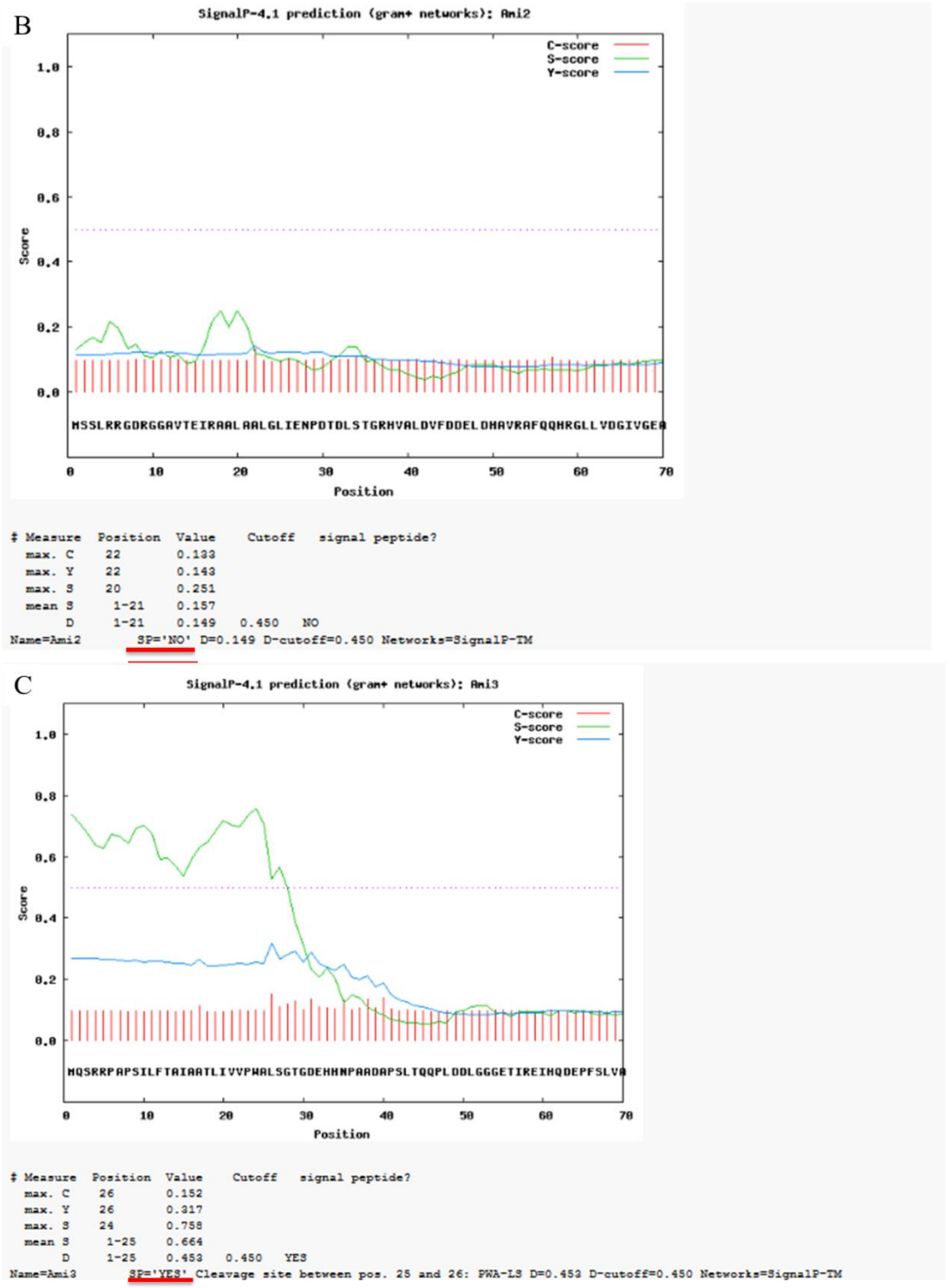


Figure D2: SignalP analysis of the three Mycobacterial amidase amino acid sequence. A: Ami1, B: Ami2 and C: Ami3

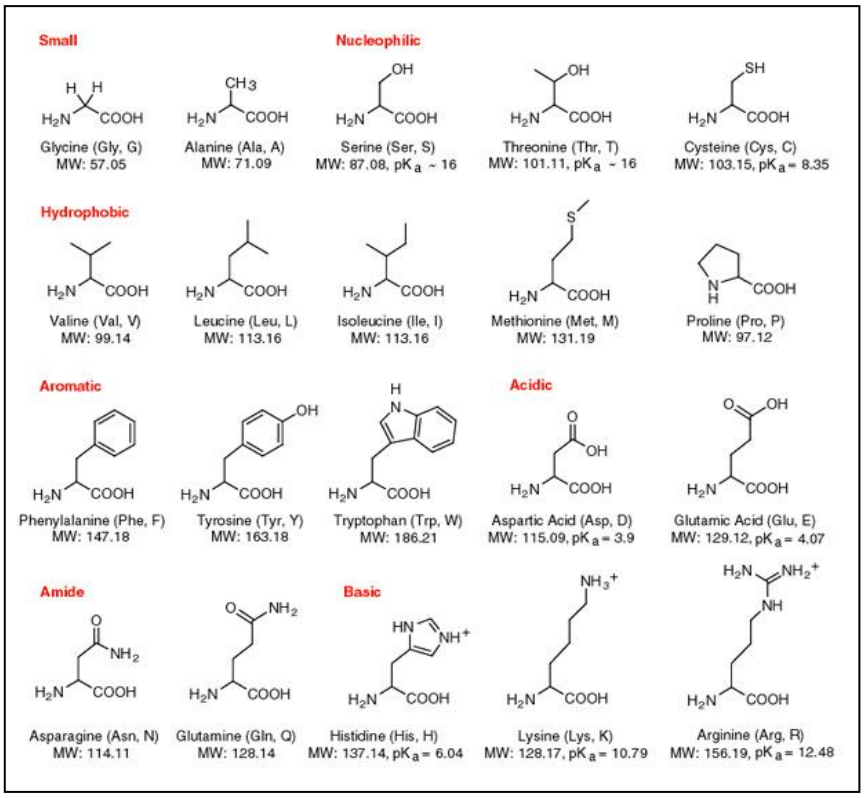


Figure D3: chart containing amino acids structure and chemical properties. (https://www.neb.com/tools-and-resources/usage-guidelines/amino-acid-structures).

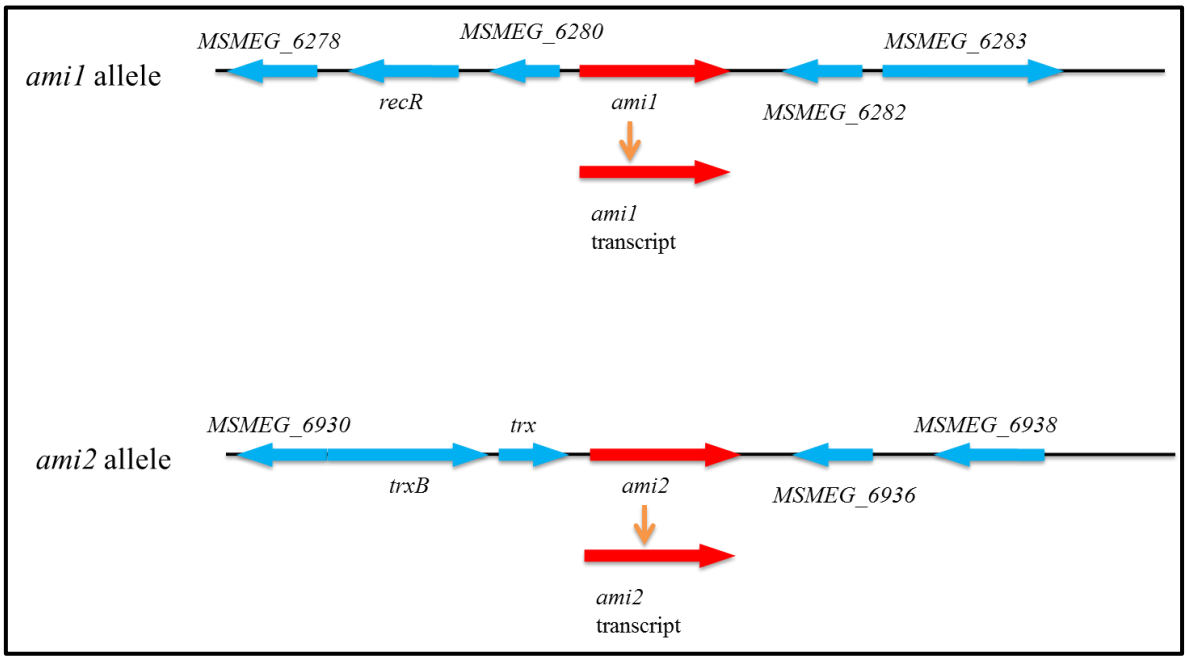


Figure D4: Diagrammatic representation of the *ami1* and *ami2* alleles and their predicted transcripts (www.Biocyc.com)

5.5 Appendix E : Flow chart

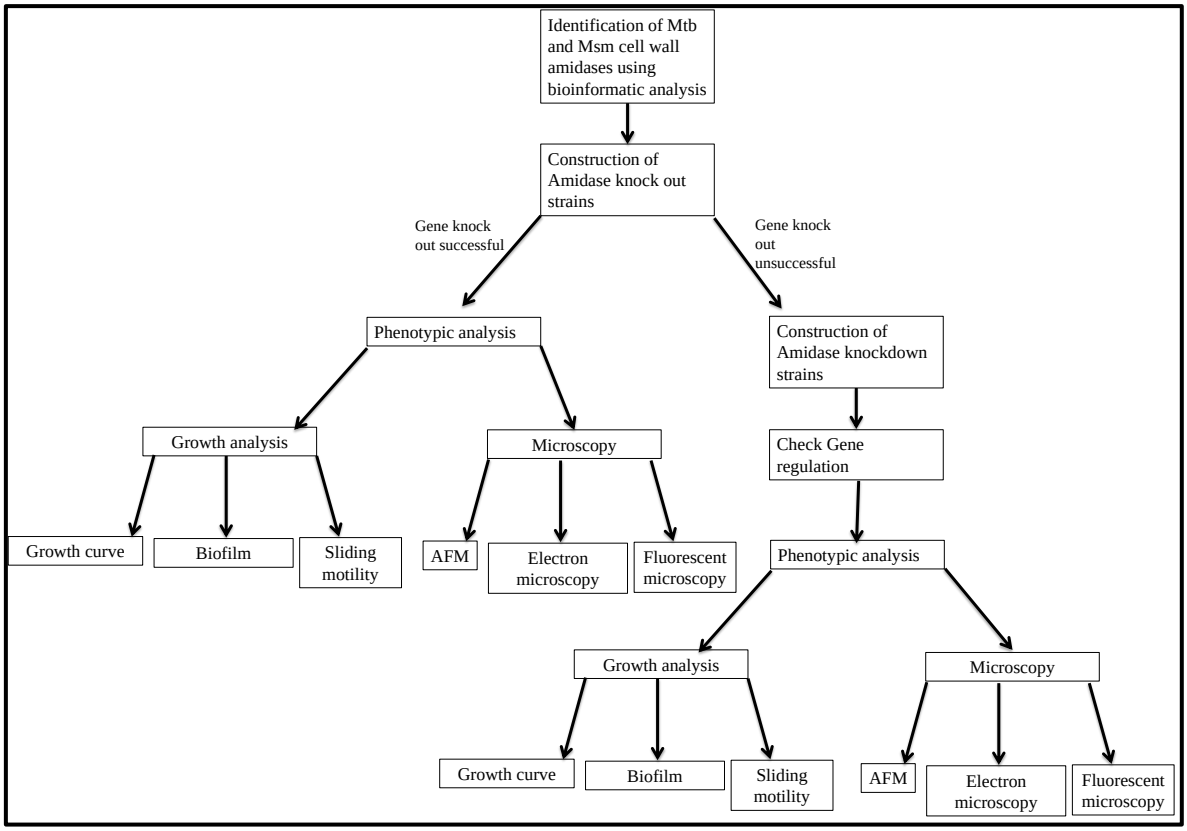


Figure E1: Diagrammatic representation of the experimental layout of the project.

6. Bibliography

Prevalence of the 23S rRNA A2058G point mutation and molecular subtypes in Treponema pallidum in the United States, 2007 to 2009. *Sex Transm Dis,* 39**,** 794-8.
ABRAHAMS, G. L., KUMAR, A., SAVVI, S., HUNG, A. W., WEN, S., ABELL, C., BARRY, C. E., 3RD, SHERMAN, D. R., BOSHOFF, H. I. & MIZRAHI, V. (2012) Pathway-selective sensitization of Mycobacterium tuberculosis for target-based whole-cell screening. *Chem Biol,* 19**,** 844-54.
ALDERWICK, L. J., BIRCH, H. L., MISHRA, A. K., EGGELING, L. & BESRA, G. S. (2007) Structure, function and biosynthesis of the Mycobacterium tuberculosis cell wall: arabinogalactan and lipoarabinomannan assembly with a view to discovering new drug targets. *Biochem Soc Trans,* 35**,** 1325-8.
BANERJEE, A., DUBNAU, E., QUEMARD, A., BALASUBRAMANIAN, V., UM, K. S., WILSON, T., COLLINS, D., DE LISLE, G. & JACOBS, W. R., JR. (1994) inhA, a gene encoding a target for isoniazid and ethionamide in Mycobacterium tuberculosis. *Science,* 263**,** 227-30.
BARNA, J. C. & WILLIAMS, D. H. (1984) The structure and mode of action of glycopeptide antibiotics of the vancomycin group. *Annu Rev Microbiol,* 38**,** 339-57.
BARRY, C. E., 3RD, BOSHOFF, H. I., DARTOIS, V., DICK, T., EHRT, S., FLYNN, J., SCHNAPPINGER, D., WILKINSON, R. J. & YOUNG, D. (2009) The spectrum of latent tuberculosis: rethinking the biology and intervention strategies. *Nat Rev Microbiol,* 7**,** 845-55.
BEN JACOB, E., BECKER, I., SHAPIRA, Y. & LEVINE, H. (2004) Bacterial linguistic communication and social intelligence. *Trends Microbiol,* 12**,** 366-72.
BERENDT, S., LEHNER, J., ZHANG, Y. V., RASSE, T. M., FORCHHAMMER, K. & MALDENER, I. (2012) Cell wall amidase AmiC1 is required for cellular communication and heterocyst development in the cyanobacterium Anabaena PCC 7120 but not for filament integrity. *J Bacteriol,* 194**,** 5218-27.
BERG, J. M., TYMOCZKO, J. L. & STRYER, L. (2007) *Biochemistry,* United States of America, Sara Tenney.
BERNHARDT, T. G. & DE BOER, P. A. (2003) The Escherichia coli amidase AmiC is a periplasmic septal ring component exported via the twin-arginine transport pathway. *Mol Microbiol,* 48**,** 1171-82.
BERRY, M. P., GRAHAM, C. M., MCNAB, F. W., XU, Z., BLOCH, S. A., ONI, T., WILKINSON, K. A., BANCHEREAU, R., SKINNER, J., WILKINSON, R. J., QUINN, C., BLANKENSHIP, D., DHAWAN, R., CUSH, J. J., MEJIAS, A., RAMILO, O., KON, O. M., PASCUAL, V., BANCHEREAU, J., CHAUSSABEL, D. & O'GARRA, A. (2010) An interferon-inducible neutrophil-driven blood transcriptional signature in human tuberculosis. *Nature,* 466**,** 973-7.
BESRA, G. S. & BRENNAN, P. J. (1997) The mycobacterial cell wall: biosynthesis of arabinogalactan and lipoarabinomannan. *Biochem Soc Trans,* 25**,** 845-50.
BIGGER, J. W. (1944) Treatment of Staphylococcal Innfections with Penicillin By Intermittent Sterilisation. *The Lancet,* 244**,** 497-500.
BIKETOV, S., MUKAMOLOVA, G. V., POTAPOV, V., GILENKOV, E., VOSTROKNUTOVA, G., KELL, D. B., YOUNG, M. & KAPRELYANTS, A. S. (2000) Culturability of Mycobacterium tuberculosis cells isolated from murine macrophages: a bacterial growth factor promotes recovery. *FEMS Immunol Med Microbiol,* 29**,** 233-40.
BLACKMAN, S. A., SMITH, T. J. & FOSTER, S. J. (1998) The role of autolysins during vegetative growth of Bacillus subtilis 168. *Microbiology,* 144 (Pt 1)**,** 73-82.
BOSHOFF, H. I. & BARRY, C. E., 3RD (2006) Is the mycobacterial cell wall a hopeless drug target for latent tuberculosis? *Drug Discovery Today: Disease Mechanisms,* 3**,** 237-245.
BOUHSS, A., TRUNKFIELD, A. E., BUGG, T. D. & MENGIN-LECREULX, D. (2008) The biosynthesis of peptidoglycan lipid-linked intermediates. *FEMS Microbiol Rev,* 32**,** 208-33.
BRAND, S., NIEHAUS, K., PUHLER, A. & KALINOWSKI, J. (2003) Identification and functional analysis of six mycolyltranferase genes of the Corynebacterium glutamicum ATCC 13032: the genes cop1, cmt1, and cmt2 can replace each other in the synthesis of trehalose dicorynomycolate, a component of the mycolic acid layer of the cell envelope. *Arch Microbiol,* 180**,** 33-44.

BUGG, T. D. H., WRIGHT, G. D., DUTKA-MALEN, S., ARTHUR, M., COURVALIN, P. & WALSH, C. (1991) Molecular basis of vancomycin resistance in *Enterococcus faesium* BM4147: biosynthesis of a depsipeptide peptidoglycan precursor by vancomycin resistance proteins VanH and VanA. *Biochemistry,* 30**,** 10408-10415.

CACERES, N. E., HARRIS, N. B., WELLEHAN, J. F., FENG, Z., KAPUR, V. & BARLETTA, R. G. (1997) Overexpression of the D-alanine racemase gene confers resistance to D-cycloserine in *Mycobacterium smegmatis*. *Journal of Bacteriology,* 179**,** 5046-5055.

CHAMBERS, H. F., MOREAU, D., YAJKO, D., MIICK, C., WAGNER, C., HACKBARTH, C., KOCAGOZ, S., ROSENBERG, E., HADLEY, W. K. & NIKAIDO, H. (1995) Can penicillins and other beta-lactam antibiotics be used to treat tuberculosis? *Antimicrob Agents Chemother,* 39**,** 2620-4.

CHAO, M. C. & RUBIN, E. J. (2010) Letting sleeping dos lie: does dormancy play a role in tuberculosis? *Annu Rev Microbiol,* 64**,** 293-311.

CHENG, X., ZHANG, X., PFLUGRATH, J. W. & STUDIER, F. W. (1994) The structure of bacteriophage T7 lysozyme, a zinc amidase and an inhibitor of T7 RNA polymerase. *Proc Natl Acad Sci U S A,* 91**,** 4034-8.

DAFFE, M., BRENNAN, P. J. & MCNEIL, M. (1990) Predominant structural features of the cell wall arabinogalactan of Mycobacterium tuberculosis as revealed through characterization of oligoglycosyl alditol fragments by gas chromatography/mass spectrometry and by 1H and 13C NMR analyses. *J Biol Chem,* 265**,** 6734-43.

DAFFE, M. & ETIENNE, G. (1999) The capsule of Mycobacterium tuberculosis and its implications for pathogenicity. *Tuber Lung Dis,* 79**,** 153-69.

DE SOUZA, G. A., LEVERSEN, N. A., MALEN, H. & WIKER, H. G. (2011) Bacterial proteins with cleaved or uncleaved signal peptides of the general secretory pathway. *J Proteomics,* 75**,** 502-10.

DRIKS, A. (2009) The Bacillus anthracis spore. *Mol Aspects Med,* 30**,** 368-73.

EHLERT, K. & HOLTJE, J. V. (1996) Role of precursor translocation in coordination of murein and phospholipid synthesis in Escherichia coli. *J Bacteriol,* 178**,** 6766-71.

EHRT, S., GUO, X. V., HICKEY, C. M., RYOU, M., MONTELEONE, M., RILEY, L. W. & SCHNAPPINGER, D. (2005) Controllong gene expression in mycobacteria with anhydrotetracycline and Tet repressor. *Nucleic Acids Res,* 33**,** e21.

FENG, Z. & BARLETTA, R. G. (2003) Roles of *Mycobacterium smegmatis* D-alanine:D-alanine ligase and D-alanine racemase in the mechanism of action of and resistance to the peptidoglycan inhibitor D-cycloserine. *Antimicrob Agents Chemother,* 47**,** 283-291.

FEUCHT, A., EVANS, L. & ERRINGTON, J. (2003) Identification of sporulation genes by genome-wide analysis of the sigmaE regulon of Bacillus subtilis. *Microbiology,* 149**,** 3023-34.

FIUZA, M., CANOVA, M. J., PATIN, D., LETEK, M., ZANELLA-CLEON, I., BECCHI, M., MATEOS, L. M., MENGIN-LECREULX, D., MOLLE, V. & GIL, J. A. (2008) The MurC ligase essential for peptidoglycan biosynthesis is regulated by the serine/threonine protein kinase PknA in Corynebacterium glutamicum. *J Biol Chem,* 283**,** 36553-63.

FLORES, A. R., PARSONS, L. M. & PAVELKA, M. S., JR. (2005) Genetic analysis of the beta-lactamases of Mycobacterium tuberculosis and Mycobacterium smegmatis and susceptibility to beta-lactam antibiotics. *Microbiology,* 151**,** 521-32.

FOSTER, S. J. (1991) Cloning, expression, sequence analysis and biochemical characterization of an autolytic amidase of Bacillus subtilis 168 trpC2. *J Gen Microbiol,* 137**,** 1987-98.

FU, L. M. & FU-LIU, C. S. (2002) Is Mycobacterium tuberculosis a closer relative to Gram-positive or Gram-negative bacterial pathogens? *Tuberculosis (Edinb),* 82**,** 85-90.

GARCIA, D. L. & DILLARD, J. P. (2006) AmiC functions as an N-acetylmuramyl-l-alanine amidase necessary for cell separation and can promote autolysis in Neisseria gonorrhoeae. *J Bacteriol,* 188**,** 7211-21.

GEFEN, O. & BALABAN, N. Q. (2009) The importance of being persistant: heterogenety of bacterial population under antibiotic stress. *FEMS microbiology Reviews,* 33**,** 704-717.

GEURTSEN, J., CHEDAMMI, S., MESTERS, J., COT, M., DRIESSEN, N. N., SAMBOU, T., KAKUTANI, R., UMMELS, R., MAASKANT, J., TAKATA, H., BABA, O., TERASHIMA, T., BOVIN, N., VANDENBROUCKE-GRAULS, C. M., NIGOU, J., PUZO, G., LEMASSU, A., DAFFE, M. & APPELMELK, B. J. (2009) Identification of mycobacterial alpha-glucan as a novel ligand for DC-SIGN: involvement of mycobacterial capsular polysaccharides in host immune modulation. *J Immunol,* 183**,** 5221-31.

GOOD, L. & STACH, J. E. (2011) Synthetic RNA silencing in bacteria - antimicrobial discovery and resistance breaking. *Front Microbiol,* 2**,** 185.

GORDHAN, B. G. & PARISH, T. (2001) Gene replacement using pre-treated DNA. *Methods in Molecular Medicine,* 54**,** 77-92.

HARSHEY, R. M. (2003) Bacterial motility on a surface: many ways to a common goal. *Annu Rev Microbiol,* 57**,** 249-73.

HEIDRICH, C., TEMPLIN, M. F., URSINUS, A., MERDANOVIC, M., BERGER, J., SCHWARZ, H., DE PEDRO, M. A. & HOLTJE, J. V. (2001) Involvement of N-acetylmuramyl-L-alanine amidases in cell separation and antibiotic-induced autolysis of Escherichia coli. *Mol Microbiol,* 41**,** 167-78.

HEIFETS, L. B. & CANGELOSI, G. A. (1999) Drug susceptibility testing of Mycobacterium tuberculosis: a neglected problem at the turn of the century. *Int J Tuberc Lung Dis,* 3**,** 564-81.

HEMPEL, A. M., WANG, S. B., LETEK, M., GIL, J. A. & FLARDH, K. (2008) Assemblies of DivIVA mark sites for hyphal branching and can establish new zones of cell wall growth in Streptomyces coelicolor. *J Bacteriol,* 190**,** 7579-83.

HETT, E. C. & RUBIN, E. J. (2008) Bacterial growth and cell division: a mycobacterial perspective. *Microbiol Mol Biol Rev,* 72**,** 126-56, table of contents.

HIGGINS, D. & DWORKIN, J. (2011) Recent progress in Bacillus subtilis sporulation. *FEMS Microbiol Rev,* 36**,** 131-48.

HOLTJE, J. V. (1996) Bacterial Lysozymes. *EXS,* 75**,** 65-74.

HUGONNET, J. E. & BLANCHARD, J. S. (2007) Irreversible inhibition of the Mycobacterium tuberculosis beta-lactamase by clavulanate. *Biochemistry,* 46**,** 11998-2004.

HUGONNET, J. E., TREMBLAY, L. W., BOSHOFF, H. I., BARRY, C. E., 3RD & BLANCHARD, J. S. (2009) Meropenem-Clavulanate Is Effective Against Extensively Drug-Resistant Mycobacterium tuberculosis. *Science,* 323**,** 1215-1218.

JACOBS, C., HUANG, L. J., BARTOWSKY, E., NORMARK, S. & PARK, J. T. (1994) Bacterial cell wall recycling provides cytosolic muropeptides as effectors for beta-lactamase induction. *EMBO J,* 13**,** 4684-94.

JOHNSON, R. E., STREICHER, E. M., LOUW, G. E., WARREN, R. M., VAN HELDEN, P. D. & VICTOR, T. C. (2003) Drug resistance in *Mycbacterium tuberculosis*. *Current issues in Molecular Biology,* 8**,** 97-112.

JORIS, B., DIVE, G., DIDEBERG, O., CHARLIER, P., FRERE, J. M. & GHUYSEN, J. M. (1982) Structure of a Zn2+containing D-alanyl-D-alanine cleavage Carboxypeptidase at 2.5 A resolution. *Nature,* 299**,** 469-470.

KANA, B. D., GORDHAN, B. G., DOWNING, K. J., SUNG, N., VOSTROKTUNOVA, G., MACHOWSKI, E. E., TSENOVA, L., YOUNG, M., KAPRELYANTS, A., KAPLAN, G. & MIZRAHI, V. (2008) The resuscitation-promoting factors of Mycobacterium tuberculosis are required for virulence and resuscitation from dormancy but are collectively dispensable for growth in vitro. *Mol Microbiol,* 67**,** 672-84.

KANA, B. D. & MIZRAHI, V. (2009) Resuscitation-promoting factors as lytic enzymes for bacterial growth and signaling. *FEMS Immunol Med Microbiol,* 58**,** 39-50.

KANA, B. D. & MIZRAHI, V. (2010) Resuscitation promoting factors in bacterial population dynamics during TB infection. *Drug Discov Today: Dis Mech*.

KANG, C. M., ABBOTT, D. W., PARK, S. T., DASCHER, C. C., CANTLEY, L. C. & HUSSON, R. N. (2005) The Mycobacterium tuberculosis serine/threonine kinases PknA and PknB: substrate identification and regulation of cell shape. *Genes Dev,* 19**,** 1692-704.

KANG, C. M., NYAYAPATHY, S., LEE, J. Y., SUH, J. W. & HUSSON, R. N. (2008) Wag31, a homologue of the cell division protein DivIVA, regulates growth, morphology and polar cell wall synthesis in mycobacteria. *Microbiology,* 154**,** 725-35.

KEEP, N. H., WARD, J. M., COHEN-GONSAUD, M. & HENDERSON, B. (2006) Wake up! Peptidoglycan lysis and bacterial non-growth states. *Trends Microbiol,* 14**,** 271-6.

KERFF, F., PETRELLA, S., MERCIER, F., SAUVAGE, E., HERMAN, R., PENNARTZ, A., ZERVOSEN, A., LUXEN, A., FRERE, J. M., JORIS, B. & CHARLIER, P. (2010) Specific structural features of the N-acetylmuramoyl-L-alanine amidase AmiD from Escherichia coli and mechanistic implications for enzymes of this family. *J Mol Biol,* 397**,** 249-59.

KIMERLING, M. E., KLUGE, H., VEZHNINA, N., IACOVAZZI, T., DEMEULENAERE, T., PORTAELS, F. & MATTHYS, F. (1999) Inadequacy of the current WHO re-treatment regimen in a central Siberian prison: treatment failure and MDR-TB. *Int J Tuberc Lung Dis,* 3**,** 451-3.

KORSAK, D., LIEBSCHER, S. & VOLLMER, W. (2005) Susceptibility to antibiotics and beta-lactamase induction in murein hydrolase mutants of Escherichia coli. *Antimicrob Agents Chemother,* 49**,** 1404-9.

KROGH, S., JORGENSEN, S. T. & DEVINE, K. M. (1998) Lysis genes of the Bacillus subtilis defective prophage PBSX. *J Bacteriol,* 180**,** 2110-2117.

KUMAR, P., ARORA, K., LLOYD, J. R., LEE, I. Y., NAIR, V., FISCHER, E., BOSHOFF, H. I. & BARRY, C. E., 3RD (2012) Meropenem inhibits D,D-carboxypeptidase activity in *Mycobacterium tuberculosis*. *Mol Microbiol,* 86**,** 367-81.

LAVOLLAY, M., ARTHUR, M., FOURGEAUD, M., DUBOST, L., MARIE, A., VEZIRIS, N., BLANOT, D., GUTMANN, L. & MAINARDI, J. L. (2008) The peptidoglycan of stationary-phase Mycobacterium tuberculosis predominantly contains cross-links generated by L,D-transpeptidation. *J Bacteriol,* 190**,** 4360-6.

LEE, W. B., KANG, J. S., YAN, J. J., LEE, M. S., JEON, B. Y., CHO, S. N. & KIM, Y. J. (2012) Neutrophils Promote Mycobacterial Trehalose Dimycolate-Induced Lung Inflammation via the Mincle Pathway. *PLoS Pathog,* 8**,** e1002614.

LIM, J. H., KIM, M. S., KIM, H. E., YANO, T., OSHIMA, Y., AGGARWAL, K., GOLDMAN, W. E., SILVERMAN, N., KURATA, S. & OH, B. H. (2006) Structural basis for preferential recognition of diaminopimelic acid-type peptidoglycan by a subset of peptidoglycan recognition proteins. *J Biol Chem,* 281**,** 8286-95.

LIVERMORE, D. M. & WOODFORD, N. (2000) Carbapenemases: a problem in waiting? *Current Opinions in Microbiology,* 3**,** 489-495.

LO, M. C., MEN, H., BRANSTROM, A., HELM, J., YAO, N., GOLDMAN, R. & WALKER, S. (2000) A new mechanism of action proposed for Ramoplanin. *J Am Chem Soc,* 122**,** 3540-3541.

MAHAPATRA, S., YAGI, T., BELISLE, J. T., ESPINOSA, B. J., HILL, P. J., MCNEIL, M. R., BRENNAN, P. J. & CRICK, D. C. (2005) Mycobacterial lipid II is composed of a complex mixture of modified muramyl and peptide moieties linked to decaprenyl phosphate. *J Bacteriol,* 187**,** 2747-57.

MARTINEZ, A., TORELLO, S. & KOLTER, R. (1999) Sliding Motility in Mycobacteria. *J Bacteriol,* 181**,** 7331-7338.

MCCALL, K. A., HUANG, C. & FIERKE, C. A. (2000) Function and mechanism of zinc metalloenzymes. *J Nutr,* 130**,** 1437S-46S.

MCDONOUGH, J. A., HACKER, K. E., FLORES, A. R., PAVELKA, M. S., JR. & BRAUNSTEIN, M. (2005) The twin-arginine translocation pathway of Mycobacterium smegmatis is functional and required for the export of mycobacterial beta-lactamases. *J Bacteriol,* 187**,** 7667-7679.

MCDONOUGH, J. A., MCCANN, J. R., TEKIPPE, E. M., SILVERMAN, J. S., RIGEL, N. W. & BRAUNSTEIN, M. (2008) Identification of functional Tat signal sequences in Mycobacterium tuberculosis proteins. *J Bacteriol,* 190**,** 6428-38.

MCKEEGAN, K. S., BORGES-WALMSLEY, M. I. & WALMSLEY, A. R. (2004) Structural understanding of efflux-mediated drug resistance: potential routes to efflux inhibition. *Curr Opin Pharmacol,* 4**,** 479-86.

MCNEIL, M., DAFFE, M. & BRENNAN, P. J. (1990) Evidence for the nature of the link between the arabinogalactan and peptidoglycan of mycobacterial cell walls. *J Biol Chem,* 265**,** 18200-6.

MEBERG, B. M., PAULSON, A. L., PRIYADARSHINI, R. & YOUNG, K. D. (2004) Endopeptidase penicillin-binding proteins 4 and 7 play auxiliary roles in determining uniform morphology of Escherichia coli. *J Bacteriol,* 186**,** 8326-36.

MELLROTH, P. & STEINER, H. (2006) PGRP-SB1: an N-acetylmuramoyl L-alanine amidase with antibacterial activity. *Biochem Biophys Res Commun,* 350**,** 994-9.

MESNAGI, S. & FOUET, A. (2002) Plasmid-Encoded Autolysin in *Bacillus anthracis*: modular structure and catalytic properties. *J Bacteriol,* 184**,** 331-334.

MILLER, C., THOMSEN, L. E., GAGGERO, C., MOSSERI, R., INGMER, H. & COHEN, S. N. (2004) SOS response induction by beta-lactams and bacterial defense against antibiotic lethality. *Science,* 305**,** 1629-31.

MIR, M., ASONG, J., LI, X., CARDOT, J., BOONS, G. J. & HUSSON, R. N. (2011) The extracytoplasmic domain of the *Mycobacterium tuberculosis* Ser/Thr kinase PknB binds specific muropeptides and is required for PknB localization. *PLoS Pathog,* 7**,** e1002182.

MISHRA, A. K., DRIESSEN, N. N., APPELMELK, B. J. & BESRA, G. S. (2011) Lipoarabinomannan and related glycoconjugates: structure, biogenesis and role in Mycobacterium tuberculosis physiology and host-pathogen interaction. *FEMS Microbiol Rev,* 35**,** 1126-57.

MITCHISON, D. A. (1998) How drug resistance emerges as a result of poor compliance during short course chemotherapy for tuberculosis. *Int J Tuberc Lung Dis,* 2**,** 10-5.

MOFFATT, B. A. & STUDIER, F. W. (1987) T7 lysozyme inhibits transcription by T7 RNA polymerase. *Cell,* 49**,** 221-7.

MUKAMOLOVA, G. V., KAPRELYANTS, A. S., YOUNG, D. I., YOUNG, M. & KELL, D. B. (1998) A bacterial cytokine. *Proc Natl Acad Sci U S A,* 95**,** 8916-21.

MUKAMOLOVA, G. V., MURZIN, A. G., SALINA, E. G., DEMINA, G. R., KELL, D. B., KAPRELYANTS, A. S. & YOUNG, M. (2006) Muralytic activity of Micrococcus luteus Rpf and its relationship to physiological activity in promoting bacterial growth and resuscitation. *Mol Microbiol,* 59**,** 84-98.

NACHEGA, J. B. & CHAISSON, R. E. (2003) Tuberculosis drug resistance: a global threat. *Clin Infect Dis,* 36**,** S24-30.

NEYROLLES, O. & GUILHOT, C. (2011) Recent advances in deciphering the contribution of Mycobacterium tuberculosis lipids to pathogenesis. *Tuberculosis (Edinb),* 91**,** 187-95.

NGUYEN, L., SCHERR, N., GATFIELD, J., WALBURGER, A., PIETERS, J. & THOMPSON, C. J. (2007) Antigen 84, an Effector of Pleiomorphism in *Mycobacterium smegmatis*. *J Bacteriol,* 189**,** 7869-7910.

NGUYEN, L. & THOMPSON, C. J. (2006) Foundations of antibiotic resistance in bacterial physiology: the mycobacterial paradigm. *Trends Microbiol,* 14**,** 304-12.

NIEDERWEIS, M., DANILCHANKA, O., HUFF, J., HOFFMANN, C. & ENGELHARDT, H. (2010) Mycobacterial outer membranes: in search of proteins. *Trends Microbiol,* 18**,** 109-16.

NIKITUSHKIN, V. D., DEMINA, G. R., SHLEEVA, M. O. & KAPRELYANTS, A. S. (2013) Peptidoglycan fragments stimulate resuscitation of "non-culturable" mycobacteria. *Antonie Van Leeuwenhoek,* 103**,** 37-46.

O'GAORA, P., BARNIN, S., HAYWARD, C., FILLEY, E., ROOK, G., YOUNG, D. & THOLE, J. (1997) Mycobacteria as immunogens: development of expression vectors for use in multiple mycobacterial species. *Medical Principles and Practices* 6**,** 91-96.

OJHA, A. K., BAUGHN, A. D., SAMBANDAN, D., HSU, T., TRIVELLI, X., GUERARDEL, Y., ALAHARI, A., KREMER, L., JACOBS, W. R., JR. & HATFULL, G. F. (2008) Growth of Mycobacterium tuberculosis biofilms containing free mycolic acids and harbouring drug-tolerant bacteria. *Mol Microbiol,* 69**,** 164-74.

OKEKE, I. N., KLUGMAN, K., P,, BHUTTA, Z. A., DUSE, A. G., JENKINS, P., O'BRIEN, T. F., PABLOS-MENDEZ. A & LAXMINARAYAN, R. (2005) Antimicrobial resistance in developing countries. Part II: strategies for containment. *Lancet Infect Dis,* 5**,** 568-580.

OLIVER, J. D. (2010) Recent findings on the viable but nonculturable state in pathogenic bacteria. *FEMS Microbiol Rev,* 34**,** 415-25.

PARISH, T. & STOKER, N. G. (2000) Use of a flexible cassette method to generate a double unmarked Mycobacterium tuberculosis tlyA plcABC mutant by gene replacement. *Microbiology,* 146 (Pt 8)**,** 1969-75.

PECSI, I., HIRMONDO, R., BROWN, A. C., LOPATA, A., PARISH, T., VERTESSY, B. G. & TOTH, J. (2012) The dUTPase enzyme is essential in Mycobacterium smegmatis. *PLoS One,* 7**,** e37461.

POPHAM, D. L., HELIN, J., COSTELLO, C. E. & SETLOW, P. (1996) Muramic lactam in peptidoglycan of Bacillus subtilis spores is required for spore outgrowth but not for spore dehydration or heat resistance. *Proc Natl Acad Sci U S A,* 93**,** 15405-10.

RAO, V., FUJIWARA, N., PORCELLI, S. A. & GLICKMAN, M. S. (2005) Mycobacterium tuberculosis controls host innate immune activation through cyclopropane modification of a glycolipid effector molecule. *J Exp Med,* 201**,** 535-43.

RASTOGI, N. & DAVID, H. L. (1988) Mechanisms of pathogenicity in mycobacteria. *Biochimie,* 70**,** 1101-20.

RASTOGI, N., FREHEL, C., RYTER, A., OHAYON, H., LESOURD, M. & DAVID, H. L. (1981) Multiple drug resistance in Mycobacterium avium: is the wall architecture responsible for exclusion of antimicrobial agents? *Antimicrob Agents Chemother,* 20**,** 666-77.

RECHT, J., MARTINEZ, A., TORELLO, S. & KOLLER, R. (2001) Sliding motility and biofilm formation in mycobacteria. *Acta Cient Venez,* 52**,** 45-49.

REYRAT, J. M., PELICIC, V., GICQUEL, B. & RAPPUOLI, R. (1998) Counterselectable markers: Untapped tolls for Bacterial Genetics and Pathogenesis. *Infect Immun,* 66**,** 4011-4017.

SASSETTI, C. M., BOYD, D. H. & RUBIN, E. J. (2003) gene required for mycobacterial growth defined by high density mutagenesis. *Mol Microbiol,* 48**,** 77-84.

SASSETTI, C. M. & RUBIN, E. J. (2003) Genetic requirements for mycobacterial survival during infection. *Proc Natl Acad Sci U S A,* 100**,** 12989-94.

SAT, B., HAZAN, R., FISHER, T., KHANER, H., GLASER, G. & ENGELBERG-KULKA, H. (2001) Programmed cell death in Escherichia coli: some antibiotics can trigger mazEF lethality. *J Bacteriol,* 183**,** 2041-5.

SAUVAGE, E., POWELL, A. J., HEILEMANN, J., JOSEPHINE, H. R., CHARLIER, P., DAVIES, C. & PRATT, R. F. (2008) Crystal structures of complexes of bacterial DD-peptidases with peptidoglycan-mimetic ligands: the substrate specificity puzzle. *J Mol Biol,* 381**,** 383-93.

SCANGA, C. A., MOHAN, V. P., JOSEPH, H., YU, K., CHAN, J. & FLYNN, J. L. (1999) Reactivation of latent tuberculosis: variations on the Cornell murine model. *Infect Immun,* 67**,** 4531-8.

SCHMIDT, J. W., GREENOUGH, A., BURNS, M., LUTERAN, A. E. & MCCAFFERTY, D. G. (2010) Generation of ramoplanin-resistant Staphylococcus aureus. *FEMS Microbiol Lett,* 310**,** 104-11.

SHAH, I. M., LAABERKI, M. H., POPHAM, D. L. & DWORKIN, J. (2008) A eukaryotic-like Ser/Thr kinase signals bacteria to exit dormancy in response to peptidoglycan fragments. *Cell,* 135**,** 486-96.

SHIDA, T., HATTORI, H., ISE, F. & SEKIGUCHI, J. (2001) Mutational analysis of catalytic sites of the cell wall lytic N-acetylmuramoyl-L-alanine amidases CwlC and CwlV. *J Biol Chem,* 276**,** 28140-6.

SHLEEVA, M., MUKAMOLOVA, G. V., YOUNG, M., WILLIAMS, H. D. & KAPRELYANTS, A. S. (2004) Formation of 'non-culturable' cells of Mycobacterium smegmatis in stationary phase in response to growth under suboptimal conditions and their Rpf-mediated resuscitation. *Microbiology,* 150**,** 1687-97.

SHLEEVA, M. O., BAGRAMYAN, K., TELKOV, M. V., MUKAMOLOVA, G. V., YOUNG, M., KELL, D. B. & KAPRELYANTS, A. S. (2002) Formation and resuscitation of "non-culturable" cells of

Rhodococcus rhodochrous and Mycobacterium tuberculosis in prolonged stationary phase. *Microbiology,* 148**,** 1581-91.
SILBERSTEIN, S. & INOUYE, M. (1975) Studies on the role of bacteriophage T7 lysozyme during phage infection. *J Mol Biol,* 96**,** 1-11.
SMITH, T. J., BLACKMAN, S. A. & FOSTER, S. J. (2000) Autolysins of Bacillus subtilis: multiple enzymes with multiple functions. *Microbiology,* 146 (Pt 2)**,** 249-62.
SNAPPER, S. B., MELTON, R. E., MUSTAFA, S., KEISER, T. & JACOBS JR, W. R., JR. (1990) Isolation and Characterization of efficient plasmid transformation mutants of *Mycobactrium smegmatis*. *Mol Microbiol,* 4**,** 1911-1919.
SOMNER, E. A. & REYNOLDS, P. E. (1990) Inhibition of peptidoglycan biosynthesis by ramoplanin. *Antimicrob Agents Chemother,* 34**,** 413-9.
STEINER, H. (2004) Peptidoglycan recognition proteins: on and off switches for innate immunity. *Immunol Rev,* 198**,** 83-96.
STORLA, D. G., YIMER, S. & BJUNE, G. A. (2008) A systematic review of delay in the diagnosis and treatment of tuberculosis. *BMC Public Health,* 8**,** 15.
STOVER, C. K., DE LA CRUZ, V. F., FUERST, T. R., BURLEIN, J. E., BENSON, L. A., BENNETT, L. T., BANSAL, G. P., YOUNG, J. F., LEE, M. H., HATFULL, G. F. & ET AL. (1991) New use of BCG for recombinant vaccines. *Nature,* 351**,** 456-60.
SUREKA, K., HOSSAIN, T., MUKHERJEE, P., CHATTERJEE, P., DATTA, P., KUNDU, M. & BASU, J. (2010) Novel role of phosphorylation-dependent interaction between FtsZ and FipA in mycobacterial cell division. *PLoS One,* 5**,** e8590.
THANKY, N. R., YOUNG, D. B. & ROBERTSON, B. D. (2006) Unusual features of the cell cycle in mycobacteria: Plar restricted growth and the snapping-model of cell division. *Tuberculosis,* 87**,** 231-236.
TRIPATHI, R. P., TEWARI, N., DWIVEDI, N. & TIWARI, V. K. (2005) Fighting tuberculosis: an old disease with new challenges. *Med Res Rev,* 25**,** 93-131.
UEHARA, T., DINH, T. & BERNHARDT, T. G. (2009) LytM-domain factors are required for daughter cell separation and rapid ampicillin-induced lysis in Escherichia coli. *J Bacteriol,* 191**,** 5094-107.
UEHARA, T. & PARK, J. T. (2007) An anhydro-N-acetylmuramyl-L-alanine amidase with broad specificity tethered to the outer membrane of Escherichia coli. *J Bacteriol,* 189**,** 5634-41.
UEHARA, T., PARZYCH, K. R., DINH, T. & BERNHARDT, T. G. (2010) Daughter cell separation is controlled by cytokinetic ring-activated cell wall hydrolysis. *EMBO J,* 29**,** 1412-22.
VAN RIE, A., PAGE-SHIPP, L., SCOTT, L., SANNE, I. & STEVENS, W. (2010) Xpert((R)) MTB/RIF for point-of-care diagnosis of TB in high-HIV burden, resource-limited countries: hype or hope? *Expert Rev Mol Diagn,* 10**,** 937-46.
VELAYATI, A. A., MASJEDI, M. R., FARNIA, P., TABARSI, P., GHANAVI, J., ZIAZARIFI, A. H. & HOFFNER, S. E. (2009) Emergence of new forms of totally drug-resistant tuberculosis bacilli: super extensively drug-resistant tuberculosis or totally drug-resistant strains in iran. *Chest,* 136**,** 420-5.
VOLLMER, W. (2012) Bacterial growth does require peptidoglycan hydrolases. *Mol Microbiol,* 86**,** 1031-1035.
VOLLMER, W., JORIS, B., CHARLIER, P. & FOSTER, S. (2008) Bacterial peptidoglycan (murein) hydrolases. *FEMS Microbiol Rev,* 32**,** 259-86.
WANG, X. & WOOD, T. K. (2011) Toxin-antitoxin systems influence biofilm and persister cell formation and the general stress response. *Appl Environ Microbiol,* 77**,** 5577-83.
WAXMAN, D. J. & STROMINGER, J. L. (1983) Penicillin-binding proteins and the mechanism of action of beta-lactam antibiotics. *Annu Rev Biochem,* 52**,** 825-69.
WAYNE, L. G. (1960) The bacteriology of respected tuberculous pulmonary lesions. 2. Observations on bacilli which are stainable but which cannot be cultured. *Am Rev Respir Dis,* 82**,** 370-7.

WAYNE, L. G. (1994) Dormancy of Mycobacterium tuberculosis and latency of disease. *Eur J Clin Microbiol Infect Dis,* 13**,** 908-14.

WEIGEL, L. M., CLEWELL, D. B., GILL, S. R., CLARK, N. C., MCDOUGAL, L. K., FLANNAGAN, S. E., KOLONAY, J. F., SHETTY, J., KILLGORE, G. E. & TENOVER, F. C. (2003) Genetic analysis of high-level Vancomycin-resistant isolate of *Staphylococcus aureus*. *Science,* 302**,** 1569-1571.

WERNER, T., LIU, G., KANG, D., EKENGREN, S., STEINER, H. & HULTMARK, D. (2000) A family of peptidoglycan recognition proteins in the fruit fly Drosophila melanogaster. *Proc Natl Acad Sci U S A,* 97**,** 13772-7.

WHO (2009) Global Tuberculosis control. *WHO report 2009.*

WHO (2011) Global Tuberculosis Report. *WHO Report 2011*.

YAGUI, M., PERALES, M. T., ASENCIOS, L., VERGARA, L., SUAREZ, C., YALE, G., SALAZAR, C., SAAVEDRA, M., SHIN, S., FERROUSIER, O. & CEGIELSKI, P. (2006) Timely diagnosis of MDR-TB under program conditions: is rapid drug susceptibility testing sufficient? *Int J Tuberc Lung Dis,* 10**,** 838-43.

YANG, D. C., TAN, K., JOACHIMIAK, A. & BERNHARDT, T. G. (2012) A conformational switch controls cell wall-remodelling enzymes required for bacterial cell division. *Mol Microbiol,* 85**,** 768-81.

ZHANG, Y. (2005) The magic bullets and tuberculosis drug targets. *Annu Rev Pharmacol Toxicol,* 45**,** 529-64.

ZHANG, Y., HEYM, B., ALLEN, B., YOUNG, D. & COLE, S. (1992) The catalase-peroxidase gene and isoniazid resistance of Mycobacterium tuberculosis. *Nature,* 358**,** 591-3.